공학박사학위논문

Synthesis and characterization of highly soluble perylene dyes for application on black matrix with low dielectric constant

저유전율 블랙 매트릭스 용 고용해성 페릴렌 염료의 합성 및 특성에 대한 연구

2019년 8월

서울대학교 대학원

재료공학부

육 심 범

Abstract

Synthesis and characterization of highly soluble perylene dyes for application on black matrix with low dielectric constant

Sim Bum Yuk

Department of Materials Science and Engineering

The Graduate School

Seoul National University

Color filters are one of the major components of display modules that convert unrefined light into red (R), green (G), and blue (B) light. A black matrix is located between RGB patterned pixels for preventing unwanted mixing of the colors. In addition, the black matrix absorbs external light to prevent malfunction of thin film transistors (TFTs). Therefore, the materials used for the preparation of black matrix requires a strong light-absorbing ability in the visible light region.

The most commonly used material for the preparation of the black matrix is carbon black. Carbon black exhibits strong absorption characteristics in the entire visible light region and high resistance to light and heat. However, films fabricated with carbon black can cause electric signal transduction errors on the adjacent TFTs because of their high electric conductivity. With the developments of thinner display panels, the distance between a TFT and color filter layers is gradually decreasing. Therefore, alternatives for carbon black with a low dielectric constant is required. Organic pigments are mixed with carbon black to lower the dielectric constant of the film. However, sufficient optical properties of the film for the black matrix are difficult to achieve due to the low molar absorbance of the pigments.

Carbon black and organic pigments have an exceedingly low solubility in industrial solvents such as propylene glycol monomethyl ether acetate (PGMEA) due to the strong intermolecular attraction. Therefore, these colorants are applied to the black matrix by the dispersion method. The dispersed particles should maintain a monodispersed state with a size of less than a few hundreds of nanometers. Using the dispersion method to a black matrix requires the development of an additional dispersion process for the colorant and new materials such as dispersants.

Organic dyes can be attractive alternatives for carbon black or organic pigments due to their strong light-absorbing ability and low dielectric constant of the film using the dyes. In addition, the black matrix can be prepared by the dissolution method through the PGMEA-soluble dyes, and the dissolution method can offer a more simplified fabrication process than the dispersion method. Generally, dyes have lower stability than pigments and carbon black, and the dyes should be designed for

improving the stability to replace these colorants.

Therefore, in this study, organic dyes highly soluble in PGMEA were developed, and the dye-type and hybrid-type (containing both the carbon black and the dyes) were fabricated. The films containing the dyes exhibited a low dielectric constant, and thus, the dyes which have strong stability and color strength can be an appropriate alternative for pigments

Highly stable perylene-3,4,9,10-tetracarboxylic dianhydride (PTCDA) was selected as the basic structure of dyes. PTCDA derivatives have been widely used in various industrial fields such as in biochemical applications, organic photovoltaics, light-emitting diodes, and TFTs due to their high thermal, chemical, and photochemical stabilities and a strong charge transfer property. In particular, the orbital energy levels of perylene can be easily adjusted by the introduction of substituents at the periphery and bay positions. Thus, PTCDA derivatives are suitable as a black matrix material to absorb the entire visible light.

Aniline derivative-substituted perylene diimides (PDIs) at the periphery position of PTCDA were synthesized, and the absorption range of the dyes was modified by the electron-donating group at the bay position. The optical and thermal properties of the dyes were investigated, and the optical, thermal, and dielectric properties of the dye-type and hybrid-type were examined. Between the two types of films, the hybrid-type black matrix showed promising results with a low dielectric constant, low transmittance spectrum, and high thermal stability.

Conjugation-extended perylenetetracarboxylic bisbenzimidazole (PTCBI) was

also synthesized for visible light absorption around 600–700 nm, the wavelength region of weakly absorbed by the PDI dyes used in a previous study. The black matrices were fabricated with a mixture of PDI and PTCBI dyes, and the optical, thermal, and dielectric properties of the films were examined. The surface morphology of the films was also probed by atomic force microscopy for further investigation.

Optical density (OD) is one of the most important factors for evaluating the light absorption ability of the black matrix. The OD values of the dye-type and hybrid-type films did not meet the industrial standard (2.5) according to a previous study. As a strategy for improving the OD of the black matrix, dimeric PDIs were synthesized, and the films were fabricated with these dyes. The solubility of the dimers was increased from the solubility of the monomeric PDIs with the same bay substituents owing to the twisted two-perylene cores. The OD of the hybrid-type black matrices using dimeric PDIs were significantly improved (up to 2.76) due to the increased dye content by the highly soluble dimeric PDIs. Additionally, the black matrices exhibited higher thermal stability, flat surface condition, and lower dielectric constant than the previously developed black matrices.

Finally, the applicability of the dyes to the black matrix was evaluated by comparing the black matrix using the dissolution method with the black matrix using the dispersion method. This comparison studies conducted using perylene dyes that have a similar structure but differ in their solubility. As a result, to develop a black matrix of thermally stable and excellent optical and surface characteristics, the strategy of improving the solubility of the perylene dye and applying the dye to the

black matrix by the dissolution method is more advantageous than the method using the dispersion method.

In conclusion, black matrices with a low dielectric constant were developed by replacing carbon black and organic pigments to organic dyes. To improve the optical and thermal stability of the films, the dyes were synthesized based on perylene chromophore with the excellent light-absorbing ability and thermal stability. The fabricated films exhibited thermally stable characteristics and surface flatness was maintained at a uniform level. In addition, the industrial standard of OD was achieved by hybrid-type black matrices using highly soluble dimeric PDIs.

KEYWORDS: Liquid crystal display, Black Matrix, Solubility, Perylene, Dyes, Dielectric constant, Light absorption

Student Number: 2009-20622

Contents

List of Tables

List of Schemes

List of Figures

Chapter 1

Introduction

1.1 An overview of LCDs

An LCD is a type of flat panel display commonly used in digital devices, for example, appliance displays, mobiles, and portable computers. The LCDs show the features of the extremely low power consumption, low voltage operation, high definition, high brightness, and flexibility of size. Currently, organic light-emitting diodes (OLEDs) with a high contrast ratio and wide color gamut occupy a large number of the display market. However, research for improving the LCDs performance has been steadily conducted due to the high yield of the panel manufacturing and the extended lifetime of the light source [1-3].

A basic structure of the LCD panel is shown in Fig. 1.1. LCD has two sheets of polarizing material with a liquid crystal solution between them. Transparent electrode deposited indium tin oxides (ITOs) are layered inside of each polarizer and the electricity is applied to the solution through ITO and thin film transistors (TFTs) and causes the crystals to align in patterns. A column spacer which made of photosensitive polymer is a material to maintain a uniform cell gap between the TFT and the color filter. A color filter is composed of red, green, blue pixels which convert

the electrically polarized light from the backlight unit to RGB color. A black matrix is located between the RGB pixels to block the light leaking from the color filter [4].

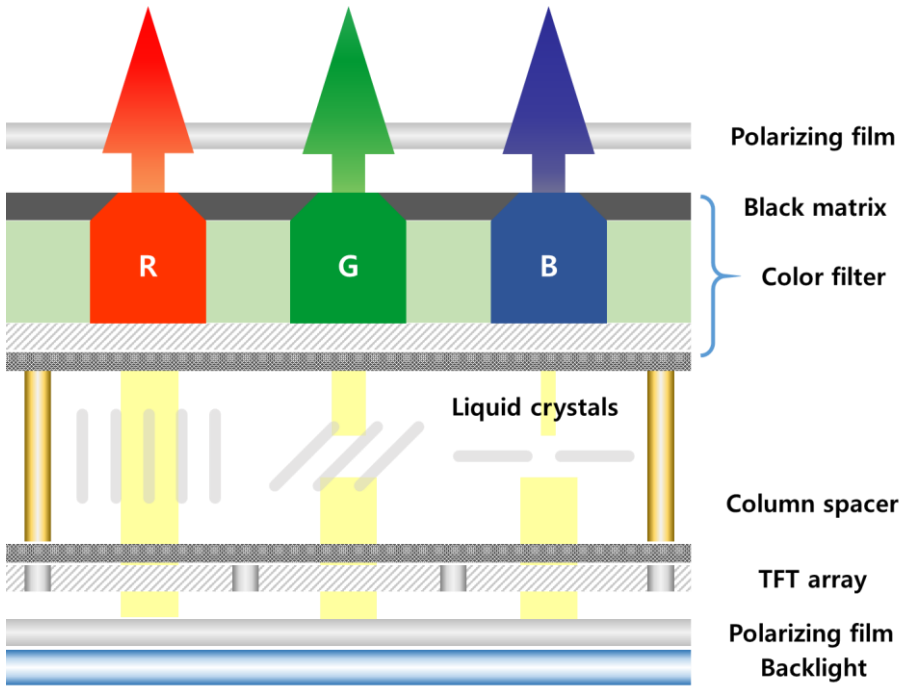

Figure 1.1. Basic structure of LCD.

1.2 Structure and requirement of black matrix

Generally, color filters consist of a clear substrate, black matrix, color filter layer (RGB colors), overcoat, and ITO film. Black matrix is coated on the clear substrate and exposed and developed to form a pattern according to the shape and size of RGB pixels. Red, green, and blue pixels are applied after black matrix patterning, and transparent overcoat layer is covered to make the different heights of the RGB pixels to the same height. ITO is placed on the overcoat layer and plays a role as an electrical signal transfer. The schematic structure of color filter, including a black matrix, is shown in Fig. 1.2 [4,5].

A black matrix, which located between RGB pixels, prevents unwanted mixing of RGB colors and blocks the light that passes through the LC even in the off state of LCD, which improves the contrast of the display. In addition, black matrices absorb external light and protect TFTs that can cause malfunction by external light. Therefore, the strong light-absorbing ability is one of the most important characteristics of black matrices. Absorption strength of black matrices is evaluated based on optical density (OD), and for practical use, black matrix with an OD of at least 2.5 μm^{-1} is required.

Black matrices are formed first in order before RGB pixels, it should go through the baking process of RGB coating. Therefore, high thermal stability is essential to sustain each severe baking process. Thermal stability of black matrices is measured by the chromatic change (ΔE_{ab}) during each baking step and retention rate (ratio between the thickness of the film after prebaking and postbaking). The films with

the ΔE_{ab} of 3 or less, and the retention rate of >80% can be sufficiently applied to the LCD color filters [6,7].

The dielectric constant is also an important factor in the characteristics of black matrices and is required to be less than 7 in the industry. Black matrices protect TFTs against an external light by being placed on the TFT layer. Black matrices having a high dielectric constant may cause a malfunction of the adjacent TFTs by sending a wrong electrical signal to the TFT. Especially, as shown in Fig. 1.3, a low dielectric constant of the black matrix is essential in the color filters on TFT array structure which is designed to reduce the display thickness.

The light stability of the pixels is important because black matrix is exposed to a lamp with ultraviolet filter for more than two million lux. The chemical stability is also important since black matrices are exposed to solvents, acids and bases during the LCD fabrication process. In detail, the cured film must be stable when exposed to solvents such as NMP and γ-butyrolactone, and to acids used in etching process or bases used in the development system [4,5].

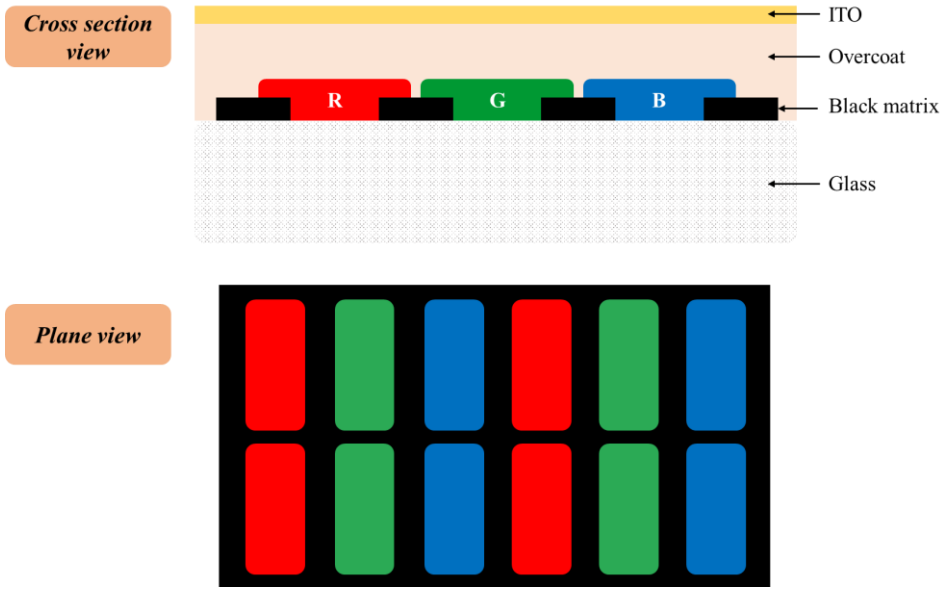

Figure 1.2. Fundamental structure of LCD color filter.

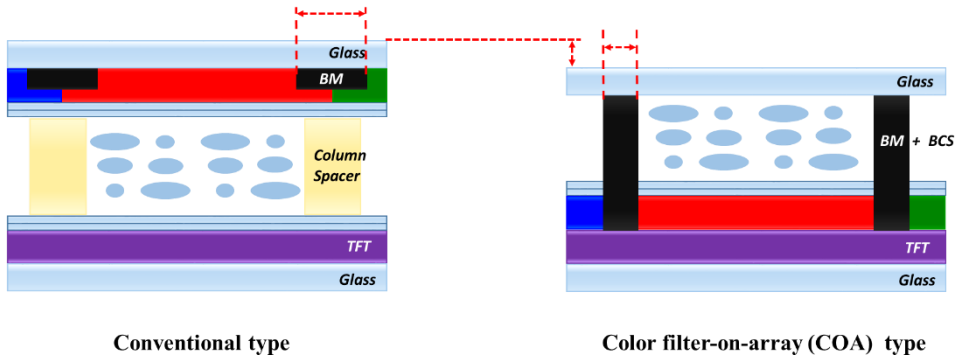

Figure 1.3. LCD structures of conventional and COA type.

1.3 Fabrication of black matrix pattern using black matrix photo-resist

Conventional fabrication process of color filter including black matrix is following photolithographic method using color and black matrix photo-resist shown as Fig. 1.4 [4,5].

1. Black matrix formation;

A black matrix is formed first in order to prevent any leakage of backlight and the RGB color mixture.

2. Color photo-resist coating;

RGB color photo-resists are coated to the entire glass.

3. Exposure;

To make the pattern insoluble, it is UV cured by exposure through a photo-mask

4. Development and baking;

After the removal of unnecessary portions of the color resist by the developing solution, the pattern is cured through baking. The above processes from step 2 and 4 are repeated three times (for RGB).

5. Overcoat layer and ITO film formation;

Transparent coating is applied over RGB pixel with slightly different height for the flat surface of the color filter. Transparent and conductive ITO film is formed by

the sputtering method.

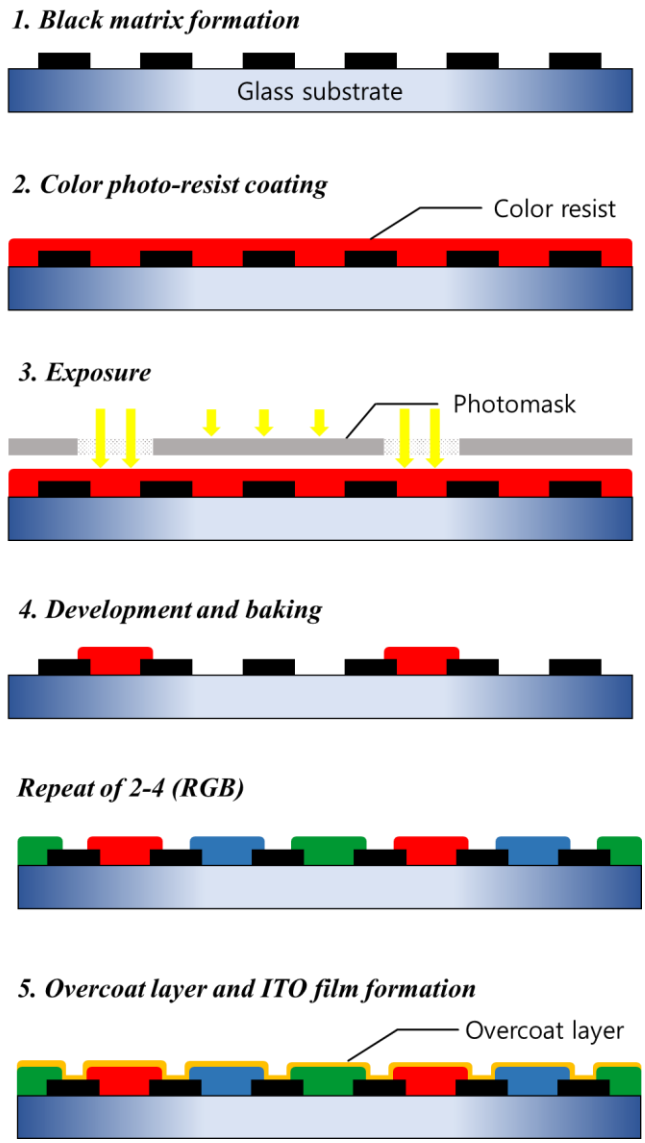

Figure 1.4. Color filter manufacturing process by the photolithographic method.

1.4 Previous research and research objectives

Current fabrication method for LCD black matrix is photolithography using dispersed carbon black [ref]. Carbon black exhibits thermally stable characteristics with strong light absorption ability against visible light, which is suitable for black matrix materials. However, the carbon black-type black matrix having a high dielectric constant may cause malfunction of the adjacent TFT layer. Therefore, research has been required to replace carbon black with other organic materials [7,8]. The dielectric constant of the black matrices can be lowered through organic pigments, however, the spectral characteristics of the black matrices may not be sufficiently high due to the low optical properties of the pigments.

Organic dyes are proposed as alternatives, and it is expected that the dielectric constant of the black matrix will be lowered as the dye content is increased. In a previous report of our research group (Prof. J.P. Kim group), studies for dye-type matrices have been studied [7,9]. However, the dye-type black matrix showed a limitation on optical properties.

In this study, we developed a hybrid-type black matrix which is fabricated with a mixture of dyes and carbon black to satisfy the industrial conditions of display. For this purpose, a chromophore with excellent thermal stability was selected as the basic structure of dyes. Various substituents were introduced on the chromophore to enhance the solubility of the dyes in an industrial solvent, and the dyes applied to black matrices through a solution process. All of the dyes designed based on perylene moiety to prevent self-agglomeration of dyes in the film state. The synthesized dyes

and carbon black were prepared in various combination ratios to analyze the film characteristics and aimed at developing a black matrix that maintains optical properties and stability while having a low dielectric constant.

1.5 References

[1] Koo H-S, Chen M, Pan P-C. LCD-based color filter films fabricated by a pigment-based colorant photo resist inks and printing technology. Thin Solid Films. 2006;515(3):896-901.

[2] Yeh P, Gu C. Optics of liquid crystal displays. John Wiley & Sons, Inc; 1999. P. 1-5.

[3] Yang DK, Wu ST. Fundamentals of liquid crystal devices. New Jersey: Wiley-SID; 2006: 278–281.

[4] Choi J, Kim SH, Lee WS, Yoon C, Kim JP. Synthesis and characterization of thermally stable dyes with improved optical properties for dye-based LCD color filters. New J. Chem. 2012; 36:812–818.

[5] Sabnis RW. Color filter technology for liquid crystal displays. Displays 1999; 20:119–29.

[6] Tsuda K. Color filters for LCDs. Displays 1993;14:115–124.

[7] Lee W, Yuk SB, Choi J, Jung DH, Choi S-H, Park J, et al. Synthesis and characterization of solubility enhanced metal-free phthalocyanines for liquid crystal

display black matrix of low dielectric constant. Dyes and Pigments. 2012;92(3):942-8.

[8] Hirayama H, Hidaka K, Imai N, Ibaraki N. Integrated black matrix on TFT arrays composed on newly developed Bi-SiOx ceramic thin film. Soc Inform Display Dig 1997;28:180-3.

[9] Choi J, Lee W, Namgoong JW, Kim T-M, Kim JP. Synthesis and characterization of novel triazatetrabenzcorrole dyes for LCD color filter and black matrix. Dyes and Pigments. 2013;99(2):357-65.

Chapter 2

Synthesis and characterization of bay-substituted perylene dyes for LCD black matrix of low dielectric constant

2.1 Introduction

Color filters are one of the most important components of liquid crystal displays (LCDs) [1, 2]. They are composed of a glass substrate, a black matrix, a color layer, and an indium tin oxide film. The black matrix plays vital roles in dividing the red, green and blue (RGB) pixels of color layer, blocking light leakage between RGB color patterns, and enhancing the contrast ratio of the LCD [3]. In addition, light shielding of the black matrix prevents malfunction of thin-film-transistors (TFT) by external incident light [4]. To perform these roles, black matrices with high optical density (OD), high light shielding ability, and low reflectance are required [1].

Recently, LCD development has focused on more simple structures with low cost and high brightness. Black matrix-on-thin film transistor (BOT) structures are a potential solution, in which the black matrix is located on the TFT array. Narrow black matrix width within the BOT structure allows a small amount of black matrix material and higher aperture ratio for the color filter to transmit more backlight than a conventional LCD. Commonly used metal materials (such as Cr/CrO_x) [1, 5] are

not suitable for BOT structures owing to their high cost and complex manufacturing process. Furthermore, electrical signal transduction errors on TFTs can occur because of the high dielectric constant of Cr/CrO_x. Accordingly, the need for new LCD development procedures using organic materials has emerged.

Carbon black is the most widely used organic material for black matrices with high OD and thermal stability [6]. However, black matrices fabricated with carbon black also have a high dielectric constant because of the high electrical conductivity of its conjugated structure. In previous studies [7-9], this disadvantage was overcome using dye-type black matrices through conducted research so far. Since organic dyes show significantly lower dielectric constants compared to carbon black, dyes can be an attractive alternative material for black matrices.

In a previous study, dye-type black matrices using organic dyes were produced to investigate ideal black matrices [9]. Two dyes with different absorption ranges were chosen, and dye-type black matrices with a low dielectric constant were fabricated. However, the dye-type black matrices showed several limitations (such as low light absorption and optical properties) because of their insufficient solubility in industrial solvents. In this study, two dyes with broad absorption were synthesized, and one was selected for black matrix production based on its spectral and thermal properties as well as its solubility in industrial solvents. Hybrid-type and dye-type black matrices were fabricated and compared with traditional carbon black-type black matrices. The spectral, optical, thermal, and dielectric properties of the fabricated black matrices were measured to evaluate the suitability of the dyes for LCD color filter manufacturing processes.

2.2 Experimental section

2.2.1 Materials and instrumentation

Perylene-3,4,9,10-tetracarboxylic dianhydride, 2,6-diisopropylaniline, m-cresol, iodine, sulfuric acid, bromine, acetic acid and potassium carbonate anhydrous purchased from Sigma-Aldrich, and carbazole, copper iodide and 18-crown-6 purchased from TCI were used as received. All the other reagents and solvents were of reagent-grade and obtained from commercial suppliers. Transparent glass substrates were provided by Paul Marienfeld GmbH & Co. KG, and acrylic binder and black matrix resist were supplied by KOLON industry Inc.

^{1}H NMR spectra were recorded on a Bruker Avance 500 spectrometer at 500 MHz using chloroform-d and TMS, as the solvent and internal standard, respectively. Matrix Assisted Laser Desorption/Ionization Time Of Flight (MALDI-TOF) mass spectra were collected on a Voyager-DE STR Biospectrometry Workstation with α-cyano-4-hydroxycinnamic acid (CHCA) as the matrix. Absorption and transmittance spectra were measured using a HP 8452A spectrophotometer. Thermogravimetric analysis (TGA) was conducted in nitrogen atmosphere at a heating rate of 10 °C min^{-1} using a TA instruments Thermogravimetric Analyzer 2050. Chromatic characteristics of the black matrices were analyzed on a Scinco color spectrometer. Dielectric constants were measured using Edward E306 thermal evaporator and an HP 4294A precision impedance analyzer. The thickness of the black matrices was

measured using a KLA-TENCOR Nanospec AFT/200 alpha step.

2.2.2 Synthesis

The dyes **2a**, **2b**, **3a,** and **3b** are already known structures and were synthesized according to the previously reported procedures [10].

2.2.2.1 N,N'-Bis(2,6-diisopropylphenyl)-1,7-dibrommoperylene-3,4,9,10-tetracarboxylicdiimide (3a)

Perylene-3,4,9,10-tetracarboxylic dianhydride (10 g, 25.44 mmol), iodine (0.24 g, 0.95 mmol), and sulfuric acid (98%, 140 ml) were mixed and stirred for 2 h at room temperature. The reaction temperature was set at 80 °C, and bromine (2.24 ml, 43.75 mmol) was added dropwise over 2 h. The mixture was reacted further at 80 °C for 16 h, cooled to room temperature, and the excess bromine gas was displaced by nitrogen gas. The precipitate obtained after adding ice-water to the mixture was collected by suction filtration. The precipitate was washed with water several times until the aqueous layer became neutral to yield dibromo dianhydride as a crude product. The crude product was dried at 100 °C under reduced pressure and used for next step without further purification.

The crude 1,7-dibromoperylene-3,4,9,10-tetracarboxylic dianhydride (6 g, 10.88 mmol), 2,6-diisopropylaniline (6.60 ml, 35.03 mmol) and acetic acid (3.45 ml) were mixed and heated at 120 ℃ in N-Methyl-2-pyrrolidine (NMP) (75 ml) under the nitrogen atmosphere for 96 h. The precipitate obtained after water to the mixture was collected by suction filtration. The crude product was washed with water, dried and purified by column chromatography on silica gel using CH_2Cl_2 as the eluent. The band containing tribromonated diimide could be separated firstly. Then, the second band containing a mixture of isomeric diimide was collected. The mixture was washed with EtOH and toluene and heated at 80 ℃ for 12 h in toluene (40 ml). The pure diimide, a red compound of **3a**, was recrystallized from the hot toluene solution (9.50 g, 43% yield). ^{1}H NMR ($CDCl_3$, 500 MHz): 9.57 (d, 2H), 9.02 (d, 2H), 8.82 (d, 2H), 7.53 (t, 2H), 7.37 (d, 4H), 2.77 (septet, 4H), 1.20 (d, 24H); MALDI-TOF MS: m/z 869.8 (100%, $[M + 2H]^+$).

2.2.2.2 N,N'-Bis(2,6-diisopropylphenyl)-1-brommoperylene-3,4,9,10-tetracarboxylicdiimide (3b)

3b could be separated by column chromatography from the same crude product of **3a**. After obtaining a mixture of diborminated isomeric diimide, **3b** was obtained as the third eluted compound (7.84 g, 39% yield). ^{1}H NMR ($CDCl_3$, 500 MHz): 9.87 (d, 1H), 9.04 (d, 1H), 8.83 (m, 3H), 8.73 (m, 2H), 7.53 (t, 2H), 7.37 (d, 4H), 2.781 (septet, 4H), 1.20 (d, 24H); MALDI-TOF MS: m/z 791.1 (100%, $[M + 2H]^+$).

2.2.2.3 N,N'-Bis(2,6-diisopropylphenyl)-1,7-di(9H-carbazole)-perylene-3,4,9,10-tetracarboxylicdiimide (4a)

A mixture of **3a** (0.60 g, 0.69 mmol), carbazole (0.35 g, 2.09 mmol), 18-crown-6 (0.15 g, 0.55 mmol), copper iodide (46 mg, 0.24 mmol) and potassium carbonate (0.96 g, 6.95 mmol) in *N*-methylpyrrolidone (45 ml) was stirred at 110 ℃ for 24 h. The reaction mixture was cooled to room temperature and poured into 5% HCl (1 L). The precipitate was filtered, repeatedly washed with water, and dried in a vacuum at 80 ℃. The crude product was purified by column chromatography on silica gel using CH_2Cl_2 as the eluent to obtain **4a** as a black solid (0.35 g, 49% yield). ^{1}H NMR (500 MHz, $CDCl_3$): 8.90 (d, 2H), 8.28 (m, 4H), 8.08 (d, 2H), 7.61 (d, 2H), 7.47 (d, 2H), 7.34 (m, 4H), 7.32 (m, 4H), 2.71 (septet, 4H), 1.15 (d, 24H); MALDI-TOF MS: m/z 1042.2 (100%, $[M + 2H]^+$).

2.2.2.4 N,N'-Bis(2,6-diisopropylphenyl)-1-(9H-carbazole)-perylene-3,4,9,10-tetracarboxylicdiimide (4b)

4b was synthesized in the same manner with **4a** using **3b** (0.60 g, 0.76 mmol), carbazole (0.17 g, 1.05 mmol), 18-crown-6 (0.15 g, 0.55 mmol), copper iodide (46 mg, 0.24 mmol) and potassium carbonate (0.96 g, 6.95 mmol) (0.29g, 44% yield). ^{1}H NMR ($CDCl_3$, 500 MHz): 8.90 (d, 1H), 8.81 (m, 2H), 8.74 (s, 1H), 8.24 (m, 2H), 7.52 (m, 3H), 7.39 (m, 6H), 7.30 (d, 2H), 7.21 (m, 2H), 2.81 (septet, 4H), 1.30 (d,

24H); MALDI-TOF MS: m/z 876.01 (100%, $[M + 2H]^+$).

2.2.3 Preparation of black matrices

The solution for a dye-type black matrix was composed of the dye (0.10 g), propylene glycol methyl ether acetate (PGMEA) (2.03 g) and acrylic binder (0.38 g). The solution for a hybrid-type black matrix was composed of the dye (0.11 g), PGMEA (2.70 g), acrylic binder (0.50 g) and carbon black resist (1 g). The prepared solutions were coated on a transparent glass substrate using a MIDAS System SPIN-1200D spin coater. The coating speed was initially 300 rpm for 20 s, which was then increased to 500 rpm and kept constant for 10s. The wet coated black matrices were dried at 80 ℃ for 20 min, prebaked 100 ℃ for 1 min, and post baked at 230 ℃ for 30 min. After each step, the coordinate values of the black matrices were measured.

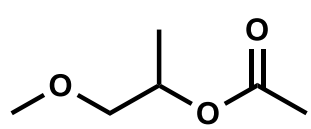

Figure 2.1. Structure of PGMEA

2.2.4 Investigation of solubility

The synthesized dyes were added to the PGMEA and CH_2Cl_2 at various concentrations. The solutions were sonificated for 5 min using ultrasonic cleaner NXP-4020. The solutions were left to stand for 48 h at room temperature and checked for precipitation to determine the solubility of the dyes.

2.2.5 Measurement of thermal stability

The thermal stability of the synthesized dyes was evaluated by TGA. The prepared dyes were heated to 230 ℃ and held at that temperature for 60 min for simulation the thermal processing condition of color filter manufacturing. The dyes were finally heated to 400 ℃ to determine their degradation temperature. The heating was carried out at the rate of 10 °C per min under nitrogen atmosphere.

2.2.6 Measurement of spectral and optical properties

The absorption spectra of the synthesized dyes and the transmittance spectra of the black matrices were measured using a UV-Vis. spectrophotometer. The chromatic values of the black matrices were recorded on a color spectrophotometer.

2.2.7 Geometry optimization of the synthesized dyes

The geometry and electric structure of the studied dyes are optimized by the density functional theory (DFT) method at the B3LYP/6-31G (d, P) performed on Gaussian 09 program.

2.3 Results and Discussion

2.3.1 Properties of the dyes

The basic structure of perylene can withstand the severe thermal conditions of the LCD color filter manufacturing process owing to its strong intermolecular π-π stacking interactions and expanded planar molecular structure [11, 12]. On the other hand, the solubility of the dye in industrial solvents (such as PGMEA) is not satisfactory. To overcome this disadvantage, two perylene diimide (PDI) dyes with enhanced solubility in industrial solvents were synthesized (by the synthetic routes shown in Scheme 2.1). First, 2,6-diisopropyl aniline was imidized on the terminal position of perylene-3,4,9,10-tetracarboxylic dianhydride (1) to reduce intermolecular crystal packing. Then, a carbazole was introduced at the bay positions

of the perylene core to distort the plane of the molecule. Both of the attached substituents decreased the planarity of the dye molecules to disturb aggregation and increase their solubility [13, 14].

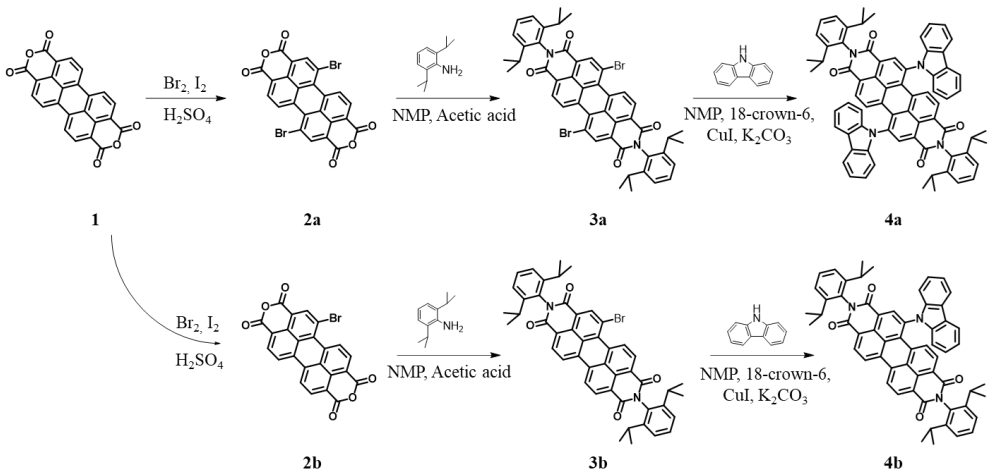

Scheme 2.1. Synthetic routes for the synthesis of PDI dyes.

Table 2.1 shows the solubility of the synthesized dyes measured in PGMEA and CH_2Cl_2, respectively. The dyes need to be dissolved in solvents at a concentration of at least 4-5 wt% to be applied in LCD color filter manufacturing processes [10]. The solubility of 3a and 3b in CH_2Cl_2 was increased sufficiently by the bulky aryl groups, which rotate 90° out of the plane of the molecule [13]. However, the solubility of 3a and 3b in PGMEA were still not enough to use as a black matrix material. By introducing additional substituents at the bay position of the dyes, the solubility of 4a and 4b was increased to more than 4 wt% in PGMEA and 6.1 wt% in CH_2Cl_2, respectively. Introducing bulky carbazole groups to the bay position of the dyes induced molecular plane distortion [14-16]. This subsequently decreased self-

organization of the dyes due to a π-π molecular orbital overlap and increased their solubility in organic solvents. The distortion angles of the perylene cores were calculated by using density functional theory (DFT) at the B3LYP/6-31G (d, p) level of theory and are presented in Fig. 2.2. We observed that the twisting angle of 4a (18.40˚) was larger than that of 4b (9.7˚, 15. 8˚), whereas 4a showed lower solubility than 4b. The asymmetric structure of 4b also affected the intermolecular crystal packing, which could offset the core twisting effect.

Table 2.1. Solubility of the dyes in PGMEA and CH_2Cl_2.

	3a	3b	4a	4b
PGMEA	2.3 wt%	2.4 wt%	4.0 wt%	5.2 wt%
CH_2Cl_2	5.5 wt%	5.7 wt%	6.1 wt%	7.5 wt%

(a)

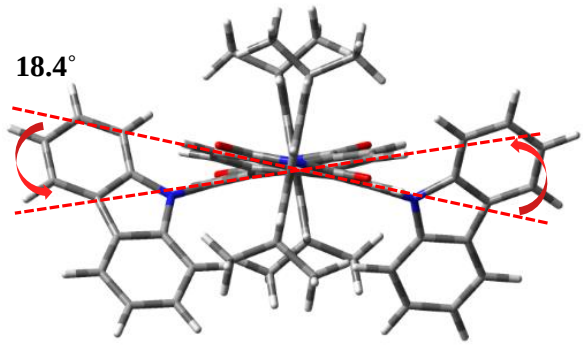

(b)

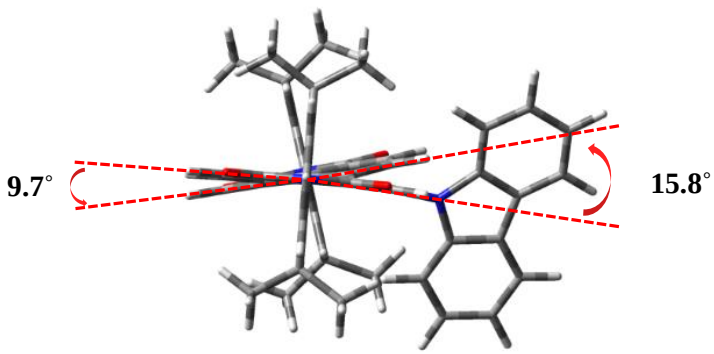

Figure 2.2. Optimized dye structures and dihedral angles of the perylene core of 4a and 4b.

The absorption spectra of dyes 4a and 4b are shown in Fig. 2.3 and the absorption maxima and molar extinction coefficient of the dyes are presented in Table 2.2. 4a has absorption maxima between 481 and 488 nm with additional broad absorption in the range of 550–650 nm. The spectral broadening of 4a may arise from the core twisting effect by the substituents and extended conjugation of the structure between the perylene core and the substituents [17-19]. Although 4b has a higher absorbance maximum than 4a, insufficient absorption above 550 nm suggests that 4b is a less effective material for black matrices (which requires a wide absorption range in the visible light region).

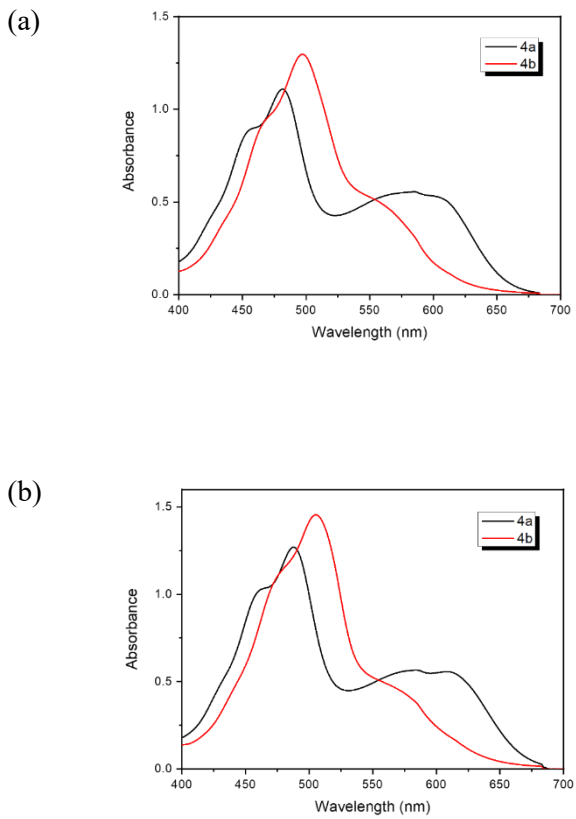

Figure 2.3. Absorption spectra of the dyes in PGMEA (a) and CH_2Cl_2 (b) (concentration at 5×10^{-5} mol l^{-1}).

Table 2.2. Absorption maxima and molar coefficients of the dyes in PGMEA and CH_2Cl_2.

	Dye	λ_{max} (nm)	ε_{max} (10^4 L mol^{-1} cm^{-1})
PGMEA	4a	481	2.22
	4b	497	2.59
CH_2Cl_2	4a	488	2.54
	4b	505	2.91

The perylene core has the advantage of thermal stability arising from its flat molecular structure that contributes to strong intermolecular π-π stacking interactions. From this point of view, the PDI dyes (based on thermally stable perylene core) are expected to endure high temperatures. The thermal stability of the dyes was investigated through TGA and the results are shown in Fig. 2.4. The experiments were conducted for 1 h at an isothermal region of 230 ℃ to mimic the conditions of the LCD color filter manufacturing process [20].

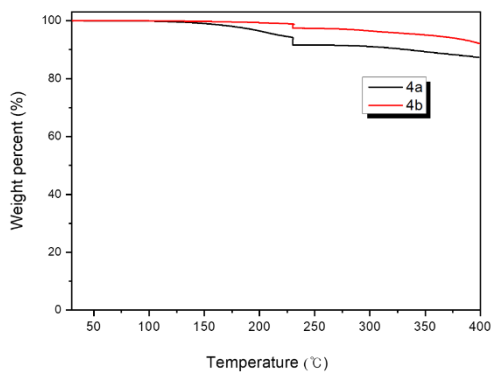

Figure 2.4. TGA analysis of the dyes.

Weight loss of the 4a and 4b in the isothermal region was 2.7% and 1.4%, respectively, which can be sufficiently applied to black matrices. The difference in thermal stability between 4a and 4b resulted from the twisted geometry of the dyes that affect π-π stacking among the dye molecules. The twisted structure introduces strong steric hindrance and reduces the tendency of the dyes to aggregate [21-24]. Hence, the small twisting angle of 4b allowed higher thermal stability than 4a.

2.3.2 Optical and thermal properties of the black matrices

Black matrices should have a wide and strong absorption spectrum to completely block the light emitted from LCD backlight [1]. Dye-type (film A, dye content: 4 wt%, thickness: 18.0 μm), hybrid –type (film B, colorant content: 8.5 wt%, dye:carbon black = 3:7, thickness: 6.8 μm), and carbon black-type (film C, carbon black content: 25 wt%, thickness: 3.0 μm) black matrices were fabricated. The spectral and optical properties of the films were measured by UV-Visible spectroscopy and OD measurements after prebaking and postbaking. The transmittance spectra of the films are shown in Fig. 2.5. Film C blocked the entire range of visible light and showed consistent transmittance spectra after prebaking and postbaking. In case of film A, a light range of 430–630 nm was blocked efficiently; however, light leakage occurred around 400 and 700 nm. This is a reflection of low absorbance at those wavelength regions for 4a in the solution state. To supplement the light leakage of film A, carbon black was added during the

fabrication process of film B. The transmittance of the visible light region is much lower than that of film A due to the effect of carbon black which has strong light absorbing ability, while small light leakage still occurred around 700 nm. In addition, the transmittance spectrum of film B after prebaking was similar to that of after postbaking, which suggests that the dye molecules endured severe baking conditions. To investigate the additional thermal stability of the films, ΔE_{ab} was measured after prebaking and postbaking (Section 2.3.3).

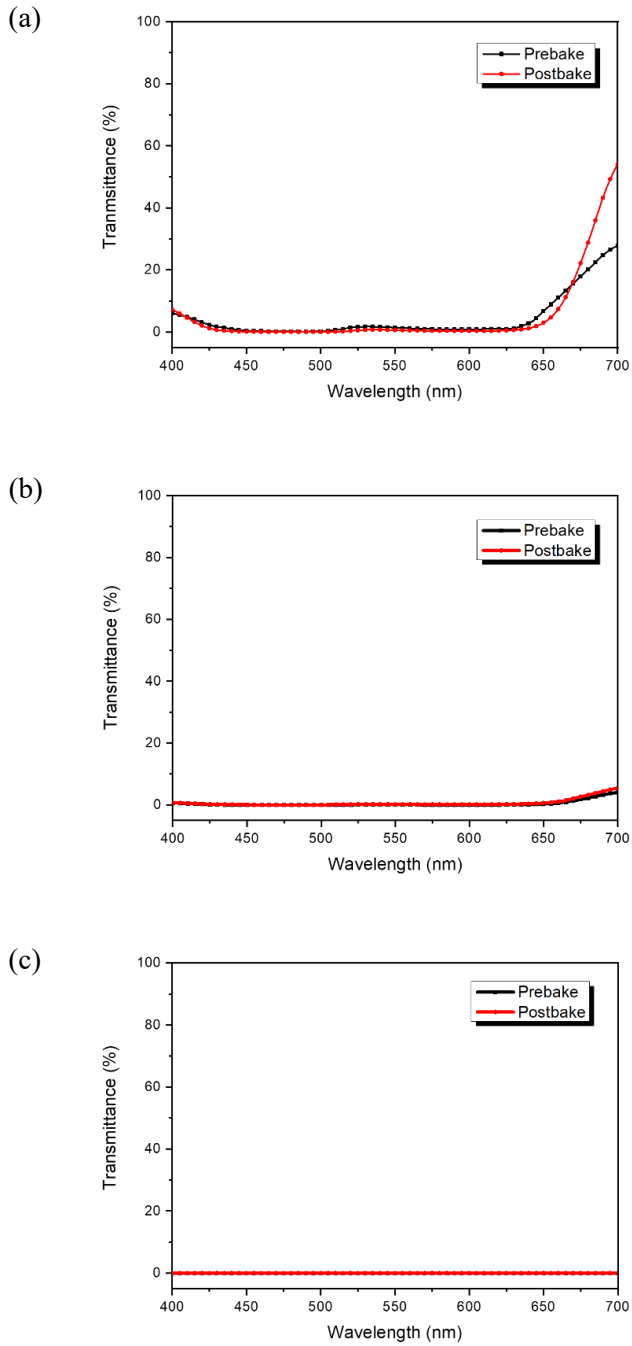

Figure 2.5. Transmittance spectra of film A (a), film B (b) and film C (c).

The opaqueness of the fabricated films was studied by OD measurements. OD is one of the most important optical characteristics of color filters [25] and can be expressed by the following equation.

$$OD = \frac{-\log(I / I_0)}{d} (\mu m^{-1})$$

A material with high OD is associated with high light shielding ability, which is advantageous for black matrix applications [26]. An OD suitable for black matrices should be more than 2.5 $\mu m^{-1,}$ and the OD of commercialized carbon black-type black matrices are 3.5–4.0 μm^{-1} [9]. The OD of the fabricated films at 550 nm is shown in Table 2.3. The OD of film A (0.12 μm^{-1}) and B (0.47 μm^{-1}) after postbaking were much lower than that of film C (3.63 μm^{-1}). This was attributed to the different colorant contents of the total black matrix resist, which contained 25 wt% of carbon black for film C, whereas film A and B contained less because of the low solubility of the dye. The OD value of film B will be calculated as 2.75 μm^{-1} if the content of colorants (dye and carbon black) is increased up to same amount of carbon black of film C. Hence, additional enhancement of the dye solubility may be needed to develop a hybrid-type black matrix with an sufficient value of OD for LCD color filters.

Table 2.3. Optical density of the black matrices at 550nm.

	Film A	Film B	Film C
After prebaking	0.12 μm^{-1}	0.47 μm^{-1}	3.63 μm^{-1}
After postbaking	0.12 μm^{-1}	0.47 μm^{-1}	3.63 μm^{-1}

High thermal stability of black matrix materials is essential because black matrices are manufactured through a baking process at high temperature. The thermal stability of the films was examined by color difference (ΔE_{ab}) after prebaking and postbaking. A film with a low ΔE_{ab} value is regarded as a thermally stable film, and the decomposition or aggregation of the resist constituents is the major cause of the increase in ΔE_{ab}. As shown in Table 2.4, the ΔE_{ab} value decreased in the order of films A, B, and C as the carbon black content of the film increased. The increment of ΔE_{ab} is due to the excellent heat resistance of carbon black. 4a also showed stable characteristics at a high temperature as revealed by the TGA experiment, however, three times of baking process was considered to be harsh for the dyes to withstand. In order to apply the film to the LCD black matrix, ΔE_{ab} of the film must be smaller than 3 [10], and films B and C, which contain carbon black satisfied this requirement. Current LCD manufacturing procedures are based on optimized dispersion of insoluble pigments and the other materials such as binder polymer and dispersant [6]. Therefore, the properties of the dye-type black matrix are expected to improve by developing a dye-favorable resist and manufacturing system.

Table 2.4. The ΔE_{ab} values of the black matrices corresponding to the CIE 1931 chromaticity diagram.

	Film A	Film B	Film C
ΔE_{ab}	5.40	2.14	0.28

2.3.3 Dielectric properties of the black matrices

In BOT structures, for improved performance of LCD color filters, the low-dielectric constant black matrix material is the main factor in avoiding TFT malfunctions[4]. The dielectric constant of the black matrix needs to be less than 7 for applications in commercial LCD panels [7]. Several points on the three types of fabricated film were selected randomly for measuring the dielectric constant at a variety of frequencies. The results are listed in Table 2.5.

Table 2.5. Dielectric constants of the black matrices.

Frequency (kHz)	Dielectric constant (ε_r, average)		
	Film A	Film B	Film C
0.1	4.01	5.49	26.39
1	4.00	5.01	25.47
10	3.92	4.90	20.65
100	3.86	4.73	18.72
200	3.84	4.68	18.22
500	3.81	4.62	17.57
700	3.80	4.59	17.34
1,000	3.79	4.67	17.10

The dielectric constant of film A was 3.79–4.01 at a varying frequency, while film C was more than 17.1. The high dielectric constant of film C was an inevitable consequence of the high electric conductivity of carbon black. On the other hand, the dielectric constant of film B (which contains both carbon black and the dye) was less than 7. This electric properties of the film B were especially noticeable at a working frequency range of 100–300 kHz where the dielectric constant was less than 4.73. The dramatic decrease in the dielectric constant was achieved by replacing up to 30% of carbon black into the dye in the hybrid-type black matrix.

2.4 Conclusions

PDI dyes with enhanced solubility in PGMEA were synthesized by substitution of donating groups at the bay positions of a thermally stable perylene core. The thermal stability and solubility of the dyes were sufficient for application in LCD manufacturing processes.

The low absorption of the dye at 400nm and 700nm led to light leakage in the visible region of the dye-type black matrices, and high electric conductivity of carbon black caused high dielectric constant of the carbon black-type black matrices. The hybrid-type black matrices showed ideal spectral, thermal, and dielectric properties. The insufficient absorptions of the dye at 400 and 700 nm were supplemented by the strong absorption of the carbon black. In addition, the thermal

stability of the hybrid-type black matrices was enhanced by the strong structural stability of the carbon black. Furthermore, the dielectric constants were significantly lower than that of carbon black-type black matrices owing to the dielectric-reducing effect of the dye.

2.5 References

[1] Sabnis, R.W.: Color filter technology for liquid crystal displays. Displays. 20, 119-129 (1999)

[2] Tsuda, K.: Colour filters for LCDs. Displays.14, 115-124 (1993)

[3] Chang, S.-C.: Improving pattern precision of chromium based black matrix by annealing. Appl. Surf. Sci. 254, 2244-2249 (2008)

[4] Jung, J., Park, Y., Jaung, J.-Y.,Park, J.: Synthesis of New Single Black Pigments Based on Azo and Anthraquinone Moieties for LCD Black Matrix. MCLC. 529, 88-94 (2010)

[5] Tan-Ching, Y.,Pei-Lum, T.: Fine line-width black matrix of a color filter by an advanced polishing method. JMiMi. 14, 867 (2004)

[6] Kudo, T., Nozaki, Y., Nanjo, Y., Yamaguchi, H., Nagao, K., Okazaki, H.,Pawlowski, G.: PIGMENTED PHOTORESIST FOR BLACK MATRIX. J.

Photopolym. Sci. Technol. 9, 121-130 (1996)

[7] Lee, W., Yuk, S.B., Choi, J., Jung, D.H., Choi, S.-H., Park, J.,Kim, J.P.: Synthesis and characterization of solubility enhanced metal-free phthalocyanines for liquid crystal display black matrix of low dielectric constant. Dyes and Pigments. 92, 942-948 (2012)

[8] Choi, J., Lee, W., Namgoong, J.W., Kim, T.-M.,Kim, J.P.: Synthesis and characterization of novel triazatetrabenzcorrole dyes for LCD color filter and black matrix. Dyes and Pigments. 99, 357-365 (2013)

[9] Lee, W., Choi, J., Kim, S.H., Park, J.,Kim, J.P.: Analysis and Characterization of Dye-Based Black Matrix Film of Low Dielectric Constant Containing Phthalocyanine and Perylene Dyes. J. Nanosci. Nanotechnol. 15, 295-302 (2015)

[10] Choi, J., Sakong, C., Choi, J.-H., Yoon, C.,Kim, J.P.: Synthesis and characterization of some perylene dyes for dye-based LCD color filters. Dyes and Pigments. 90, 82-88 (2011)

[11] Wang, W., Han, J.J., Wang, L.-Q., Li, L.-S., Shaw, W.J.,Li, A.D.Q.: Dynamic π–π Stacked Molecular Assemblies Emit from Green to Red Colors. Nano Letters. 3, 455-458 (2003)

[12] Alibert-Fouet, S., Dardel, S., Bock, H., Oukachmih, M., Archambeau, S., Seguy, I., Jolinat, P.,Destruel, P.: Electroluminescent Diodes from Complementary Discotic Benzoperylenes. Chemphyschem 4, 983-985 (2003)

[13] Seybold, G.,Wagenblast, G.: New perylene and violanthrone dyestuffs for

fluorescent collectors. Dyes and Pigments. 11, 303-317 (1989)

[14] Ma, Y.-S., Wang, C.-H., Zhao, Y.-J., Yu, Y., Han, C.-X., Qiu, X.-J.,Shi, Z.: Perylene Diimide Dyes Aggregates: Optical Properties and Packing Behavior in Solution and Solid State. Supramol. Chem. 19, 141-149 (2007)

[15] Würthner, F., Sautter, A.,Thalacker, C.: Substituted Diazadibenzoperylenes: New Functional Building Blocks for Supramolecular Chemistry. Angew. Chem. Int. Ed. 39, 1243-1245 (2000)

[16] Würthner, F., Thalacker, C., Diele, S.,Tschierske, C.: Fluorescent J-type Aggregates and Thermotropic Columnar Mesophases of Perylene Bisimide Dyes. Chem. Eur. J. 7, 2245-2253 (2001)

[17] Struijk, C.W., Sieval, A.B., Dakhorst, J.E.J., van Dijk, M., Kimkes, P., Koehorst, R.B.M., Donker, H., Schaafsma, T.J., Picken, S.J., van de Craats, A.M., Warman, J.M., Zuilhof, H.,Sudhölter, E.J.R.: Liquid Crystalline Perylene Diimides: Architecture and Charge Carrier Mobilities. J. Am. Chem. Soc. 122, 11057-11066 (2000)

[18] Langhals, H.,Blanke, P.: An approach to novel NIR dyes utilising α-effect donor groups. Dyes and Pigments. 59, 109-116 (2003)

[19] Würthner, F., Chen, Z., Hoeben, F.J.M., Osswald, P., You, C.-C., Jonkheijm, P., Herrikhuyzen, J.v., Schenning, A.P.H.J., van der Schoot, P.P.A.M., Meijer, E.W., Beckers, E.H.A., Meskers, S.C.J.,Janssen, R.A.J.: Supramolecular p−n-Heterojunctions by Co-Self-Organization of Oligo(p-phenylene Vinylene) and Perylene Bisimide Dyes. J. Am. Chem. Soc. 126, 10611-10618 (2004)

[20] Ohmi, T.: Manufacturing Process of Flat Display. JSME Int J., Ser. B 47, 422-428 (2004)

[21] Chunlong, Z., Nianchun, M.,Liyun, L.: An investigation of the thermal stability of some yellow and red azo pigments. Dyes and Pigments. 23, 13-23 (1993)

[22] Das, S., Basu, R., Minch, M.,Nandy, P.: Heat-induced structural changes in merocyanine dyes: X-ray and thermal studies. Dyes and Pigments. 29, 191-201 (1995)

[23] Giles, C.H., Duff, D.G.,Sinclair, R.S.: The Relationship between Dye Structure and Fastness Properties. Rev. Prog. Color. 12, 58-65 (1982)

[24] Su, W., Zhang, Y., Zhao, C., Li, X.,Jiang, J.: Self-Assembled Organic Nanostructures: Effect of Substituents on the Morphology. Chemphyschem 8, 1857-1862 (2007)

[25] Bui, T.S., Kim, J., Jung, E., Le, H.S., Nguyen, N.T.,Bae, J.-Y.: High optical density and low dielectric constant black matrix containing graphene oxide and carbon black on color filters. Displays. 34, 192-199 (2013)

[26] Kuo, K.-H., Chiu, W.-Y., Hsieh, K.-H.,Don, T.-M.: Novel UV-curable and alkali-soluble resins for light-shielding black matrix application. Eur. Polym. J. 45, 474-484 (2009)

Chapter 3

Application of perylene dyes for low dielectric hybrid-type black matrices

3.1 Introduction

Liquid crystal displays (LCD) are composed of liquid crystals (LCs), thin-film transistors (TFTs), and color filters [1]. Among these elements of the LCD modules, color filters play an important role in converting white backlight to red, green and blue (RGB) colors. The black matrix located between the RGB color pixels prevents the unintended mixture of colors and improves the contrast ratio of the color filter. Additionally, malfunction of the TFT channels arising from an external light can be avoided by the light shielding ability of the black matrix [2, 3]. In order to perform these roles, materials comprising the black matrix should have high optical density (OD) and sufficient stability to endure the severe fabrication process of LCDs.

In the early stages of the development of LCDs, chromium was the most commonly used material for the black matrix [1]. However, black matrices based on organic compounds have recently been developed in order to avoid the disadvantages of the chromium-based black matrices such as high cost and environmental pollution.

Furthermore, the fabrication process of the black matrix is much easier with organic compounds than with chromium [4]. Organic materials with refractive indices similar to indium-tin-oxide (ITO) glass can also reduce the reflectance of the display from external incident lights [5]. Carbon black is the most widely used organic material for this application because of its high OD and thermal stability. However, in accordance with the trend of developing thinner displays, electrical TFT malfunctions can occur in the presence of highly conductive carbon black [6, 7]. In the color filter-on-TFT array (COA) structure, which has received more attention than the conventional structure, the color filter is directly layered on the TFT [8]. Therefore, the dielectric constant of the black matrix material is one of the key issues in the development of COA structures and low dielectric constant organic materials are required to replace carbon black. In this respect, organic dyes which show lower dielectric constants than carbon black are excellent alternatives for black matrices.

In our previous research, dye-type black matrices were fabricated using dyes of different chromophores (perylene and phthalocyanine) [8]. However, the dye-only type black matrices showed limitations such as insufficient absorption of visible light and reduced surface uniformity arising from the different aggregation behaviors of each dye. Afterward, a hybrid-type black matrix using dyes and carbon black together was tested to overcome the shortcomings of the dye-only type matrix [9]. However, leakage of light still occurred. Although this light leakage problem could be easily solved by increasing the amount of carbon black, there would be an undesirable increase in the dielectric constant.

In this study, hybrid-type black matrices were fabricated with various blend ratios of dyes and carbon black to fully absorb the visible light and maintain low dielectric

constants. The dyes were designed and synthesized based on the perylene moiety. Owing to their excellent chemical, thermal and photostability [10-12], perylene derivatives are suitable organic materials for black matrices. Additionally, various perylene dyes with different colors can be easily obtained by changing the donating power and conjugation length of the substituents attached at the bay and periphery positions [13-16]. In this respect, perylene diimide (PDI) and perylenetetracarboxylic bisbenzimidazole (PTCBI) dyes were designed to have different absorption ranges in order to prevent light leaking. The PTCBI dye was newly synthesized for visible light absorption around 600–700 nm, which cannot be absorbed by the PDI dye. Furthermore, the dielectric constant of the black matrix fabricated using these dyes could be improved by using a lower content of carbon black as compared to the hybrid-type film in previous research [9]. The issue of a non-uniform surface of the black matrix film was expected to be solved by using the dyes derived from the same perylene moiety. The optical and thermal properties and the solubility of the dyes were determined to confirm their applicability on the black matrix. Dye-type black matrices were also fabricated by using the two perylene-based dyes for comparison with hybrid-type black matrices. The optical, thermal, and dielectric properties of the fabricated black matrices were investigated. The surface morphologies of the black matrices were also probed by atomic force microscopy (AFM) to identify the effect of the dyes with the same moiety on surface roughness.

3.2 Experimental section

3.2.1 Materials and instrumentation

Perylene-3,4,9,10-tetracarboxylic dianhydride, 2,6-diisopropylaniline, m-cresol, iodine, sulfuric acid, bromine, acetic acid, propionic acid, and potassium carbonate anhydrous purchased from Sigma-Aldrich, and 1,2-diaminobenzene, 4-hydroxy-3-tert-butylanisole, carbazole, copper iodide and 18-crown-6 purchased from TCI were used as received. All the other reagents and solvents were of reagent-grade and obtained from commercial suppliers. Transparent glass substrates were provided by Paul Marienfeld GmbH & Co. KG, and acrylic binder and black matrix resist were supplied by KOLON industry Inc. and Dongwoo Fine-Chem.

^{1}H and ^{13}C NMR spectra were recorded on a Bruker Avance 500 spectrometer (National Center for Inter-university Research Facilities at Seoul National University) at 500 MHz using chloroform-d, acetic acid-d and TMS, as the solvents and internal standard, respectively. Matrix Assisted Laser Desorption/Ionization Time of Flight (MALDI-TOF) mass spectra were collected on a Voyager-DE STR Biospectrometry Workstation (National Center for Inter-university Research Facilities at Seoul National University) with α-cyano-4-hydroxycinnamic acid (CHCA) as the matrix. Absorption and transmittance spectra were measured using a Perkin-Elmer Lambda 25 spectrophotometer. Thermogravimetric analysis (TGA) was conducted in a nitrogen atmosphere at a heating rate of 10 ℃ min^{-1} using a TA instruments

Thermogravimetric Analyzer 2050. Chromatic characteristics of the black matrices were analyzed on a Scinco color spectrometer. Dielectric constants were measured using Edward E306 thermal evaporator and an HP 4294A precision impedance analyzer. The thickness of the black matrices was measured using a KLA-TENCOR Nanospec AFT/200 alpha step. The roughness of the black matrices was measured using Nanostation II.

3.2.2 Synthesis

The dyes **2**, **3a** and **3b** are already known structures and were synthesized according to the previously reported procedures [9, 13].

3.2.2.1 N,N'-bis(2,6-diisopropylphenyl)-1,7-dibromoperylene-3,4,9,10-tetracarboxylicdiimide (3a)

Perylene-3,4,9,10-tetracarboxylic dianhydride (10 g, 25.44 mmol), iodine (0.24 g, 0.95 mmol), and sulfuric acid (98%, 140 ml) were mixed and stirred for 2 h at room temperature. The reaction temperature was set at 80 ℃, and bromine (2.24 ml, 43.75 mmol) was added dropwise over 2 h. The mixture was reacted further at 80 ℃ for 16 h, cooled to room temperature, and the excess bromine gas was displaced by nitrogen gas. The precipitate obtained after adding ice-water to the mixture was

collected by suction filtration. The precipitate was washed with water several times until the aqueous layer became neutral to yield dibromo dianhydride as a crude product. The crude product was dried at 100 ℃ under reduced pressure and used for next step without further purification.

The crude 1,7-dibromoperylene-3,4,9,10-tetracarboxylic dianhydride (6 g, 10.88 mmol), 2,6-diisopropylaniline (6.60 ml, 35.03 mmol) and acetic acid (3.45 ml) were mixed and heated at 120 ℃ in N-Methyl-2-pyrrolidine (NMP) (75 ml) under the nitrogen atmosphere for 96 h. The precipitate obtained after water to the mixture was collected by suction filtration. The crude product was washed with water, dried and purified by column chromatography on silica gel using CH_2Cl_2 as the eluent. The band containing tribromonated diimide could be separated firstly. Then, the second band containing a mixture of isomeric diimide was collected. The mixture was washed with EtOH and toluene and heated at 80 ℃ for 12 h in toluene (40 ml). The pure diimide, a red compound of **3a**, was recrystallized from the hot toluene solution (9.50 g, 43% yield). ^{1}H NMR ($CDCl_3$, 500 MHz): 9.57 (d, 2H), 9.02 (d, 2H), 8.82 (d, 2H), 7.53 (t, 2H), 7.37 (d, 4H), 2.77 (septet, 4H), 1.20 (d, 24H); MALDI-TOF MS: m/z 869.8 (100%, $[M + 2H]^+$).

3.2.2.2 N,N'-bis(2,6-diisopropylphenyl)-1,7-di(9H-carbazole)-perylene-3,4,9,10-tetracarboxylicdiimide (3b)

A mixture of **3a** (0.60 g, 0.69 mmol), carbazole (0.35 g, 2.09 mmol), 18-crown-6

(0.15 g, 0.55 mmol), copper iodide (46 mg, 0.24 mmol) and potassium carbonate (0.96 g, 6.95 mmol) in *N*-methylpyrrolidone (45 ml) was stirred at 110 °C for 24 h. The reaction mixture was cooled to room temperature and poured into 5% HCl (1 L). The precipitate was filtered, repeatedly washed with water, and dried in a vacuum at 80 °C. The crude product was purified by column chromatography on silica gel using CH_2Cl_2 as the eluent to obtain **4b** as a black solid (0.35 g, 49% yield). ^{1}H NMR (500 MHz, $CDCl_3$): 8.90 (d, 2H), 8.28 (m, 4H), 8.08 (d, 2H), 7.61 (d, 2H), 7.47 (d, 2H), 7.34 (m, 4H), 7.32 (m, 4H), 2.71 (septet, 4H), 1.15 (d, 24H); MALDI-TOF MS: m/z 1042.2 (100%, $[M + 2H]^+$).

3.2.2.3 1,7-dibromoperylene-3,4,9,10-tetracarboxylic bisbenzimidazole (4a)

A mixture of **2** (1.00 g, 1.82 mmol), 1,2-diaminobenzene (1.18 g, 10.91 mmol) and propanoic acid (100 ml) was stirred for 24 h at 150 °C. The reaction mixture was cooled to room temperature and poured into water. The precipitate was filtered and dried in a vacuum at 80 °C. The crude products were purified by silica gel column chromatography with dichloromethane (CH_2Cl_2) as eluent to obtain **4a** as a purple-black solid compound (0.85 g, 67% yield) [18]. ^{1}H NMR (CF_3COOD, 500 MHz): δ 9.24 (d, 2H), 9.11 (s, 2H), 9.07 (d, 2H), 8.85 (d, 2H), 7.91 (d, 2H), 7.67 (m, 4H); ^{13}C NMR (CF_3COOD, 125 MHz): δ 157.98, 145.12, 143.71, 141.58, 139.18, 138.76, 137.10, 131.85, 131.27, 126.78, 124.91, 122.88, 122.57, 121.94, 121.57, 117.38, 114.69; MALDI-TOF MS: m/z 695.2 (100%, $[M + H]^+$); Elemental analysis: Calcd

for $C_{36}H_{14}Br_2N_4O_2$: C, 62.27; H, 2.03; N, 8.07; O, 4.61. Found: C, 62.28; H, 2.02; N, 8.07; O, 4.55.

3.2.2.4 1,7-di-2-(tert-butyl)-4-methoxyphenyl-perylene-3,4,9,10-tetracarboxylic bisbenzimidazole (4b)

4a (1.00 g, 1.44 mmol), 4-hydroxy-3-*tert*-butylanisole (1.04 g, 5.76 mmol) and potassium carbonate (0.40 g, 2.88 mmol) in N-Methyl-2-pyrrolidone (NMP) (120 ml) was stirred for 24 h at 120 ℃. The reaction mixture was cooled to room temperature and poured into 1M HCl (500 ml). The precipitate was filtered, repeatedly washed with water, and dried in vacuum at 80 ℃. The crude products were purified by silica gel column chromatography with CH_2Cl_2 as eluent to obtain **4b** as a blue-purple solid compound (0.63 g, 49% yield). ^{1}H NMR ($CDCl_3$, 500 MHz): δ 9.31 (d, 2H), 9.17 (s, 2H), 8.99 (d, 2H), 8.74 (d, 2H), 7.85 (d, 2H), 7.70 (m, 4H), 7.08 (m, 6H), 3.45 (s, 6H), 1.45 (d, 18H); ^{13}C NMR ($CDCl_3$, 125 MHz): δ 158.89, 158.65, 157.06, 147.77, 143.96, 143.25, 131.52, 131.13, 130.82, 129.11, 128.79, 128.05, 127.17, 126.87, 126.26, 124.05, 122.97, 122.46, 120.50, 120.00, 115.44, 115.12, 112.10, 55.93, 30.76, 29.88; MALDI-TOF MS: m/z 893.1 (100%, $[M + H]^+$); Elemental analysis : Calcd for $C_{58}H_{44}N_4O_6$: C, 78.01; H, 4.97; N, 6.27; O, 10.75. Found: C, 76.69; H, 5.78; N, 5.70; O, 11.83.

3.2.3 Preparation of black matrices

Three kinds of black matrices were fabricated and depicted in Fig. 3.1. The solutions for hybrid-type black matrices (A, B) were composed of the dyes (0.10 g), propylene glycol methyl ether acetate (PGMEA) (1.68 g, 2.02 g), acrylic binder (6.67 g, 7.20 g) and carbon black resist (1.56 g, 0.67 g). The solutions for a dye-type black matrix (C) were composed of the dyes (0.10 g), PGMEA (1.90 g) and acrylic binder (8.00 g). The prepared solutions were coated on a transparent glass substrate using a MIDAS System SPIN-1200D spin coater. The coating speed was initially 250 rpm for 20 sec, which was then increased to 400 rpm and kept constant for 10 sec. The wet coated black matrices were then dried at 40 ℃ for 20 min, prebaked 100 ℃ for 100 sec, and post baked at 230 ℃ for three times every 30 min. After each step, the coordinate values of the black matrices were measured.

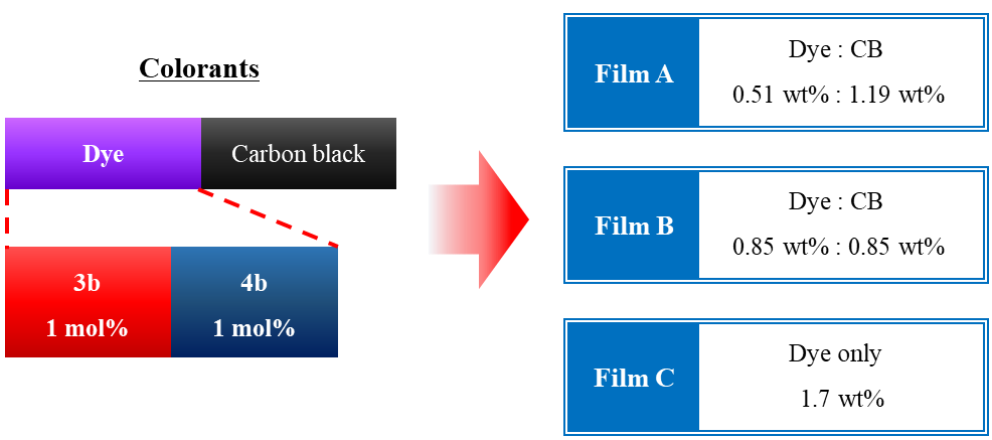

Figure 3.1. Blend ratio of the fabricated black matrices.

3.2.4 Measurement of spectral and optical properties

The absorption spectra of the synthesized dyes and the transmittance spectra of the black matrices were measured using a UV-visible spectrophotometer and fluorescence spectrometer. The chromatic values of the black matrices were recorded on a color spectrophotometer.

3.2.5 Investigation of solubility

The synthesized dyes were added to the PGMEA and CH_2Cl_2 at various concentrations. The solutions were sonicated for 5 min using ultrasonic cleaner NXP-4020. The solutions were left to stand for 48 h at room temperature and checked for precipitation to determine the solubility of the dyes.

3.2.6 Measurement of thermal stability

The thermal stability of the synthesized dyes was evaluated by TGA. The prepared dyes were heated to 230 ℃ and held at that temperature for 30 min for simulation the thermal processing condition of color filter manufacturing process. The dyes were finally heated to 400 ℃ to determine their degradation temperature. The

heating was carried out at the rate of 10 ℃ per min under nitrogen atmosphere.

3.2.7 Geometry optimization of the synthesized dyes

The geometry and electric structure of the studied dyes are optimized by the density functional theory (DFT) method at the B3LYP/6-31G (d, p) performed on Gaussian 09 program.

3.2.8 Atomic force microscopy

The surface morphologies of the black matrices were observed at room temperature using Nanostation II in non-contact mode.

3.3 Results and Discussion

3.3.1 Properties of dyes

Perylene-3,4,9,10-tetracarboxylic dianhydride shows strong intermolecular π-π interactions and a high resonance stabilization energy because of its planar molecular structure [19-21]. For this reason, organic materials based on the perylene moiety tend to be thermally stable and black matrices fabricated with such dyes can withstand the severe thermal conditions of the LCD manufacturing process without undergoing any color change [3, 8, 9]. However, the solubility of the basic perylene structure in industrial solvents such as PGMEA is not satisfactory for the black matrix manufacturing process. Therefore, additional substituents were introduced into the periphery and bay positions of the perylene core in order to enhance the solubility of the dyes [22], as shown in Scheme 3.1. The bulky isopropyl groups of 3b increased the steric repulsion toward the perylene core and induced the rotation of the C–N bond at the peripheral position. These deviated substituents from the plane of the molecule interrupted the face-to-face stacking of the perylene core of 3b [21, 23], thereby increasing the solubility of the dye. Carbazoles and 2-*tert*-butyl-methoxy phenols, attached at the bay positions of 3b and 4b, also contributed to the enhancement of their solubility by twisting the main body [9]. The conjugation length of 4b was increased in the direction of the longer axis (peripheral position) by the condensation reaction between 2 and benzimidazole. The conjugation-expanded

PTCBI structure showed an increased absorption above 650 nm in comparison to dye 3b [21].

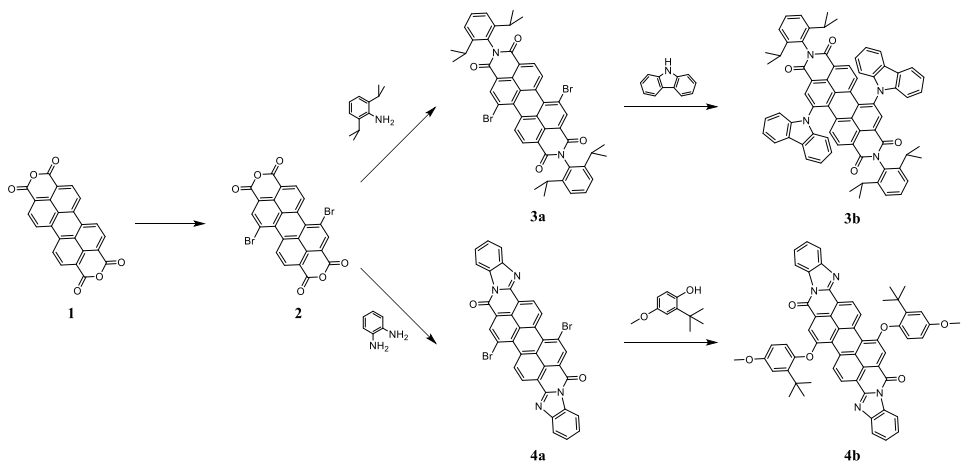

Scheme 3.1. Synthesis of perylene dyes.

3.3.1.1 Spectral properties of the synthesized dyes

The absorption spectra of dyes 3b and 4b are shown in Fig. 3.2 and their absorption maxima and molar extinction coefficients are presented in Table 3.1. The absorption spectrum of 3b shows a dual band in the visible region, one of which is denoted as the α-band (broad band) and the other one is denoted as the β-band (sharp band). The β-band, originating from the π-π* transition of the perylene core, is within the usual absorption range of the unsubstituted perylene dye. The α-band is the result of electron density reallocation from the HOMO of the donating group at the bay

position to the LUMO of the perylene core by photoinduced electronic transition [17]. Since the molar extinction coefficient of 3b (α-band) is low, it is not sufficient to be applied alone in a black matrix. Hence, 4b was synthesized to absorb the longer wavelength region by core extension along the long-axis direction [21]. The maximum absorption wavelengths of 4b in PGMEA and CH_2Cl_2 are 604, and 611 nm and the absorption maxima are 43,300, and 52,800 M^{-1} cm^{-1}, respectively. The dye 4b is also unsatisfactory for use in a single dye-type black matrix because of its low absorption in the 400–450 nm region. However, since the two dyes absorb in visible regions that are complementary to each other, the color of this binary dye mixture is close to being completely black. Therefore, the black matrices were fabricated by either using a mixed solution of these dyes and carbon black or simply the dyes alone in order to investigate the spectral features of the dyes in the film state.

Table 3.1. Absorption maxima and molar extinction coefficients of the dyes in PGMEA and CH_2Cl_2.

	Dye	λ_{max} (nm)	ε_{max} (10^4 l mol^{-1} cm^{-1})
PGMEA	3b	482	2.32
	4b	604	3.77
CH_2Cl_2	3b	488	2.54
	4b	611	5.28

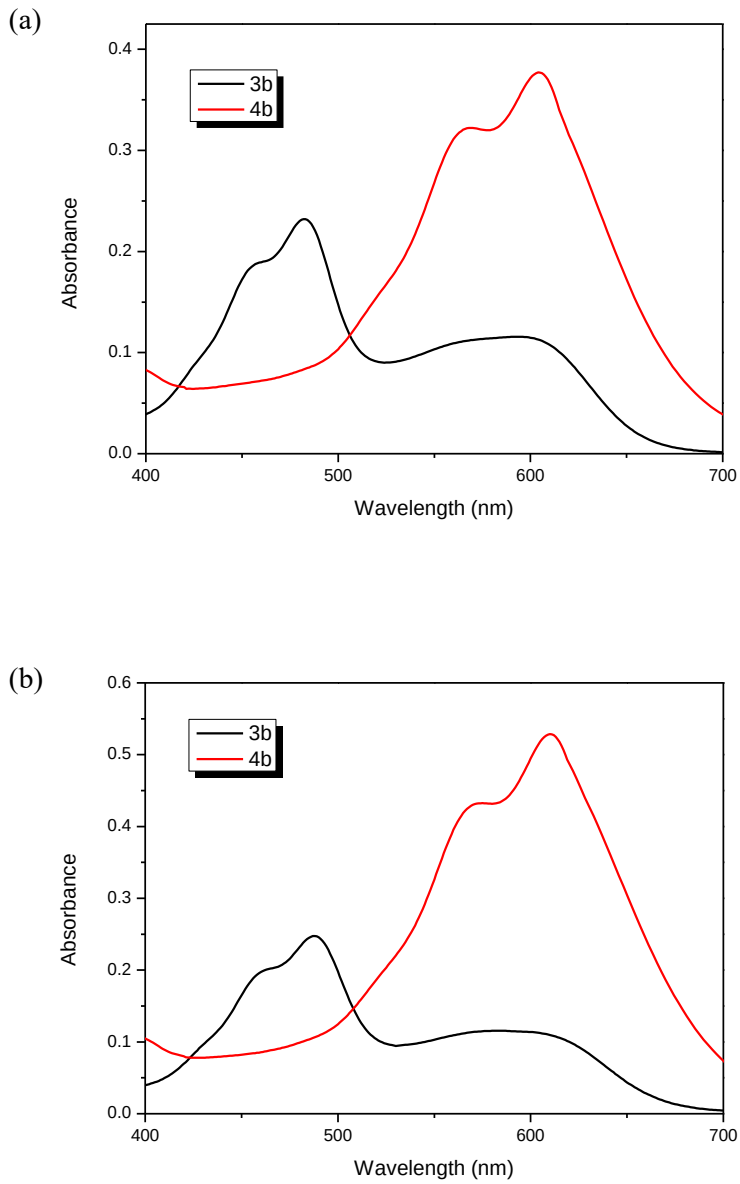

Figure 3.2. Absorption spectra of the dyes in (a) PGMEA and (b) CH_2Cl_2.

3.3.1.2 Thermal stability of the dyes

The fabrication of black matrices requires thermally stable dyes because of the severe manufacturing conditions for LCDs, in which the temperature typically exceeds 200 °C [15, 24]. The dyes were heated to 230 °C and held at that temperature for 1 h to simulate the analogous color filter photolithography process conditions. The applicability of the dyes in a black matrix was examined by analyzing the weight loss in this temperature range.

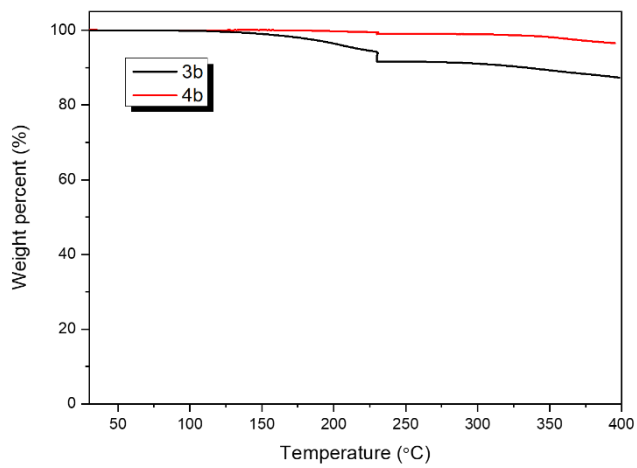

Figure 3.3. TGA analysis of the dyes.

Perylene, which contains several benzene rings, has a planar structure. This structural feature strengthens the intermolecular π-π interactions even after various synthetic transformations whereby different substituents are attached to the perylene core [17]. The synthesized dyes are therefore expected to endure high temperatures. As shown in Fig. 3.3, the weight losses of dyes 3b and 4b during their isothermal

treatment were 2.6 and 0.4 wt%, respectively, which indicated that the dyes were thermally stable for application in black matrices. The dye 4b was more stable than 3b because of its molecular planarity. This planarity was a result of the extended conjugation structure that induced strong intermolecular π-π interactions between the PTCBI backbones [21, 25]. The molecular planarity was verified by computational calculations, as described in the following section; 4b had a smaller distortion angle than 3b.

3.3.1.3 Geometrical optimization and solubility of dyes

Since molecular planarity and intermolecular distance are related to the photophysical properties and solubility of the dyes, DFT computational calculations were conducted to predict the optimized dye structures. The distortion angles and molecular sizes of the dyes are shown in Fig. 3.4. Dye 3b, as determined in previous research [9], showed a distortion angle of 18.40° and a molecular height of 9.34 Å. This twisted structure is a result of the bulky substituents attached at the periphery and bay positions and affects the physical, chemical, and electronic properties of the dyes [26]. As the distortion angle and molecular size increase, the π-π interactions between the perylene cores are decreased and the dye aggregation tendency is hindered [25]. Since the amount of dye required to make a black matrix with a high OD would be quite large, bulky substituents that can enhance the solubility of the dyes are essential. Dye 2 was found to be insoluble in organic solvents PGMEA and

CH_2Cl_2, as listed in Table 3.2. However, the solubility of 3a was improved significantly by attaching the diisopropyl aniline substituent to its periphery. Furthermore, a higher solubility was achieved with 3b.

The structural design of 4b was focused on the absorption of a long wavelength in the visible light region by expanding its conjugation structure. By DFT calculation, the distortion angle and molecule height of the dye were determined to be 13.04° and 7.87 Å, respectively. These parameters indicate an efficient crystal packing of 4b and provide an explanation for its reduced solubility [27] compared to that of 3b in organic solvents.

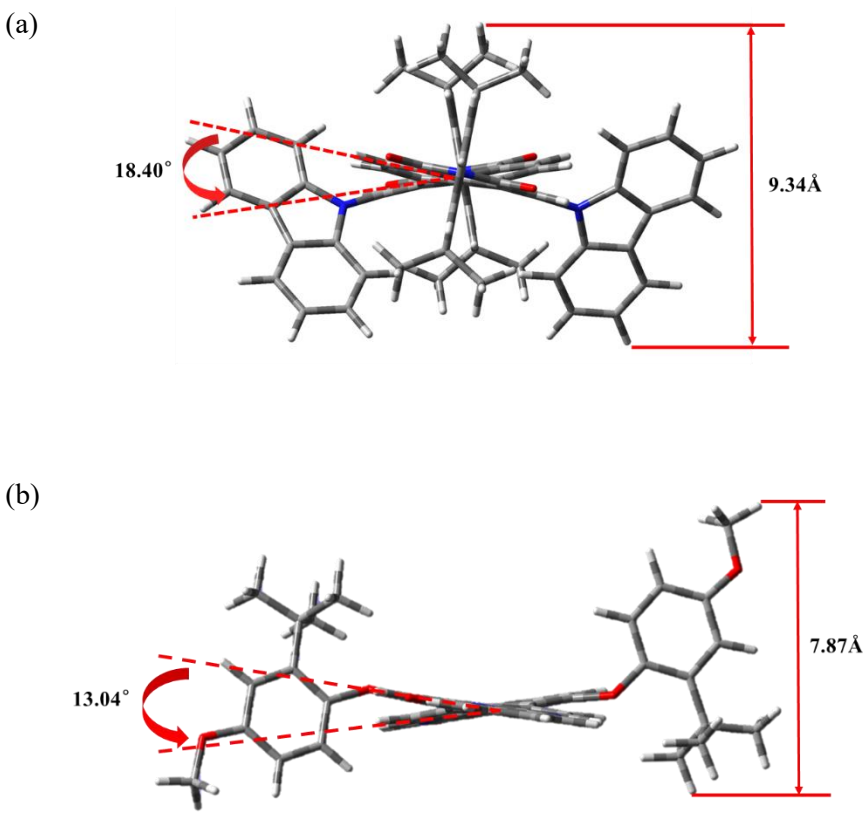

Figure 3.4. Optimized structure of (a) 3b and (b) 4b.

Table 3.2. Solubility of the dyes in PGMEA and CH_2Cl_2.

	2 (wt%)	3a (wt%)	3b (wt%)	4a (wt%)	4b (wt%)
PGMEA	Insoluble	2.3	4.6	Insoluble	3.2
CH_2Cl_2	Insoluble	5.4	6.1	1.4	4.6

3.3.2 Characterization of dye-type and hybrid-type black matrices

As shown in Fig. 3.1, three films were fabricated with different content ratios of the synthesized dyes and carbon black. However, the molar ratio of the two dyes used in the films was identical (3b:4b = 1 mol:1 mol).

Film A, with a blend ratio commonly employed in industry, contained more carbon black than the dyes. On the other hand, the dye content was increased in film B for a lower dielectric constant, which is required for COA-type displays. The optical and electrical properties of the fabricated hybrid-type films (films A and B) were compared with the dye-type film (film C).

3.3.2.1 Spectral and optical properties of the black matrices

The spectral and optical properties of the fabricated films were measured by using a UV-Vis spectrometer, a fluorescence spectrometer, and an OD meter. Fig. 3.5

shows the transmittances of the films after prebaking and postbaking processes. These films blocked the entire visible light effectively, except for the dye-type films (film C) around at 700 nm. The transmittances of the films at 700 nm differed depending on the content of carbon black. Film C did not completely absorb light at 700 nm after postbaking, and its transmittance was 6.94%. This transmittance value implied that the absorptions of the dyes were still insufficient, and an additional colorant such as carbon black was required to absorb light at ~700 nm. The transmittances of film A after postbaking was 0.44% and that of film B was 0.79%. Furthermore, films A and B showed excellent light-shielding properties. Thus, it could be concluded that the carbon black included absorbed visible light strongly and the hybrid-type films had an advantage in light-shielding ability when compared to the dye-type films.

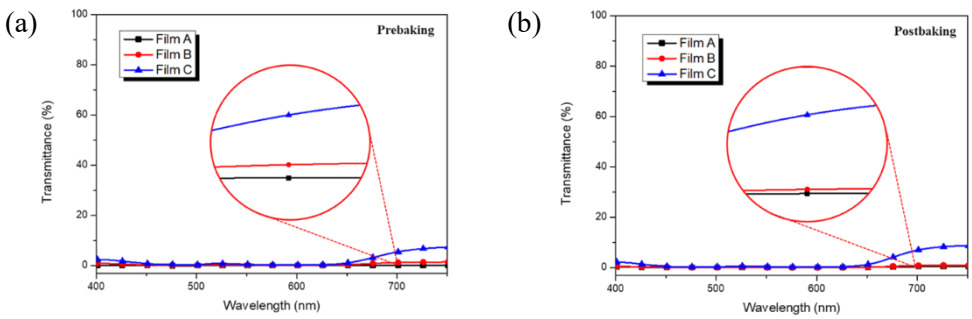

Figure 3.5. Transmittance spectra of the films after (a) prebaking and (b) postbaking.

Perylene is a strong fluorescent dye [28, 29] and its fluorescence in the visible region may have an unfavorable effect on the optical properties of the black matrix.

Therefore, the fluorescence levels of the films were measured in order to reveal the influence of the dyes and these are plotted in Fig. 3.6. Films 3b, 4b, and CB (carbon black), which contained one kind of colorant, were fabricated as well for the sake of comparison with films A–C. While film 3b showed fluorescence beyond 700 nm with an additional shoulder in the visible region, film 4b showed emissions only in the IR region. The fluorescence in the IR region does not significantly affect the light shielding performance of the LCD black matrix. Consequently, 4b can be considered to have sufficient visible light blocking power. All the films, with the exception of films 4b and CB, showed fluorescence below 700 nm and the film 3b showed the highest fluorescence. Therefore, the fluorescence of films A–C and film 3b below 700 nm was considered to originate from that of dye 3b. The fluorescence intensity of the films decreased as their carbon black content was increased (film C < film B < film A) since carbon black can absorb the re-emitted light from 3b. This spectral property of the films is reflected in their transmittance; consequently, the least fluorescent film A showed the best light-shielding ability among the films.

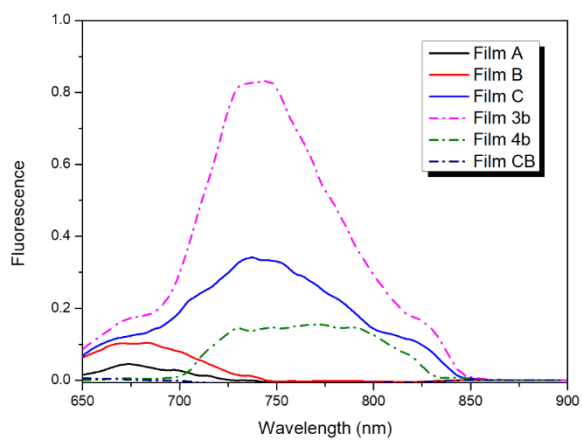

Figure 3.6. Fluorescence spectra of films A-C (solid line), 3b, 4b and carbon black (dashed line) after postbaking.

The OD of these films were also measured. OD is one of the major optical properties of the black matrix and represents the absorption ability of a material divided by its thickness. It can be expressed by the following equation:

$$\mathrm{OD} = \frac{-\log(I/I_0)}{d} \quad (\mu m^{-1})$$

The ODs of the films at 550 nm were evaluated to be 0.24–0.49 μm^{-1}, as listed in Table 3.3. As a result of the strong light absorption ability of carbon black, film A showed the highest OD among all the films. Therefore, owing to limitations in visible light coverage and absorption, using a hybrid-type black matrix would be a better option in the industry.

Table 3.3. Optical density of the black matrices after postbaking at 550nm.

	Film A	Film B	Film C
OD	0.49	0.30	0.24

3.3.2.2 Thermal stability of the black matrices

The black matrix is coated on the substrate prior to the coating of the R, G, and B color pixels [4]. A black matrix material with high thermal stability is thus crucial to endure the baking process at each coating step. Therefore, an evaluation of the film stability and that of the dye itself is necessary. As shown in Fig. 3.5, the difference

in transmittance between the prebaked and postbaked hybrid-type films is less than 1.23% at 700 nm. The small difference in the transmittance as a result of the baking process indicates that the fabricated films are thermally stable. The thermal stability of the films is measured by its color difference (ΔE_{ab}) during the baking process, and these values are listed in Table 3.4.

Table 3.4. The ΔE_{ab} values of the black matrices.

	Pre – Post 1st	Post 1st – Post 2nd	Post 2nd – Post 3rd
Film A	4.26	2.44	0.78
Film B	4.10	2.54	1.56
Film C	6.99	4.31	1.97

As verified before, the hybrid-type films showed lower differences in transmittance than the dye-type films because of the thermal stability of carbon black. In this regard, the color differences of the films during the three postbaking steps are similar (film A < film B < film C) to those observed from the transmittances. Since the ΔE_{ab} values of the films were within 3.00 as the postbaking progressed, which is an industrial standard, it was concluded that the fabricated films showed sufficient stability for their application to the LCD manufacturing process.

3.3.2.3 Dielectric properties of the black matrices

It is important to analyze the electric conductivity of the black matrix because an electrical malfunction of the TFT can occur due to a film with a high dielectric constant. Since the distance between the TFT and the color filter is getting closer in the COA structure [4], it is essential to develop a black matrix material with a lower dielectric constant. The dielectric constants of the fabricated films were measured at a frequency of 10. The dye-type film showed low dielectric constants (3.72) compared to those of the carbon black-type black matrix (17.1) [3]. This is because the electrons in the organic dyes cannot migrate effectively in the high-frequency electric field [30]. The dielectric constants of films A and B, which contain highly conductive carbon black, were higher than that of film C. However, the measured values of the films (6.25 for film A and 4.05 for film B) were still much lower than that of the carbon black-type black matrix. Therefore, these films can be applied to conventional LCDs, which demand dielectric constants of less than 7. In the COA structure, however, films B and C will be more suitable than film A because of its much lower dielectric constant.

Table 3.5. Dielectric constant of the black matrices.

	Film A	Film B	Film C
Dielectric constant	6.25	4.05	3.72

3.3.2.4 AFM images of the black matrices

In a previous study on the dye-type black matrices using dyes of different moieties, the dye aggregates were found to be perpendicular to the surface of the film [8]. Owing to this self-aggregation tendency of the dyes, the surface of the film was not smooth enough for the color filter. Therefore, in this study, two dyes having the same moiety were synthesized for better miscibility and a smoother surface of the black matrix.

Both 3b and 4b were synthesized with the same perylene moiety and were thus expected to show similar aggregation behaviors on the fabricated film with a smooth surface [31]. Fig. 3.7 shows the surface images of the films scanned by AFM.

A flawless and smooth surface is observed in the dye-type films, suggesting that the dyes synthesized based on the same moiety were miscible with each other and no surface aggregation behavior was detected. On the other hand, aggregated particles and an uneven surface were found on film A. For a more accurate analysis, the Rq of each film surface was calculated and listed in Table 3.6. Films with Rq values of less than 4 are considered to have enough smoothness for a black matrix. The Rq of films B and C are 1.80 and 0.38, respectively, whereas that of film A is 5.90. The high Rq value of film A is a result of the high carbon black content. The Rq value was minimized and dye aggregation could be prevented by using the dyes with the same moiety in films B and C. However, with an increase in the ratio of carbon black which is immiscible with the dyes, the surfaces became rougher. As

mentioned previously, carbon black can block visible light effectively but adversely affects the smoothness of the hybrid-type film surfaces. Hence, an appropriate blend ratio of the black matrix resist is needed to maintain low film roughness. From this perspective, film B with a mixture of dyes and carbon black at a 1:1 weight ratio is a better option.

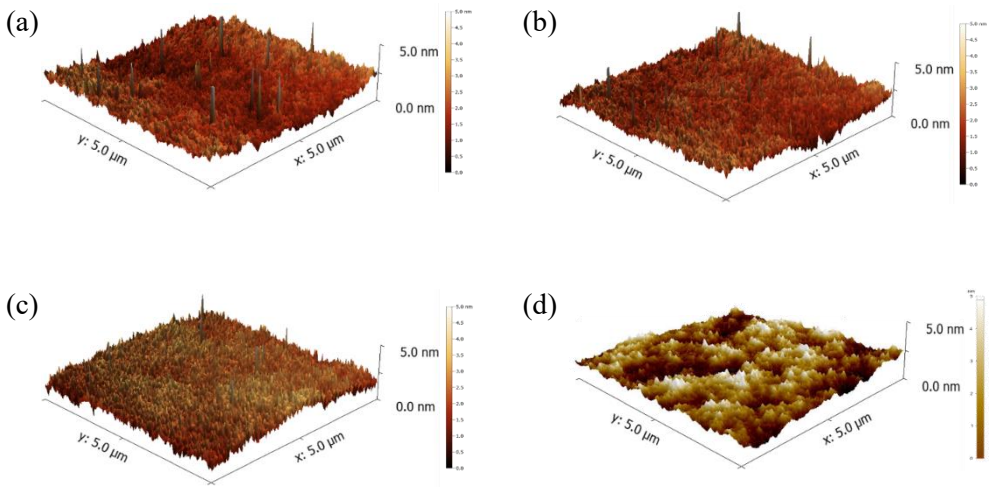

Figure 3.7. AFM images of the black matrices: (a) Film A; (b) Film B; (c) Film C; (d) Film carbon black.

Table 3.6. Surface roughness (Rq) of the black matrices after postbaking.

	Film A	Film B	Film C
Rq	5.90	1.80	0.38

3.4 Conclusions

Dyes having the same moiety were synthesized in order to prevent their self-aggregation on the surface of the black matrix. Incorporation of various aryl substituents into the bay and periphery positions of perylene core facilitated an efficient tuning of the absorption range of the dyes to cover the entire visible light region. Computational analysis was performed to predict the twisting angles, and the height of the dye molecules, and the results were consistent with the experimentally determined solubility and thermal stability. The spectral and thermal stabilities of the dyes were sufficient for application in the black matrix manufacturing process.

The films fabricated using these dyes showed excellent light shielding ability in the visible region, except film C. The dye-only type film showed a light leaking problem at 700 nm because of the fluorescence of 3b. The hybrid-type films showed higher thermal stability and had excellent optical and electrical properties. Furthermore, the film smoothness was significantly improved compared to that found in previous research by applying these dyes having the same perylene moiety.

3.5 References

[1] K. Tsuda, Displays, 14 (1993) 115-124.

[2] J. Jung, Y. Park, J.-Y. Jaung, J. Park, Molecular Crystals and Liquid Crystals, 529 (2010) 88-94.

[3] W. Lee, S.B. Yuk, J. Choi, D.H. Jung, S.-H. Choi, J. Park, J.P. Kim, Dyes and Pigments, 92 (2012) 942-948.

[4] R.W. Sabnis, Displays, 20 (1999) 119-129.

[5] Y. Xing, W.M. Frank, J.P. David, F.S. Martin, K. Jong Kyu, C. Jaehee, E.F. Schubert, Japanese Journal of Applied Physics, 48 (2009) 120203.

[6] T.S. Bui, J. Kim, E. Jung, H.S. Le, N.T. Nguyen, J.-Y. Bae, Displays, 34 (2013) 192-199.

[7] C.-S. Lee, H.-J. Yoon, S.-I. Yoon, S.-H. Yoon, D.-W. Kim, M.-S. Jung, T. Won, Molecular Crystals and Liquid Crystals, 436 (2005) 29/[983]-938/[992].

[8] W. Lee, J. Choi, S.H. Kim, J. Park, J.P. Kim, Journal of Nanoscience and Nanotechnology, 15 (2015) 295-302.

[9] S.B. Yuk, W. Lee, J.W. Namgoong, J. Choi, J.B. Chang, S.H. Kim, J.Y. Kim, J.P. Kim, Journal of Inclusion Phenomena and Macrocyclic Chemistry, 82 (2015) 187-194.

[10] Z. Chen, U. Baumeister, C. Tschierske, F. Wurthner, Chemistry, 13 (2007) 450-

465.

[11] W. Jiang, C. Xiao, L. Hao, Z. Wang, H. Ceymann, C. Lambert, S. Di Motta, F. Negri, Chemistry, 18 (2012) 6764-6775.

[12] L.E. Shoer, S.W. Eaton, E.A. Margulies, M.R. Wasielewski, J Phys Chem B, 119 (2015) 7635-7643.

[13] J. Choi, C. Sakong, J.-H. Choi, C. Yoon, J.P. Kim, Dyes and Pigments, 90 (2011) 82-88.

[14] J.Y. Kim, C. Sakong, S.-a. Choi, H. Jang, S.H. Kim, K.S. Chang, M.S. Han, J.S. Lee, J.P. Kim, Dyes and Pigments, 131 (2016) 293-300.

[15] C. Sakong, Y.D. Kim, J.-H. Choi, C. Yoon, J.P. Kim, Dyes and Pigments, 88 (2011) 166-173.

[16] L. Flamigni, B. Ventura, A. Barbieri, H. Langhals, F. Wetzel, K. Fuchs, A. Walter, Chemistry, 16 (2010) 13406-13416.

[17] C.C. Chao, M.K. Leung, Y.O. Su, K.Y. Chiu, T.H. Lin, S.J. Shieh, S.C. Lin, J Org Chem, 70 (2005) 4323-4331.

[18] M. Mamada, C.s. Pérez-Bolívar, P. Anzenbacher Jr, Organic letters, 13 (2011) 4882-4885.

[19] F. Wurthner, Chem Commun (Camb), (2004) 1564-1579.

[20] M. Li, J.-R. Xu, Y. Zeng, H.-J. Ben, F.-L. Yao, S. Yang, E.-Q. Chen, X.-K. Ren, Dyes and Pigments, 139 (2017) 79-86.

[21] C. Huang, S. Barlow, S.R. Marder, J Org Chem, 76 (2011) 2386-2407.

[22] Z. An, S.A. Odom, R.F. Kelley, C. Huang, X. Zhang, S. Barlow, L.A. Padilha, J. Fu, S. Webster, D.J. Hagan, E.W. Van Stryland, M.R. Wasielewski, S.R. Marder, The Journal of Physical Chemistry A, 113 (2009) 5585-5593.

[23] J. Choi, W. Lee, C. Sakong, S.B. Yuk, J.S. Park, J.P. Kim, Dyes and Pigments, 94 (2012) 34-39.

[24] C. Yoon, H.-S. Kwon, J.-S. Yoo, H.-Y. Lee, J.-H. Bae, J.-H. Choi, Coloration Technology, 131 (2015) 2-8.

[25] F. Wurthner, C.R. Saha-Moller, B. Fimmel, S. Ogi, P. Leowanawat, D. Schmidt, Chem Rev, 116 (2016) 962-1052.

[26] S. Leroy-Lhez, J. Baffreau, L. Perrin, E. Levillain, M. Allain, M.J. Blesa, P. Hudhomme, J Org Chem, 70 (2005) 6313-6320.

[27] J.B. Chang, J.W. Namgoong, S.H. Kim, S.H. Park, B.H. Hwang, J.P. Kim, Dyes and Pigments, 121 (2015) 30-37.

[28] R. Mishra, J.M. Lim, M. Son, P. Panini, D. Kim, J. Sankar, Chemistry, 20 (2014) 5776-5786.

[29] F. Würthner, S. Ahmed, C. Thalacker, T. Debaerdemaeker, Chemistry - A European Journal, 8 (2002) 4742-4750.

[30] H. Chen, F. Peng, Z. Luo, D. Xu, S.-T. Wu, M.-C. Li, S.-L. Lee, W.-C. Tsai, Opt. Mater. Express, 4 (2014) 2262-2273.

[31] C. Ramanan, A.L. Smeigh, J.E. Anthony, T.J. Marks, M.R. Wasielewski, J Am Chem Soc, 134 (2012) 386-397.

Chapter 4

Synthesis of bay-linked perylene dimers with enhanced solubility for high optical density black matrix material

4.1 Introduction

Perylene-3,4,9,10-tetracarboxylic acid diimide (PDI) derivatives can be easily synthesized from commercially available perylene-3,4,9,10-tetracarboxylic dianhydride (PTCDA). They are widely used in biochemical applications, organic photovoltaics, light-emitting diodes, and thin-film transistors (TFT) due to their high thermal, chemical, and photochemical stability and strong charge transfer property [1, 2]. Additionally, PDIs exhibit strong optical absorption from the visible to the near-infrared spectral region and can be implemented in various colors ranging from red to black by tuning the energy level of the molecule through changing substituents at imide or bay positions. However, the strong aggregation ability and low solubility in organic solvents of PDIs induced by the planar and rigid structure of the perylene core severely limit their applications in industries using the solution-process method [3, 4]. A blending method is applied, in which solvated dyes are mixed with dispersed pigments to improve color purity and electrical properties of color filters included in liquid crystal display (LCD) and organic light-emitting diodes (OLED). To adopt PDIs in this method, solubility enhancement of the dyes is essential.

Black matrix, a component of the LCD color filter, separates the RGB color pixels to prevent undesired color mixing and protects the TFT from external light to suppress the generation of leakage current. Therefore, black matrix materials require high optical density (OD), which indicates the ability for light absorption and strong thermal stability to withstand the manufacturing process. Currently, organic materials are used for black matrix, and carbon black has been reported as a representative material because it exhibits stable characteristics against heat and light and shows strong absorption strength.

Recently, however, the display industry is demanding thinner panels, and black matrix fabricated with carbon black poses a limitation. A carbon black, which has high electrical conductivity, is one of the most commonly used conductive additives in capacitors [5] and can cause malfunction of TFTs adjacent to the black matrix. Therefore, hybrid-type black matrices using a mixture of organic dyes or pigments with carbon black are currently being developed to lower the electric conductivity. A highly stable PDI with strong light-absorbing ability can be an effective alternative for lowering the dielectric constant of the black matrix.

Several hybrid-type black matrices using PDIs were fabricated in the previous study [6, 7]. The fabricated black matrices showed high thermal stability, electric and surface properties. However, the dye content of the black matrix solutions was insufficient due to the low solubility of the PDIs, and the OD value was measured lower than the commercial standard (> 2.5). Thus, an increase in dye solubility is essential to improve the optical property of a hybrid-type black matrix containing solvated dyes and dispersed carbon black. In this study, bay-linked dimers were

synthesized to reduce intermolecular stacking ability for enhancing the solubility of the dyes. A diphenyl ring was bonded between two PDI molecules to prevent aggregation of the dyes by forming a twisting angle and widening the gap between the PDI cores. The dyes absorb visible light in different ranges by introducing substituents having different electron donating power. Therefore, the absorption of the full spectrum of visible light was achieved by mixing the synthesized dimers. In this strategy, highly soluble dimeric PDIs were synthesized, and the optical and physical properties of the dimers were evaluated and compared with those of the monomeric PDIs. Hybrid-type black matrices using the dimers showed improved optical characteristics compared to the previous studies, and their optical, physical, and electrical properties were investigated in detail along with surface morphology.

4.2 Experimental section

4.2.1 Materials and instrumentation

Perylene-3,4,9,10-tetracarboxylic dianhydride, 2,6-diisopropylaniline, m-cresol, iodine, sulfuric acid, bromine, acetic acid, propionic acid, and potassium carbonate anhydrous purchased from Sigma-Aldrich, tetrakis(triphenylphosphine) palladium(0), 3-methoxy-1-butanol, 1-butoxy-2-propanol, 3,4,5-trimethoxybenzyl alcohol, 2-ethylhexylamine, and 3-isopropoxypropylamine purchased from TCI, and biphenyl-4,4’-diboronic acid bis(pinacol) ester purchased from Alfa Aesar were used as received. All the other reagents and solvents were reagent-grade and obtained

from commercial suppliers. Transparent glass substrates were provided by Paul Marienfeld GmbH & Co. KG, and acrylic binder and black matrix resist were supplied by ChemE Inc.

^{1}H and ^{13}C NMR spectra were recorded on a Bruker Avance 500 spectrometer (National Center for Inter-university Research Facilities at Seoul National University) at 500 MHz using chloroform-d and TMS, as the solvents and internal standard, respectively. Matrix Assisted Laser Desorption/Ionization Time of Flight (MALDI-TOF) mass spectra were collected on a Voyager-DE STR Biospectrometry Workstation (National Center for Inter-university Research Facilities at Seoul National University) with α-cyano-4-hydroxycinnamic acid (CHCA) as the matrix. Absorption and transmittance spectra were measured using a Perkin-Elmer Lambda 25 spectrophotometer and fluorescence spectra were measured using a Perkin-Elmer LS 55. Thermogravimetric analysis (TGA) was conducted in a nitrogen atmosphere at a heating rate of 10 °C min^{-1} using a TA instruments Thermogravimetric Analyzer 2050. Chromatic characteristics of the black matrices were analyzed on a Scinco color spectrometer. Dielectric constants of the black matrices were measured using Edward E306 thermal evaporator and an HP 4294A precision impedance analyzer. The thickness of the black matrices was measured using a KLA-TENCOR Nanospec AFT/200 alpha step. The OD value of the black matrices was measured using X-rite 301 densitometer. The roughness of the black matrices was measured using NX-10.

4.2.2 Synthesis

The dyes **2** and **3** are already known structures and were synthesized according to the previously reported procedures [7-9].

4.2.2.1 N,N'-Bis(2,6-diisopropylphenyl)-1-bromo-7-(3-methoxybutoxy)-perylene-3,4,9,10-tetracarboxylicdiimide (4a)

3 (1.00 g, 1.15 mmol), 3-methoxy-1-butanol (0.60 g, 5.76 mmol) and potassium carbonate (0.80 g, 5.76 mmol) in *N,N*-dimethylmethanamide (DMF) (60 ml) was stirred under nitrogen atmosphere for 3 h at 80 °C. The reaction mixture was cooled to room temperature and poured into 0.5 M HCl (300 ml). The precipitate was filtered, repeatedly washed with water, and dried in vacuum at 80 °C. The crude product was purified by silica gel column chromatography with CH_2Cl_2 as eluent to obtain unreacted **3** (0.65 g, 65% yield) and desired **4a** as a red solid compound (0.19 g, 19% yield). ^{1}H NMR ($CDCl_3$, 500 MHz): δ 9.66 (d, 1H, *J* = 12.8 Hz), 9.55 (d, 1H, *J* = 13.6 Hz), 9.03 (s, 1H), 8.78 (d, 1H, *J* = 13.6 Hz), 8,71 (d, 1H, *J* = 12.8 Hz), 8.62 (s, 1H), 7.53-7.50 (m, 2H), 7.38-7.36 (m, 4H), 4.70-4.64 (m, 2H), 3.72 (sextet, 1H), 3.39 (s, 3H), 2.80 (septet, 4H), 2.25-2.73 (m, 2H), 1.32 (d, 4H, *J* = 10.4 Hz), 1.20-1.89 (m, 24H); ^{13}C NMR (125 MHz, $CDCl_3$): δ 163.61, 163.59, 163.56, 162.97, 157.83, 145.86, 145.82, 138.56, 134.77, 134.22, 133.42, 131.87, 130.62, 130.58, 130.09, 129.96, 129.83, 129.15, 128.67, 128.54, 128.30, 124.37, 124.34, 123.33, 122.53, 121.65, 120.75, 119.98, 118.85, 77.48, 77.22, 76.97, 73.83, 67.96, 56.46,

36.75, 29.45, 24.23, 19.46; MALDI-TOF (m/z): calcd for $[M+3H]^{3+}$: 893.20. Found: 893.42; Elemental analysis: calcd for $C_{53}H_{51}N_2O_6$: C, 71.37; H, 5.76; N, 3.14; O, 10.76. Found: C, 71.35; H, 5.90; N, 3.00; O, 10.84.

4.2.2.2 N,N'-Bis(2,6-diisopropylphenyl)-1-bromo-7-(1-butoxy-2-propanyloxy)-perylene-3,4,9,10-tetracarboxylicdiimide (4b)

4b was synthesized following the same procedure for **4a** using **3** (1.00 g, 1.15 mmol), 1-butoxy-2-propanol (0.76 g, 5.76 mmol) and potassium carbonate (0.80 g, 5.76 mmol) in DMF (60 ml). The crude product was purified by silica gel column chromatography with CH_2Cl_2 as eluent to obtain unreacted **3** (0.61 g, 61% yield) and desired **4b** as a red solid compound (0.17 g, 0.16% yield). ^{1}H NMR ($CDCl_3$, 500 MHz): δ 9.64 (d, 1H, *J* = 12.8 Hz), 9.62 (d, 1H, *J* = 10.4 Hz), 9.02 (s, 1H), 8.76 (d, 1H, *J* = 12.8 Hz), 8.69 (d, 1H, *J* = 12.8 Hz), 8.63 (s, 1H), 7.53-7.50 (m, 2H), 7.37-7.36 (m, 4H), 5.22-5.20 (m, 1H), 3.84-3.76 (m, 2H), 3.56-3.51 (m, 2H), 2.79-2.72 (septet, 4H), 1.57-1.56 (m, 2H), 1.55 (s, 1H), 1.20-1.19 (m, 24H), 0.85 (t, 3H, *J* = 12.0 Hz); ^{13}C NMR (125 MHz, $CDCl_3$): δ 163.66, 163.60, 163.56, 163.50, 163.01, 157.69, 157.42, 157.16, 145.82, 138.45, 134.77, 133.40, 131.89, 130.65, 130.61, 130.10, 130.00, 129.96, 129.93, 129.86, 129.08, 129.05, 128.49, 128.21, 123.28, 122.51, 121.69, 121.55, 120.49, 119.89, 118.85, 74.16, 71.76, 69.31, 31.92, 29.44, 24.23, 19.44, 17.39, 14.04; MALDI-TOF (m/z): calcd for $[M+3H]^{3+}$: 921.32. Found: 921.49; Elemental analysis: Calcd for $C_{55}H_{55}N_2O_6$: C 71.81; H 6.03; N 3.05; O 10.43. Found: C 71.85; H 6.17; N 3.17; O 10.18.

4.2.2.3 N,N'-Bis(2,6-diisopropylphenyl)-1-bromo-7-(3,4,5-trimethoxybenzyloxy)-perylene-3,4,9,10-tetracarboxylicdiimide (4c)

4c was synthesized following the same procedure for **4a** using **3** (1.00 g, 1.15 mmol), 3,4,5-trimethoxybenzyl alcohol (1.14 g, 5.76 mmol) and potassium carbonate (0.80 g, 5.76 mmol) in DMF (60 ml). The crude product was purified by silica gel column chromatography with CH_2Cl_2 as eluent to obtain unreacted **3** (0.33 g, 33% yield) and desired **4c** as a red solid compound (0.60 g, 53% yield). ^{1}H NMR ($CDCl_3$, 500 MHz): δ 9.67 (d, 1H, *J* = 13.6 Hz), 9.57 (d, 1H, *J* = 4.8 Hz), 9.03 (s, 1H), 8.72 (s, 1H), 8.72 (d, 1H, *J* = 2.4 Hz), 8.71 (d, 1H, *J* = 2.4 Hz), 7.54-7.50 (m, 2H), 7.38-7.35 (m, 4H), 6.80 (s,2H), 5.57 (s, 2H), 3.87 (s, 3H), 3.85 (s, 6H), 2.79-2.70 (septet, 4H), 1.20-1.18 (m, 24H); ^{13}C NMR (125 MHz, $CDCl_3$): δ 163.53, 162.89, 157.14, 153.91, 145.83, 145.78, 138.36, 137.05, 134.67, 134.02, 133.50, 131.76, 130.56, 130.51, 130.08, 130.02, 129.91, 129.20, 128.93, 128.80, 128.25, 124.51, 124.37, 124.33, 123.33, 122.62, 121.81, 121.40, 120.20, 119.34, 105.47, 77.48, 77.22, 76.97, 72.93, 61.13, 56.44, 29.46, 24.20; MALDI-TOF (m/z): calcd for $[M+3H]^{3+}$: 987.30. Found: 987.34; Elemental analysis: Calcd for $C_{58}H_{53}N_2O_8$: C 70.65; H 5.42; N 2.84; O 12.98. Found: C 70.62; H 5.49; N 2.75; O 12.73.

4.2.2.4 N,N'-Bis(2,6-diisopropylphenyl)-1-bromo-7-((2-ethylhexyl)amino)-perylene-3,4,9,10-tetracarboxylicdiimide (4d)

4d was synthesized following the same procedure for **4a** using **3** (1.00 g, 1.15 mmol) and 2-ethylhexylamine (0.76 g, 5.76 mmol) in DMF (60 ml). The crude product was purified by silica gel column chromatography with CH_2Cl_2:n-Hexane (1:1) as eluent to obtain **4d** as a green solid compound (0.90 g, 85% yield). ^{1}H NMR ($CDCl_3$, 500 MHz): δ 9.51 (d, 1H, *J* = 12.8 Hz), 9.01 (s, 1H), 8.91 (d, 1H, *J* = 12.8 Hz), 8.71 (d, 1H, *J* = 12.8 Hz), 8.54 (d, 1H, *J* = 12.8 Hz), 8.34 (s, 1H), 7.53-7.49 (m, 2H), 7.37-7.35 (m, 4H), 6.11(s, 1H), 3.47 (d, 2H, *J* = 8.8 Hz), 2.79-2.72 (septet, 4H), 1.79-1.76 (m, 1H), 1.57-1.52 (m, 2H), 1.51-1.46 (m, 2H), 1.39-1.33 (m, 4H), 1.21-1.19 (m, 24H), 1.03 (t, 3H, *J* = 12.0 Hz), 0.93 (t, 3H, *J* = 11.2 Hz); ^{13}C NMR (125 MHz, $CDCl_3$): δ 163.70, 163.67, 163.30, 162.84, 147.78, 145.73, 145.67, 138.69, 135.91, 135.19, 131.76, 131.69, 130.68, 130.61, 129.80, 129.75, 129.69, 129.09, 128.96, 126.10, 124.80, 124.22, 124.17, 123.39, 122.55, 121.52, 120.97, 119.79, 119.27, 118.61, 114.59, 77.35, 77.09, 76.84, 47.61, 39.32, 31.62, 29.30, 28.98, 24.93, 24.11, 23.09, 14.10, 11.11; MALDI-TOF (m/z): calcd for $[M+3H]^{3+}$: 918.36. Found: 918.33; Elemental analysis: Calcd for $C_{56}H_{58}N_3O_4$: C 73.35; H 6.38; N 4.58; O 6.98. Found: C 73.26; H 6.42; N 4.46; O 7.00.

4.2.2.5 N,N'-Bis(2,6-diisopropylphenyl)-1-bromo-7-(3-isopropoxypropyl(amino))-perylene-3,4,9,10-tetracarboxylicdiimide (4e)

4e was synthesized following the same procedure for **4a** using **3** (1.00 g, 1.15 mmol) and 3-isopropoxypropylamine (0.60 g, 5.76 mmol) in DMF (60 ml). The crude product was purified by silica gel column chromatography with CH_2Cl_2 as

eluent to obtain **4e** as a green solid compound (0.67 g, 64%). ^{1}H NMR ($CDCl_3$, 500 MHz): δ 9.49 (d, 1H, *J* = 13.6 Hz), 9.07 (d, 1H, *J* = 12.8 Hz), 8.98 (s, 1H), 8.71 (d, 1H, *J* = 12.8 Hz), 8.52 (d, 1H, *J* = 12.8 Hz), 8.31 (s, 1H), 7.52-7.48 (m, 2H), 7.36 (d, 4H, *J* = 12.8 Hz), 3.66-3.62 (m, 4H), 3.47-3.43 (m, 1H), 2.79-2.71 (septet, 4H), 2.15-2.12 (m, 2H), 1.20-1.66 (m, 24H), 0.86 (d, 6H, *J* = 9.6 Hz); ^{13}C NMR (125 MHz, $CDCl_3$): δ 163.88, 163.34, 163.01, 148.02, 145.87, 145.84, 145.81, 145.74, 138.71, 135.96, 135.31, 134.22, 132.32, 132.23, 131.85, 130.81, 130.74, 130.68, 129.87, 129.85, 129.14, 128.78, 126.06, 124.80, 124.32, 124.27, 123.46, 122.62, 121.96, 121.61, 119.58, 119.47, 119.34, 118.58, 114.72, 77.48, 77.22, 76.97, 72.46, 68.56, 45.31, 29.90, 29.44, 29.41, 29.05, 24.21, 24.18, 21.95, 21.89; MALDI-TOF (m/z): calcd for $[M+3H]^{3+}$: 906.31. Found: 906.29; Elemental analysis: Calcd for $C_{54}H_{54}N_3O_5$: C 71.67; H 6.01; N 4.64; O 8.84. Found: C 71.72; H 6.06; N 4.67; O 8.85.

4.2.2.6 4,4'-(Biphenyl)bis(N,N'-bis(2,6-diisopropylphenyl)-1-bromo-7-(3-methoxybutoxy)-perylene-3,4,9,10-tetracarboxylicdiimide) (5a)

4a (0.60 g, 0.67 mmol), biphenyl-4,4'-diboronic acid bis(pinacol) ester (0.14 g, 0.33 mmol) and $Pd(PPh_3)_4$ (0.4 g, 0.03 mmol) were added in degassed aqueous 2M potassium carbonate (24 ml) and tetrahydrofuran (THF, 48 ml). The reaction mixture was heated at reflux under nitrogen atmosphere for 18 h. After cooled to room temperature, the mixture was diluted with ethyl acetate and the aqueous layer was removed. Upon drying over anhydrous $MgSO_4$, the organic layer was condensed in

vacuum. The crude product was purified by silica gel column chromatography with CH_2Cl_2 as eluent to obtain **5a** as a red solid compound (0.39 g, 65% yield). ^{1}H NMR ($CDCl_3$, 500 MHz): δ 9.61 (d, 2H, *J* = 12.8 Hz), 8.79 (d, 4H, *J* = 11.2 Hz), 8.61 (s, 2H), 8.22 (quartet, 4H, *J* = 12.8 Hz), 7.87 (d, 4H, *J* = 13.6 Hz), 7.72 (d, 4H, *J* = 12.8 Hz), 7.52-7.47 (m, 4H), 7.37-7.33 (m, 8H), 4.72-4.66 (m, 4H), 3.74-3.72 (m, 2H), 3.40 (s, 6H), 2.83-2.72 (m, 8H), 2.28-2.25 (m, 4H), 1.34 (d, 8H, *J* = 9.6 Hz), 1.21-1.17 (m, 48H); ^{13}C NMR (125 MHz, $CDCl_3$): δ 163.97, 163.92, 163.86, 163.65, 163.60, 158.13, 157.78, 145.88, 145.83, 142.52, 142.30, 141.98, 140.42, 140.36, 136.03, 135.26, 135.22, 134.57, 134.36, 133.63, 132.79, 131.90, 131.80, 131.22, 130.89, 130.68, 130.23, 130.04, 129.87, 129.81, 129.62, 129.40, 129.18, 128.97, 128.79, 128.52, 128.42, 124.65, 124.30, 123.87, 122.25, 122.19, 122.15, 121.98, 121.90, 121.82, 121.58, 119.03, 118.78, 77.48, 77.22, 76.97, 73.84, 67.91, 56.51, 36.79, 29.44, 29.36, 24.28, 24.25, 24.22, 19.50; MALDI-TOF (m/z): calcd for $[M+H]^+$: 1776.82. Found: 1776.76; Elemental analysis: Calcd for $C_{118}H_{110}N_4O_{12}$: C 79.79; H 6.24; N 3.15; O 10.81. Found: C 79.34; H 6.15; N 2.99; O 10.43.

4.2.2.7 4,4'-(Biphenyl)bis(N,N'-bis(2,6-diisopropylphenyl)-1-bromo-7-(1-butoxy-2-propanyloxy)-perylene-3,4,9,10-tetracarboxylicdiimide) (5b)

5b was synthesized following the same procedure for **5a** using **4b** (0.60 g, 0.65 mmol), biphenyl-4,4'-diboronic acid bis(pinacol) ester (0.13 g, 0.33 mmol) and $Pd(PPh_3)_4$ (0.4 g, 0.03 mmol) in degassed aqueous 2 M potassium carbonate (24 ml) and THF (48 ml). The crude products were purified by silica gel column

chromatography with CH_2Cl_2 as eluent to obtain **5b** as a red solid compound (0.41 g, 69% yield). ^{1}H NMR ($CDCl_3$, 500 MHz): δ 9.70 (d, 2H, *J* = 12.8 Hz), 8.77-8.76 (m, 4H), 8.64 (d, 2H, *J* = 12.0 Hz), 8.18 (s, 4H), 7.87 (d, 4H, *J* = 12.8 Hz), 7.72 (d, 4H, *J* = 14.4 Hz), 7.52-7.46 (m, 4H), 7.37-7.32 (m, 8H), 5.24-5.19 (m, 2H), 3.85-3.84 (m, 2H), 3.81-3.80 (m, 2H), 3.57-3.54 (m, 4H), 2.80-2.72 (m, 8H), 1.59 (d, 6H, *J* = 10.4 Hz), 1.57 (s, 4H), 1.35-1.30 (m, 4H), 1.21-1.13 (m, 48H), 0.86 (t, 6H, *J* = 12.0 Hz); ^{13}C NMR (125 MHz, $CDCl_3$): δ 163.98, 163.69, 163.53, 157.10, 145.86, 145.78, 142.40, 141.88, 140.35, 140.27, 135.94, 135.25, 134.68, 134.53, 133.61, 132.77, 131.82, 131.10, 130.91, 130.73, 130.37, 129.84, 129.63, 129.32, 129.15, 128.97, 128.83, 128.72, 128.37, 124.72, 124.30, 124.27, 124.15, 123.92, 122.90, 122.59, 122.18, 122.12, 121.73, 120.84, 120.53, 74.29, 71.79, 31.95, 29.44, 24.30, 19.47, 17.52, 14.06; MALDI-TOF (m/z): calcd for $[M+H]^+$: 1832.88. Found: 1832.32; Elemental analysis: Calcd for $C_{122}H_{118}N_4O_{12}$: C 79.97; H 6.49; N 3.06; O 10.48. Found: C 79.51; H 6.32; N 2.95; O 10.94.

4.2.2.8 4,4'-(Biphenyl)bis(N,N'-bis(2,6-diisopropylphenyl)-1-bromo-7-(3,4,5-trimethoxybenzyloxy)-perylene-3,4,9,10-tetracarboxylicdiimide) (5c)

5c was synthesized following the same procedure for **5a** using **4c** (0.60 g, 0.61 mmol), biphenyl-4,4'-diboronic acid bis(pinacol) ester (0.12 g, 0.31 mmol) and $Pd(PPh_3)_4$ (0.4 g, 0.03 mmol) in degassed aqueous 2 M potassium carbonate (24 ml) and THF (48 ml). The crude products were purified by silica gel column chromatography with CH_2Cl_2 as eluent to obtain **5c** as a red solid compound (0.29 g,

49% yield). ^{1}H NMR ($CDCl_3$, 500 MHz): δ 9.65 (d, 2H, *J* = 16.0 Hz), 8.78 (s, 2H), 8.74 (s, 2H), 8.72 (d, 2H, *J* = 4.8 Hz), 8.23-8.19 (m, 4H), 7.87 (d, 4H, *J* = 13.6 Hz), 7.72 (d, 4H, *J* = 5.6 Hz), 7.52-7.48 (m, 4H), 7.37-7.32 (m, 8H), 6.84 (s, 4H), 5.60 (s, 4H), 3.85 (s, 6H), 3.88 (s, 6H), 3.87 (s, 12H), 2.81-2.70 (m, 8H), 1.20-1.14 (m, 48H); ^{13}C NMR (125 MHz, $CDCl_3$): δ 163.85, 163.82, 163.57, 163.54, 157.43, 157.06, 153.90, 145.79, 142.41, 142.32, 142.05, 140.51, 140.45, 140.37, 138.56, 136.07, 135.19, 135.00, 134.62, 133.50, 132.83, 131.69, 131.22, 130.79, 130.71, 130.62, 130.29, 129.99, 129.92, 129.88, 129.80, 129.60, 129.34, 129.19, 128.80, 128.75, 128.63, 124.86, 124.31, 124.17, 122.27, 122.23, 122.16, 121.98, 119.56; MALDI-TOF (m/z): calcd for $[M+H]^+$: 1964.83. Found: 1965.00; Elemental analysis: Calcd for $C_{128}H_{114}N_4O_{16}$: C 78.27; H 5.85; N 2.85; O 13.03. Found: C 78.28; H 5.97; N 2.76; O 12.39.

4.2.2.9 4,4'-(Biphenyl)bis(N,N'-bis(2,6-diisopropylphenyl)-1-bromo-7-((2-ethylhexyl)amino)-perylene-3,4,9,10-tetracarboxylicdiimide) (5d)

5d was synthesized following the same procedure for **5a** using **4d** (0.60 g, 0.65 mmol), biphenyl-4,4'-diboronic acid bis(pinacol) ester (0.13 g, 0.33 mmol) and $Pd(PPh_3)_4$ (0.4 g, 0.03 mmol) in degassed aqueous 2 M potassium carbonate (24 ml) and THF (48 ml). The crude products were purified by silica gel column chromatography with CH_2Cl_2 as eluent to obtain **5d** as a green solid compound (0.33 g, 55% yield). ^{1}H NMR ($CDCl_3$, 500 MHz): δ 8.96 (d, 2H, *J* = 12.8 Hz), 8.76 (s, 2H),

8.72 (d, 2H, J = 12.8 Hz), 8.33 (s, 2H), 8.07-8.03 (quartet, 4H), 7.83 (d, 4H, J = 12.8 Hz), 7.72 (d, 4H, J = 13.6 Hz), 7.52-7.46 (m, 4H), 7.37-7.32 (m, 8H), 6.11-6.10 (m, 2H), 3.50-3.48 (m, 4H), 2.81-2.73 (m, 8H), 1.83-1.78 (m, 2H), 1.57-1.50 (m, 4H), 1.53-1.50 (m, 4H), 1.41-1.37 (m, 8H), 1.25-1.18 (m, 48H), 1.04 (t, 6H, J = 12.0 Hz), 0.95 (t, 6H, J = 11.2 Hz); ^{13}C NMR (125 MHz, $CDCl_3$): δ 163.92, 163.88, 163.82, 147.76, 145.86, 145.84, 142.21, 140.32, 139.26, 136.94, 136.30, 134.27, 132.95, 131.81, 131.20, 131.03, 130.81, 130.42, 130.12, 129.88, 129.80, 129.60, 129.01, 126.32, 124.64, 124.30, 124.25, 123.04, 122.32, 121.34, 120.99, 120.20, 119.43, 115.63, 77.48, 77.22, 76.97, 47.76, 39.48, 31.78, 29.91, 29.43, 29.34, 29.15, 25.07, 24.28, 24.25, 24.22, 23.24, 14.26, 11.27; MALDI-TOF (m/z): calcd for $[M+H]^+$: 1825.95. Found: 1826.77; Elemental analysis: Calcd for $C_{124}H_{124}N_6O_8$: C 81.55; H 6.84; N 4.60; O 7.01. Found: C 81.31; H 6.81; N 4.42; O 6.84.

4.2.2.10 4,4'-(Biphenyl)bis(N,N'-bis(2,6-diisopropylphenyl)-1-bromo-7-(3-isopropoxypropyl(amino))-perylene-3,4,9,10-tetracarboxylicdiimide) (5e)

5e was synthesized following the same procedure for **5a** using **4e** (0.60 g, 0.66 mmol), biphenyl-4,4'-diboronic acid bis(pinacol) ester (0.13 g, 0.33 mmol) and $Pd(PPh_3)_4$ (0.4 g, 0.03 mmol) in degassed aqueous 2 M potassium carbonate (24 ml) and THF (48 ml). The crude products were purified by silica gel column chromatography with CH_2Cl_2 as eluent to obtain **5e** as a green solid compound (0.48 g, 81% yield). ^{1}H NMR ($CDCl_3$, 500 MHz): δ 9.10 (d, 2H, J = 12.8 Hz), 8.74 (s, 2H),

8.72 (d, 2H, J = 12.8 Hz), 8.31 (s, 2H), 8.06-8.01 (m, 4H), 7.84 (d, 4H, J = 11.2 Hz), 7.72 (d, 4H, J = 12.8 Hz), 7.51-7.45 (m, 4H), 7.36-7.31 (m, 8H), 3.69-3.68 (m, 4H), 3.67-3.63 (m, 4H), 3.53-3.48 (m, 2H), 2.81-2.72 (septet, 8H), 2.16-2.14 (m, 4H), 1.21-1.16 (m, 48H), 0.95 (d, 12H, J = 9.6 Hz); ^{13}C NMR (125 MHz, $CDCl_3$): δ 163.95, 163.74, 147.83, 145.84, 142.24, 140.27, 139.06, 136.84, 136.20, 134.22, 132.98, 132.19, 131.11, 130.88, 130.32, 130.16, 129.87, 129.76, 129.33, 128.98, 126.19, 124.52, 124.29, 124.23, 122.90, 122.26, 121.81, 121.31, 119.89, 119.58, 119.66, 77.48, 77.22, 76.97, 72.51, 68.35, 45.21, 29.91, 29.43, 29.33, 29.26, 24.27, 24.20, 22.07, 21.93; MALDI-TOF (m/z): calcd for $[M+H]^+$: 1802.88. Found: 1802.97; Elemental analysis: Calcd for $C_{120}H_{116}N_6O_{10}$: C 79.97; H 6.49; N 4.66; O 8.88. Found: C 79.81; H 6.46; N 4.42; O 8.36.

4.2.3 Preparation of black matrices

Six kinds of hybrid-type and six kinds of dye-type black matrices were fabricated and listed in Table 4.1. The inks for hybrid-type black matrices (H_{ad}-H_{ce}) were composed of the dyes (0.52 g), propylene glycol methyl ether acetate (PGMEA) (4.53 g), acrylic binder (6.40 g) and carbon black resist (2.56 g). The inks for dye-type black matrices (D_{ad}-D_{ce}) were composed of the dyes (1.00 g), PGMEA (5.99 g) and acrylic binder (6.20 g). The prepared inks were coated on a transparent glass substrate using a MIDAS System SPIN-1200D spin coater. The coating speed was initially 250 rpm for 20 sec, which was then increased to 400 rpm and kept constant

for 10 sec. The wet coated black matrices were then dried at 40 ℃ for 20 min, prebaked 100 ℃ for 100 sec, and post baked at 230 ℃ for three times every 30 min. After each step, the coordinate values of the black matrices were measured.

4.2.4 Geometry optimization of the synthesized dyes

The geometry and electric structure of the studied dyes are optimized by the density functional theory (DFT) method at the B3LYP/6-31G (d, p) performed on Gaussian 09 program.

Table 4.1. Blend ratio of fabricated black matrices.

Type	Film	Dye		Carbon black (wt%)
		Hydroxy Substituent	Amino Substituent	
Hybrid-type	H_{ad}	5a / 1.83	5d / 1.83	3.66
	H_{ae}	5a / 1.83	5e / 1.83	3.66
	H_{bd}	5b / 1.83	5d / 1.83	3.66
	H_{be}	5b / 1.83	5e / 1.83	3.66
	H_{cd}	5c / 1.83	5d / 1.83	3.66
	H_{ce}	5c / 1.83	5e / 1.83	3.66
Dye-type	D_{ad}	5a / 3.66	5d / 3.66	-
	D_{ae}	5a / 3.66	5e / 3.66	-
	D_{bd}	5b / 3.66	5d / 3.66	-
	D_{be}	5b / 3.66	5e / 3.66	-
	D_{cd}	5c / 3.66	5d / 3.66	-
	D_{ce}	5c / 3.66	5e / 3.66	-

4.3 Results and Discussion

4.3.1 Synthesis

Synthesis procedure and structure of the synthesized dyes are depicted in scheme 4.1. 2,6-diisopropyl aniline was imidized on the periphery position of the dyes for solubility enhancement [10, 11]. To investigate the difference in the spectroscopic and physical properties of PDI by a hetero atom directly linked at the bay position, hydroxy or amine groups were introduced at the bay position through nucleophilic substitution. The unsymmetric PDIs (4a-e), in which the substituent was introduced only at one of two bay positions, were synthesized by controlling the temperature and the reaction time. The monomeric PDIs were finally synthesized to dimeric PDIs (5a-e) containing diphenyl group as a linker through the Suzuki–Miyaura coupling reaction. Structure of intermediates and dyes were confirmed by ^{1}H NMR, ^{13}C NMR, and MALDI-TOF spectroscopy and elemental analysis.

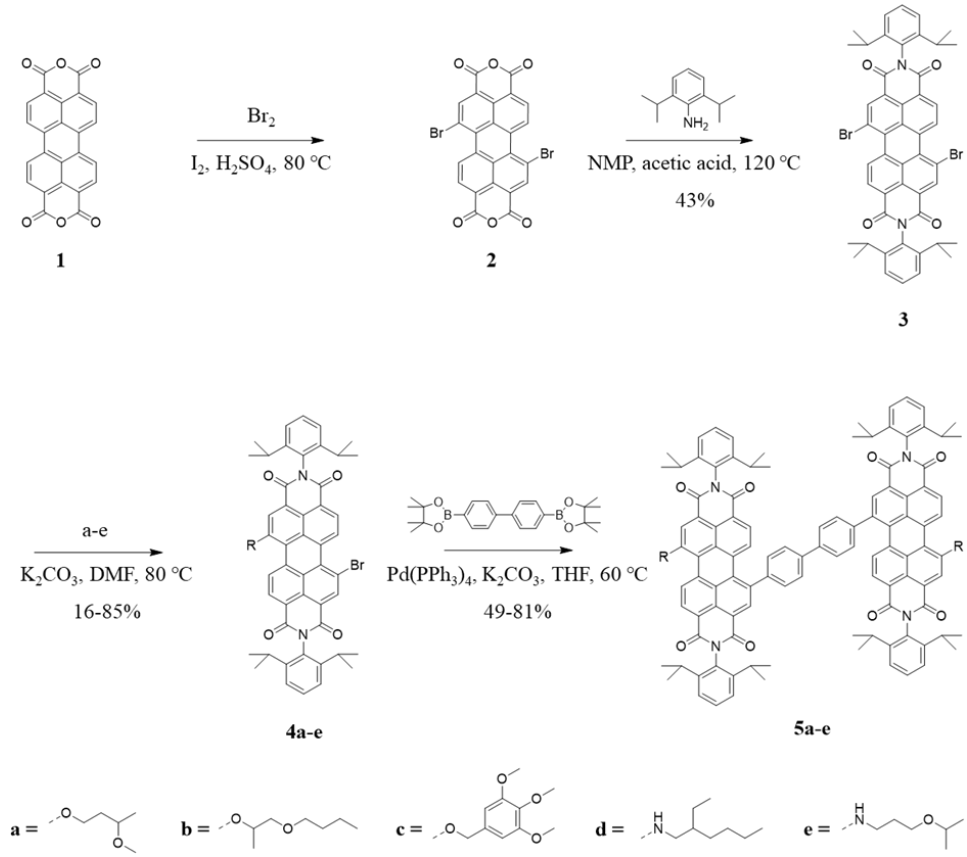

Scheme 4.1. Synthesis of diphenyl linked PDI dimers.

4.3.2 Spectral properties and solvatochromism of the dyes

Absorption and emission spectra of the synthesized monomeric and dimeric PDIs were measured in various solvents, and spectra for PGMEA used in the black matrix fabrication are shown in Fig. 4.1 and the spectroscopic data are given in Table 4.2. Absorption range of the monomers varied depending on the bay-linked substituents, and the maximum absorption wavelength was at approximately 560 nm and 647 nm

for dyes with ether group (4a-c) and amino group (4d, 4e), respectively. The different absorption spectra correspond to the changes in the highest occupied molecular orbital (HOMO) level due to the electron donating power of the bay substituent and were consistent with the computational calculation detailed in section 4.3.3.

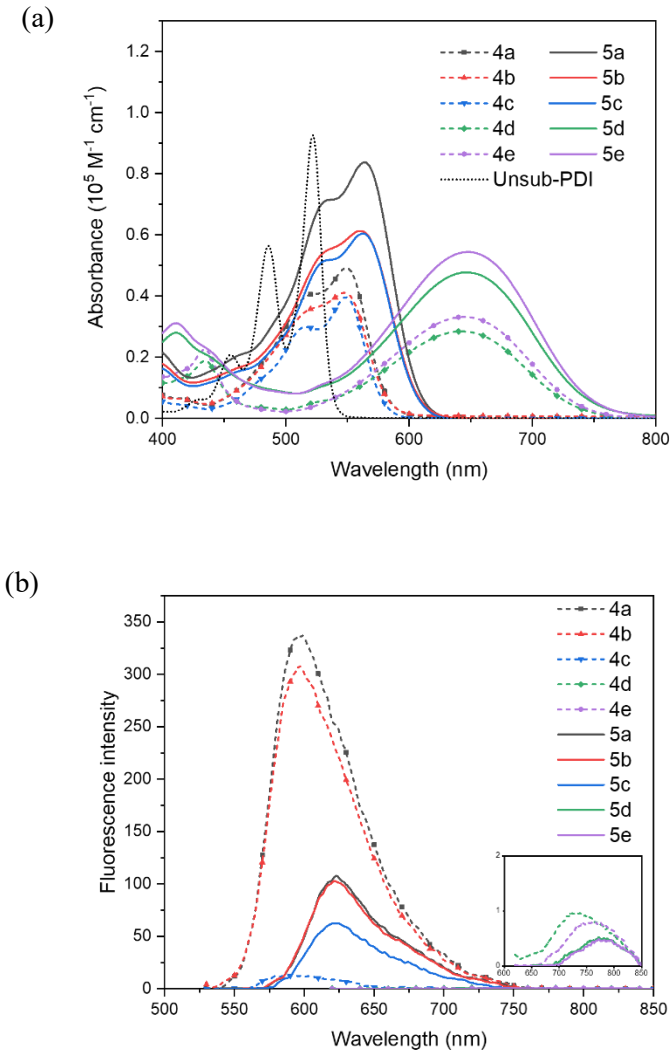

Figure 4.1. Absorption (a) and emission spectra (b) of the dyes in PGMEA.

Table 4.2. Spectroscopic data of the dyes in PGMEA.

	λ_{abs} (nm)	λ_{em} (nm)	ε (10^4 M^{-1} cm^{-1})	FWMH (nm)[a]	Φ_F
Unsubstituted PDI	522, 486	-	9.26, 5.65	-	-
4a	549	598	4.92	39	0.81
4b	548	597	4.11	42	0.75
4c	549	588	3.96	35	0.04
4d	642	729	2.12	117	0.02
4e	645	759	3.32	117	0.01
5a	564	623	8.38	49	0.33
5b	561	622	6.13	55	0.32
5c	562	624	6.05	53	0.14
5d	647	778	4.78	119	0.00
5e	647	782	5.44	121	0.00

[a] The FWHM value was estimated by doubling the right half-width of the absorption band.

The spectral broadness varied according to the type of bay substituents. An unsubstituted PDI which shows flat structure exhibits a sharp absorption spectrum, as shown in Fig. 4.1. (a), including clear 0-0 and 0-1 transitions at 522 and 486 nm, respectively. The introduction of the substituent at the bay position of the PDI changes the molecular conformation of the perylene core and then can affect the

shape of the vibronic absorption spectrum by altered vibrational overlap. The absorption spectra of 4a-4c exhibited less pronounced vibronic structure than that of unsubstituted PDI and the vibronic structure of the absorption spectrum completely disappeared in 4d and 4e. To analyze the line broadening feature, the dihedral angles of the dyes between naphthalene subunits attached to the central benzene ring (Φ_a for unsubstituted PDI, Φ_b, and Φ_c for monomers, and $\Phi_{b'}$ and $\Phi_{c'}$ for dimers were depicted in Fig. 4.2) were calculated by geometry optimization and are listed in Table 4.3. The unsubstituted PDI maintained the flat structure, and the dihedral angles of the synthesized dyes were calculated to be affected by the structure of the substituents. Similar Φ_c values were observed in all monomers due to the same bromine-substituted bay position. On the other hand, Φ_b, the dihedral angles of donating group-substituted bay position of monomer, showed different angles according to the donating groups. The Φ_b values of 4d and 4e (21.41°, 21.73°, respectively) were larger than those of other monomers due to sterically hindered hydrogen attached at the amino group. As the dihedral angle increases, the absorption spectrum becomes broadened [9, 12]. Additionally, the large value of Φ_b, which represents low core planarity, is considered to have influenced the absorbance (Table 4.2) of 4d and 4e to be lower than that of 4a-c [13]

Table 4.3. Distortion angles[a] of the dyes calculated by DFT at B3LYP/6-31G level.

	Φ_a	Φ_b	Φ_c	
Unsubstituted PDI	0.08			
4a		15.62	21.44	
4b		15.91	21.45	
4c		14.71	21.63	
4d		21.41	21.97	
4e		21.73	21.96	
		$\Phi_{b'}$	$\Phi_{c'}$	Ψ
5a		15.03	19.21	76.92
5b		15.48	19.16	79.48
5c		14.75	19.79	78.93
5d		20.80	19.76	74.66
5e		21.49	20.48	66.99

[a] Distortion of angles of bay positions (Φ) and intra-PDI core (Ψ) shown in Fig. 4.2.

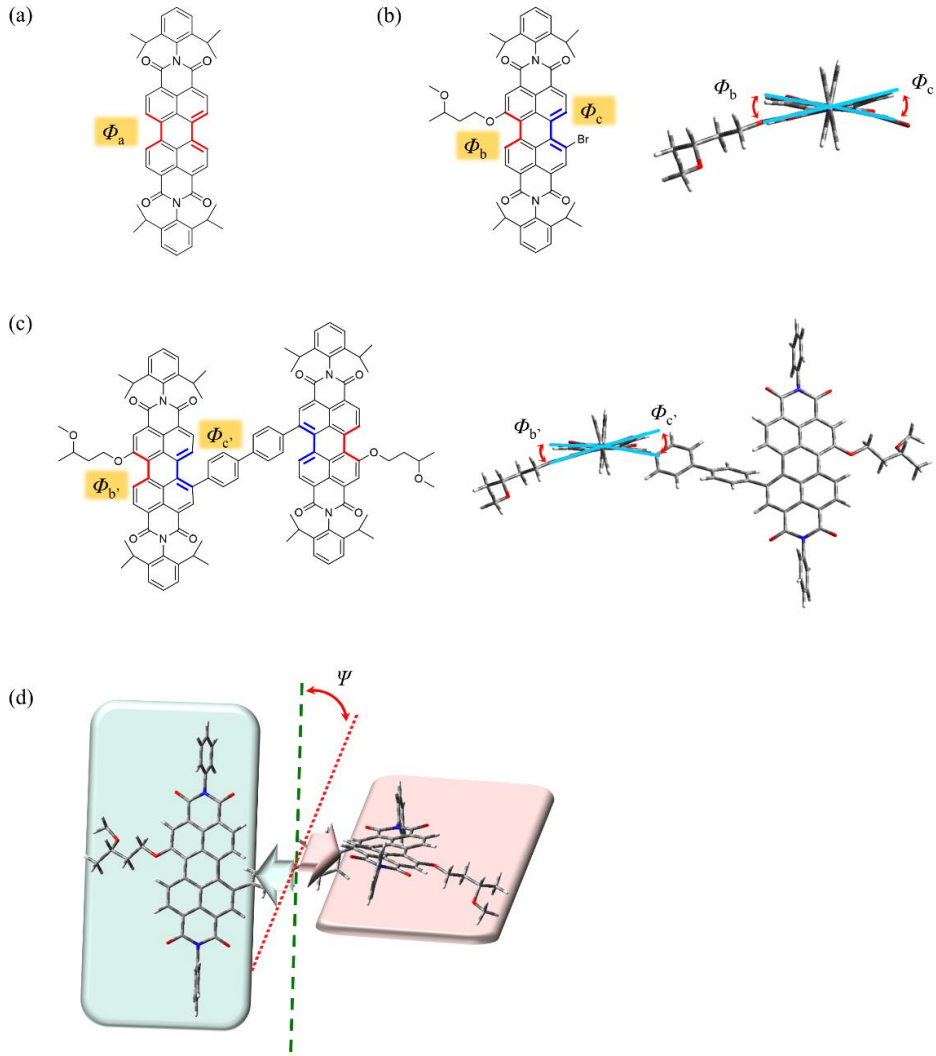

Figure 4.2. Description of the distortion angles (a) Φ_a of unsubstituted PDI, (b) Φ_b and Φ_c of monomer, (c) $\Phi_{b'}$ and $\Phi_{c'}$ of dimer and (d) Ψ of dimer.

The $\Phi_{b'}$ of the dimers is analogous to that of the monomers with the same substituent, and the $\Phi_{c'}$ (dihedral angle of diphenyl linked bay position) of all dimers showed similar values. The vibronic structure of the absorption spectra of the dimers, which is similar to the monomers, resulted from these structural features. Absorption spectra of the dimeric PDIs (5a-e) were red shifted by 2–10 nm compared to monomeric PDIs due to conjugation extension through diphenyl linker, and the absorbance of the dimers increased up to 2.31–fold that of the monomers. The full width at half maximum (FWHM) of the dyes was also enlarged by 2–18 nm relative to the monomers with the same substituent as a result of the photoinduced charge transfer between the diphenyl linker and the perylene units [14]. This charge transfer can be confirmed from the calculated frontier molecular orbital (FMO) shown in Fig. 4.3. According to the FMO calculation, the dimers showed typical orbital characteristics of charge transfer that delocalized electron density through the whole dimer molecule, including the diphenyl linker at the HOMO state, while the lowest unoccupied molecular orbital (LUMO) is delocalized mainly on the perylene core and the diimide groups [15]. Enhanced optical property can be expected in a black matrix fabricated using dimers that appeared with higher absorbance and broader FWHM than that of the monomers.

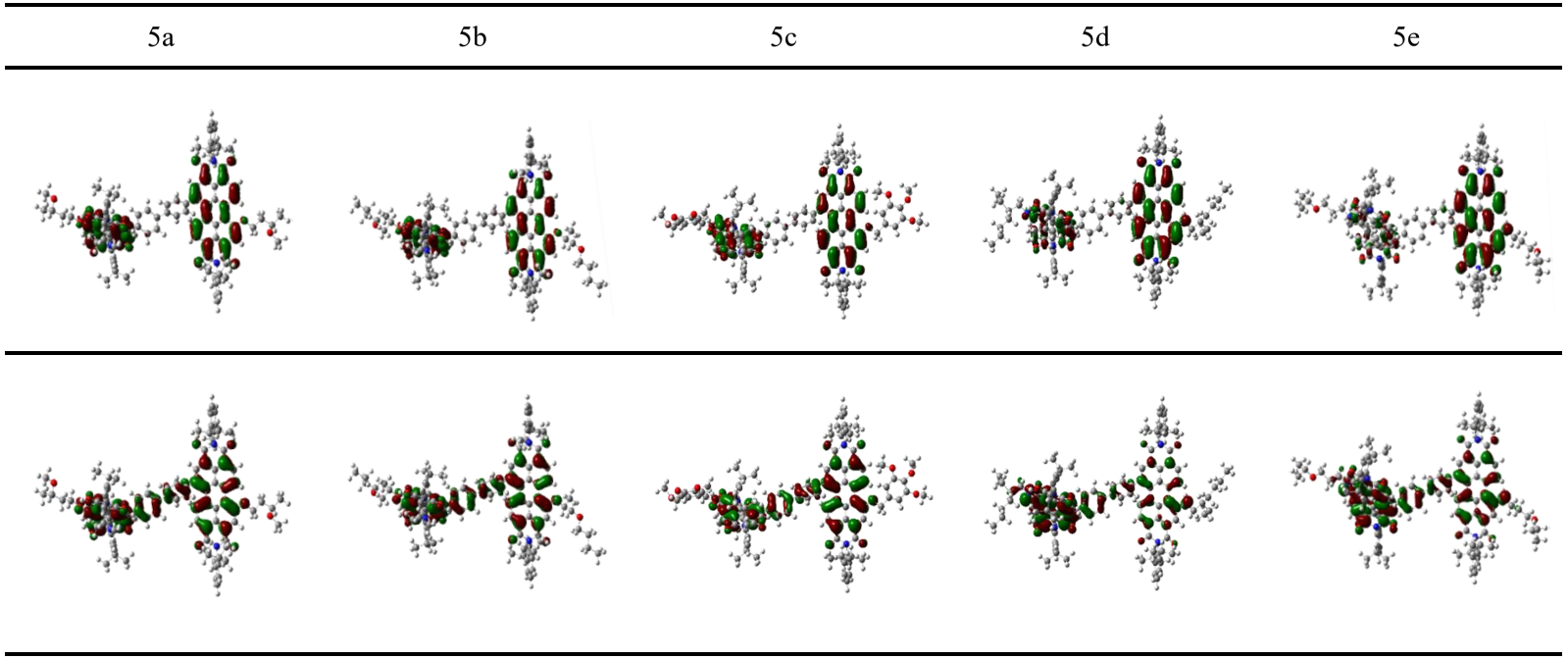

Figure 4.3. The frontier molecular orbitals of the LUMO (top) and HOMO (bottom) of 5a-e calculated by DFT at B3LYP/6-31G level.

The solvatochromic Stokes shift of the dyes was measured in solvents with various polarities and the data analysis was carried out using the Lippert–Mataga equation.

$$\Delta\nu = \nu_f - \nu_a = 2(\mu_e - \mu_g)^2 \Delta f/(hca_0^3) + C$$

where

$$\Delta f = [(\epsilon - 1)/(2\epsilon + 1)] - [(n^2 - 1)/2n^2 + 1)]$$

In the equation, ν_f and ν_a are the wavenumber corresponding to spectral maxima in fluorescence and absorption spectra, respectively. μ_e and μ_g are the ground- and excited-state dipole moments, respectively. c is the velocity of light, a_0 is the radius of the Onsager cavity around the fluorophore, h is the Plank's constant, Δf is known as the solvent polarity parameter, and ϵ and n are the dielectric constant and refractive index, respectively. The ground state dipole moment of the dyes was calculated using DFT calculation. Onsager cavity radius is the theoretically predicted from Atomic and Bond Contribution of van der Waals volume (VABC).

As shown in Fig. 4.4, the Lippert–Mataga plot of the dyes created a positive, linear relationship between the Stokes shift values ($\Delta\nu$) and Δf. The positive slope indicates that the fluorescence of the dye red-shifted with increased solvent polarity, and these results were also represented in Table 4.4. In a polar solvent environment, the dipole-dipole interaction between the dyes and solvent molecules led to the stabilization of the excited state relative to the ground state, which induced an energy gap contraction [16-18]. The increase in solvent polarity also affected the fluorescence quenching (in Table 4.4), especially in protic solvents. The non-

radiative decay process is presumably via intersystem crossing, solvent relaxation and hydrogen bonding between the dyes and solvent molecules [19-25]. As listed in Table 4.2 and Table 4.4, fluorescence quantum yield (Φ_F) of the dyes with the amino group is lower than that of the dyes with the ether group and Φ_F tends to decrease with increasing solvent polarity. Since perylene has high electron deficient characteristics due to having four electron withdrawing carbonyl groups, charge separation occurs even through a substituent of moderate electron donating ability [26]. Therefore, electron-rich amino substituents influence fluorescence quenching significantly. The dyes with low Φ_F are suitable as black matrix materials, for which strong light-blocking ability is required.

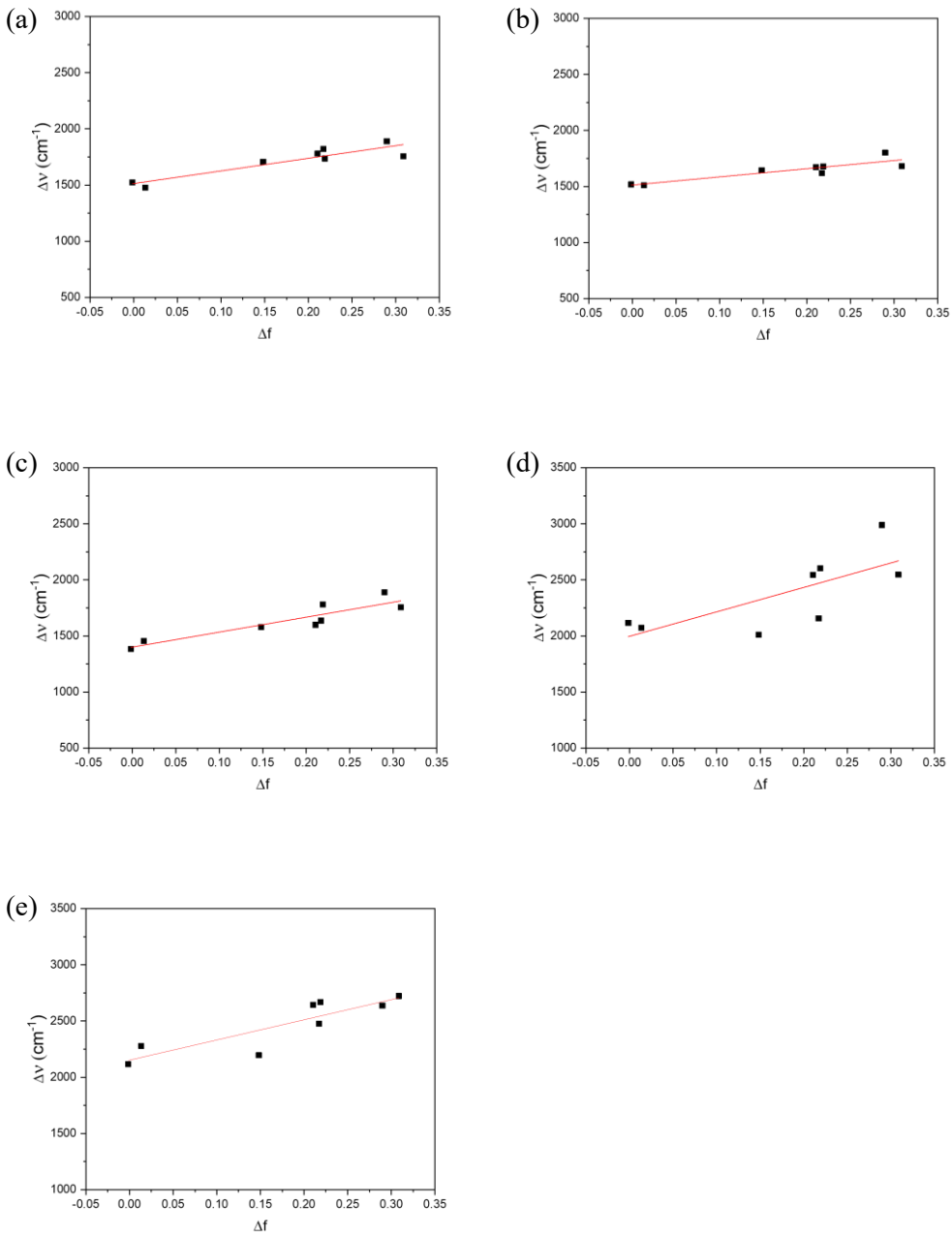

Figure 4.4. Lippert-Mataga plots for the dyes in various solvents: (a) 5a; (b) 5b; (c) 5c; (d) 5d; (e) 5e.

The electron donating ability also influenced the change of the maximum absorption wavelength depending on the solvent, especially 5d and 5e. The ground and Frank–Condon state are easily affected by the solvent polarity, and thus PDIs substituted with a strong electron-donating amino group (5d and 5e) showed a larger solvatochromic shift in absorption spectra (52 nm and 42 nm) than those of PDIs substituted with an ether group (5a-5c).

The difference of electron donating power was found in the chemical shift of the NMR peak of the protons (a and b) adjacent to the N or O atom of the dyes. As shown in Fig. 5, the protons of 5d and 5e are upfield-shifted compare to the protons of 5a-c by the influence of high electron donating ability around the amino groups.

The large bathochromic shift and quenching of the fluorescence is a typical phenomenon of the intramolecular charge transfer (ICT) between the donor (bay substituent) and the acceptor (PDI) [27]. Furthermore, the strong electron-donating ability increases intramolecular resonance with the π electron of the molecule and enhances electron transfer from donor to acceptor in excited states [20, 28]. Thus, it is concluded that ICT was strengthened by the amino group [20, 29].

Table 4.4. Summary of spectroscopic data of the dyes in various solvents. Solvents are listed in their order of the orientation polarizability.

		Hexane	Toluene	CF	THF	MC	EtOH	MeOH
	Δf	0	0.014	0.148	0.210	0.217	0.289	0.309
5a	λ_{abs} (nm)	552	569	568	563	570	567	568
	λ_{em} (nm)	602	622	627	621	628	631	628
	ε (10^4 M^{-1} cm^{-1})	8.14	8.16	8.84	8.22	9.18	8.19	8.37
	Φ_F	0.87	0.85	0.80	0.43	0.45	0.04	0.02
5b	λ_{abs} (nm)	551	568	566	558	566	563	564
	λ_{em} (nm)	601	620	627	619	631	630	626
	ε (10^4 M^{-1} cm^{-1})	6.09	6.07	6.64	6.28	6.73	6.36	5.36
	Φ_F	0.88	0.85	0.74	0.40	0.38	0.03	0.02
5c	λ_{abs} (nm)	551	567	566	562	567	565	566
	λ_{em} (nm)	596	618	622	618	625	632	629
	ε (10^4 M^{-1} cm^{-1})	6.02	6.05	7.30	6.97	7.01	6.84	6.58
	Φ_F	0.94	0.71	0.59	0.71	0.23	0.01	0.01
5d	λ_{abs} (nm)	615	639	646	647	650	644	667
	λ_{em} (nm)	707	737	743	775	756	798	803
	ε (10^4 M^{-1} cm^{-1})	4.64	4.70	5.09	4.45	5.36	4.56	4.62
	Φ_F	0.03	0.02	0.02	0.01	0.01	0.00	0.00
5e	λ_{abs} (nm)	621	646	648	646	653	663	663
	λ_{em} (nm)	715	758	755	779	779	803	809
	ε (10^4 M^{-1} cm^{-1})	4.14	5.20	5.30	5.19	5.69	5.14	5.18
	Φ_F	0.02	0.01	0.01	0.01	0.01	0.00	0.00

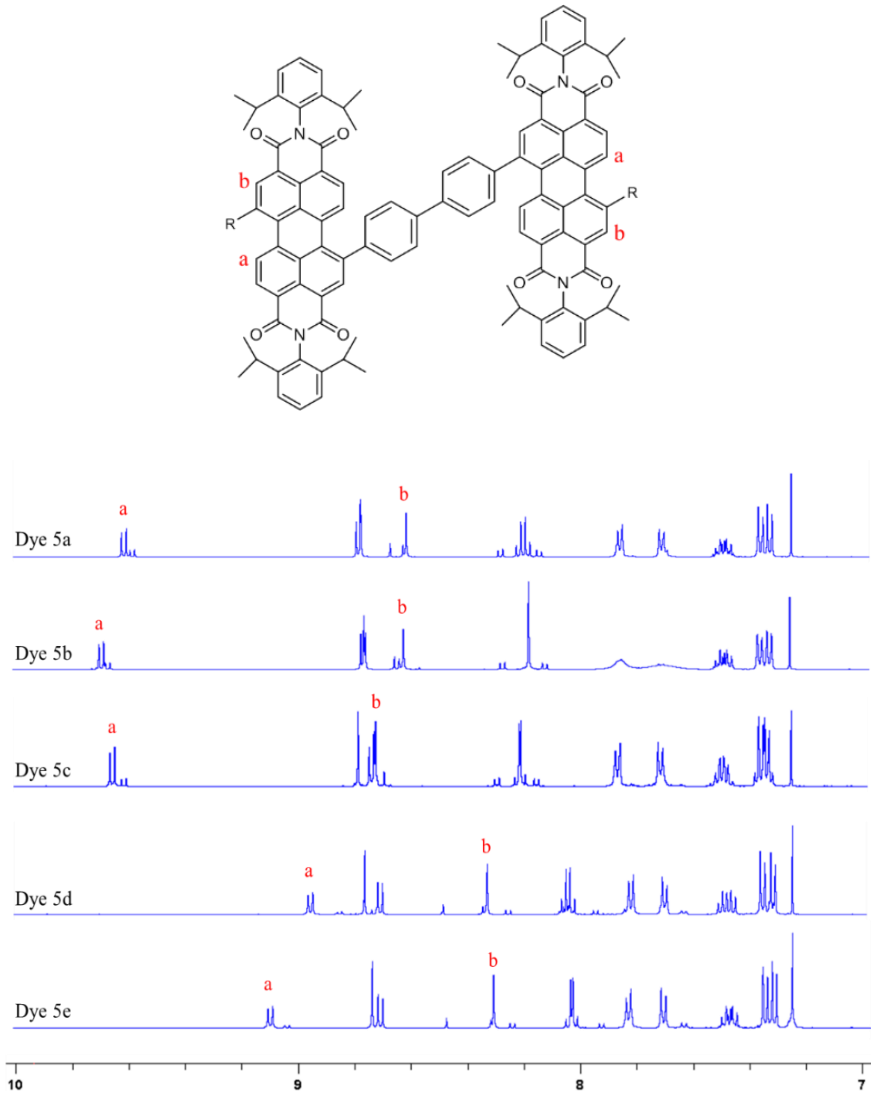

Figure 4.5. ^{1}H NMR (500 MHz) spectra of the aromatic region of 5a-5e. The labeled peaks correspond to the protons of PDI core adjacent to the N or O atoms of the dyes.

4.3.3 Computational studies and solubility of the dyes

The perylene core is an electron-deficient compound, and typically, the HOMO level of the molecule increases without affecting the LUMO level by substitution of electron donating group at the bay position [30]. As listed in Table 4.5, the LUMO levels of the monomers were similar to unsubstituted PDI, while the HOMO levels increased to different values depending on the type of substituents (the ether and the amino group). Consequently, the amino substituents were found to have higher electron-donating power than the ether substituents, which is consistent with the theoretical tendency of the electron donating ability of molecules. The energy gap between HOMO and LUMO levels of the monomers is smaller than that of unsubstituted PDI, and the energy gap change with the substituents showed the same trend as the measured spectral characteristics of the synthetic dyes. The LUMO level of the dimers showed an analogous value with the monomers and the HOMO level was slightly increased relative to the monomers. The red-shifted absorption spectra of the dimers (2–18 nm) were measured experimentally, and this result is consistent with the HOMO-LUMO gap calculated from DFT.

Table 4.5. Energy levels of the dyes calculated by DFT at B3LYP/6-31G level and solubility of the dyes in PGMEA.

	HOMO (eV)	LUMO (eV)	Solubility (wt%)
Unsubstituted PDI	-6.01	-3.49	-
4a	-5.76	-3.34	6.68
4b	-5.81	-3.39	9.77
4c	-5.75	-3.33	4.14
4d	-5.58	-3.30	10.80
4e	-5.59	-3.31	10.51
5a	-5.55	-3.25	11.45
5b	-5.62	-3.32	15.78
5c	-5.35	-3.35	7.92
5d	-5.39	-3.21	12.81
5e	-5.42	-3.25	12.81

Molecules with strong intermolecular π–π interactions, such as unsubstituted PDI, have low solubility in most organic solvents and limited use in electronic and organic photovoltaic materials. Therefore, to improve the solubility of the dye, various methods such as the introduction of bulky substituents on the perylene core or synthesis of imide-/bay-linked dimer have been attempted [31, 32]. Black matrix with enhanced optical properties can be achieved by increasing the dye content; thus, the solubility of the dyes needs to be improved for this purpose. In this study, the solubility of the dimers and monomers was measured in various organic solvents and is shown in Table 4.5 and Table 4.6. The dihedral angles (Φ) of the two naphthalene subunits of the dyes and twisting angle (Ψ) of the dimers between two PDI planes were calculated by DFT, and the relationship between the angles and solubility was investigated.

Table 4.6. Solubility of the dyes in various solvents.

	Solubility (wt%)						
	Hexane	Toluene	CF	THF	MC	EtOH	MeOH
4a	Insoluble[a]	3.56	14.66	5.06	11.54	0.59	Insoluble
4b	-[b]	5.97	20.22	17.71	10.99	1.25	-
4c	-	6.10	24.15	7.32	15.19	1.22	-
4d	0.52	5.52	23.80	13.32	11.95	1.07	-
4e	-	8.70	18.21	18.17	11.85	1.07	-
5a	0.18	5.29	24.09	8.66	16.84	0.98	-
5b	0.16	18.11	21.46	21.68	20.84	1.39	-
5c	-	8.57	28.53	19.97	24.13	1.38	-
5d	0.70	14.03	25.41	21.12	19.46	1.71	-
5e	-	16.72	20.72	20.86	24.25	1.44	-

[a] Less than 0.05 wt%.

[b] Less than 0.10 wt%.

As shown in Table 4.3, the amino group induced a larger core distortion than the ether group. This structural feature, which prevents intermolecular stacking, enhanced the solubility [33]. Mono-substituted PDIs generally exhibit low solubility due to a small core distortion compared to 1,7-disubstituted PDIs [11]. However, the synthesized monomers showed improved solubility in comparison to the 1,7-diaryl-substituted PDIs (6.4 wt% in PGMEA) used in previous research [6]. This suggested that alkyl substituents have favorable effects on solubility improvement than aryl substituents. The lowest solubility of the 4c containing aryl substituent among the

synthesized mono-substituted PDI also supports this speculation.

The solubility of the dimers was increased compared to that of the monomers with the same substituent due to the highly twisted dimeric backbone (Ψ) and the solubility difference between the dimers and monomers in PGMEA is shown in Fig. 6. The distorted structure of the dimers also reduced the intermolecular stacking of the dyes [14], and both Ψ and Φ values influenced the solubility of the dimers simultaneously. The highest solubility in PGMEA was observed with 5b, which had the largest Ψ. 5d and 5e with the larger Φ showed higher solubility than 5a and 5c, despite having the smaller Ψ values.

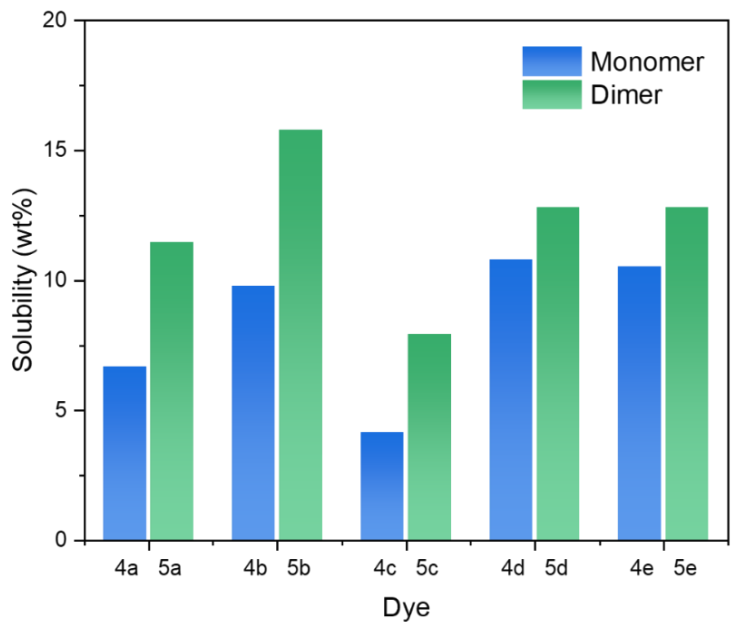

Figure 4.6. Solubility of the dyes in PGMEA.

4.3.4 Thermal stability of the dyes

The thermal behavior of the synthesized dyes was studied by TGA, and the possibility of application of the dyes to black matrix baked at high temperature was examined. The TGA was conducted until the temperature reached 400 ℃, including the isothermal region at 230 ℃ for 30 min. The thermal stability was evaluated by the weight loss at the isothermal region and the results are shown in Table 4.7 and Fig. 4.7. Generally, dyes can be considered as sufficiently stable when weight loss is less than 3 wt% in this region.

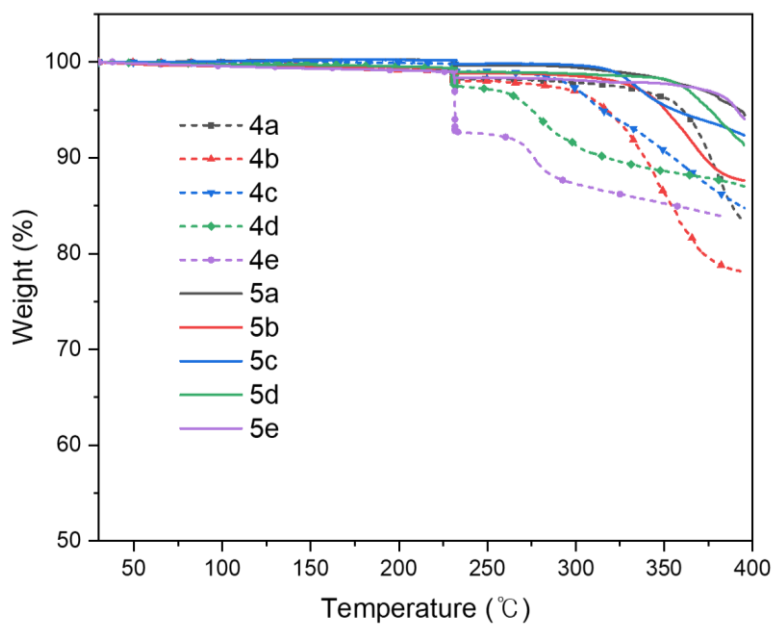

Figure 4.7. TGA of the dyes.

Table 4.7. Weight loss of the dyes during TGA.

	Weight loss (%)									
	4a	4b	4c	4d	4e	5a	5b	5c	5d	5e
Isothermal region	0.88	1.07	0.77	1.84	6.24	0.32	0.49	0.19	0.45	0.63
at 400 ℃	16.80	21.90	15.24	15.95	16.23	6.24	12.37	7.64	8.65	5.95

The thermal stability of the PDI is enhanced by strong intermolecular π–π interaction induced by minimizing the twisting angle of the perylene core. Therefore, unsubstituted PDI with a low core distortion showed high thermal stability (a decomposition temperature of 400 ℃). On the other hand, the strong intermolecular packing caused by a planar molecular structure lowered the solubility of the dyes in organic solvents [34]. Therefore, a suitable molecular structure design satisfying both stability and solubility is required to apply the dyes to the black matrix. For this purpose, in this study, the dimeric structure was synthesized using bay-substituted perylene monomer through the diphenyl linker.

The dimers exhibited less than 0.63% weight loss in the isothermal region and 12.37% weight loss during the heating up to 400 ℃, which is lower than that of the monomers (0.77–6.24%, 15.24–21.90 %), indicating that the dimerization improved the thermal stability. 5c and 4c substituted with an aryl group were most stable among the dimers and monomers, respectively. The difference in the physical property was thought to be attributed to the stability of the aryl groups against heat. The other dyes, substituted with an alkyl group showed similar thermal stability regardless of the structure of substituent.

4.3.5 Optical and thermal properties of the black matrices

Since the synthesized dye alone cannot absorb all the visible light, two dyes with different light absorption regions (one from the ether group substituted dyes and the other one from the amino group substituted dyes) were mixed to form six combinations of dyes (Table 4.1) applied to the black matrix. The hybrid-type black films were prepared using these combinations of the dyes with dispersed carbon black. In the previous study, the content of the dyes in the black matrix resist was limited due to the low solubility of the dyes. The content of carbon black contained in the hybrid-type films also was much lower than that of the commonly used carbon black-type film because dye-to-carbon black ratios (0.85 wt%: 0.85 wt%, 0.51 wt%: 1.19 wt%) were fixed to lower the dielectric constant of the films [6]. In this study, the solubility of the dyes in PGMEA was enhanced by dimerization, and the optical properties of the films were improved by increasing the amount of the dyes added to the black matrix resist. The dye-type films without carbon black were also fabricated for comparison.

In general, the fluorescence of PDI in the solid state tends to be quenched by the inter- and intra-layer energy transfers induced from aggregated perylene molecules [35]. The spectral characteristics of the films with each dye (D_a, D_b, D_c, D_e, and D_f) were examined to confirm this fluorescence quenching of solid state. As shown in Fig. 4.8, the fluorescence of the films was quenched markedly. Fluorescence was detected in films D_a and D_b, which were strongly fluorescent in a solution state. However, the intensities of the fluorescence were very small (under 4) and the

maximum fluorescence wavelengths were located in the infrared region (D_a: 730.5 nm, D_b: 715 nm). Such low-intensity film fluorescence is expected to be advantageous for the optical properties of the black matrix. Increased absorptivity and a broadened absorption band were observed in the film due to dye aggregation arising from increased dye concentration. The broad absorption band and high absorbance of the film is a favorable characteristic to the black matrix. However, the aggregation of the dyes may hinder the flatness of film. Therefore, surface morphology was evaluated and analyzed in section 4.3.6.

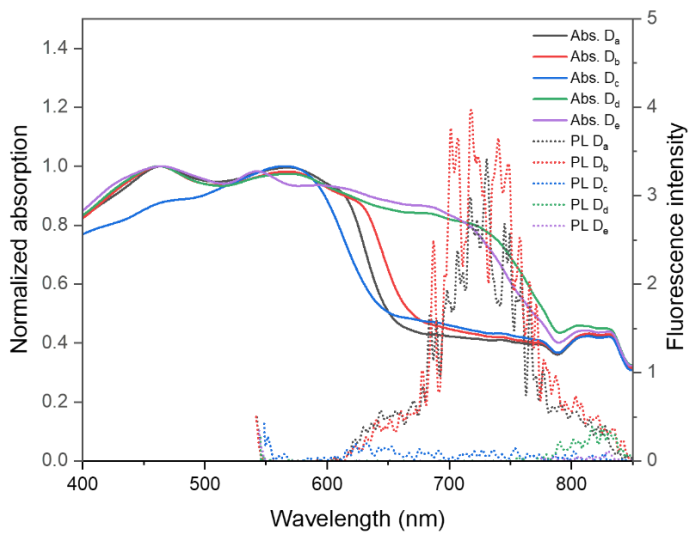

Figure 4.8. Normalized absorption and emission spectra of the dyes in solid state.

Transmittances of the hybrid-type and dye-type films listed in Table 4.8 were less than 0.24% and 2.68%, respectively, and the films showed more effective light-shielding abilities in the visible region than those of the films of the previous study (hybrid-type film: 0.79%, dye-type film: 6.94%) [6]. These results showed that improved optical property can be achieved through dyes having enhanced solubility.

Table 4.8. Transmittance of the fabricated black matrices after 3rd postbaking at a specific wavelength.

	H_{ad}	H_{ae}	H_{bd}	H_{be}	H_{cd}	H_{ce}
400 nm	0.22	0.22	0.23	0.23	0.23	0.23
550 nm	0.11	0.11	0.11	0.11	0.11	0.11
700 nm	0.23	0.23	0.23	0.23	0.24	0.23
	D_{ad}	D_{ae}	D_{bd}	D_{be}	D_{cd}	D_{ce}
400 nm	2.67	2.39	2.39	2.41	2.36	2.31
550 nm	0.67	0.61	0.61	0.62	0.59	0.58
700 nm	2.08	2.60	2.51	2.61	2.68	2.47

Since every film had very low transmittance in the visible region, the light-shielding ability of the films cannot be distinguished using the transmittance of the films. Therefore, the OD value was measured in addition to evaluate optical characteristics of the films according to the dyes, and the OD values of the hybrid-type films are shown in Table 4.9. A black matrix with an OD value greater than 2.5 is used in the display industry. The hybrid-type films showed an OD value greater than 2 (0.49 μm^{-1} in the previous study) and the OD values of H_{ad} and H_{ae} containing 5a with the highest absorbance among the dyes were 2.64 μm^{-1} and 2.76 μm^{-1}, respectively. The tendency of the OD value of the fabricated hybrid-type and dye-type films (Table 4.10) was correlated with the absorbance of the dyes used in the films.

Table 4.9. OD values of the hybrid-type black matrices.

	H_{ad}	H_{ae}	H_{bd}	H_{be}	H_{cd}	H_{ce}
OD value	2.64	2.76	2.08	2.09	2.20	2.10

Table 4.10. OD values of the dye-type black matrices.

	D_{ad}	D_{ae}	D_{bd}	D_{be}	D_{cd}	D_{ce}
OD value	0.60	0.60	0.57	0.58	0.55	0.57

Strong thermal stability must be ensured for the black matrix material since high-temperature baking needs to be performed three times after deposition of the black matrix on the color filter for applying RGB pixels. The thermal stability of the films was evaluated under similar conditions of the display fabrication process, including prebaking at 100 ℃ and postbaking at 230 ℃. In this process, the color difference values (ΔE_{ab}) of the film between the baking procedures were determined as the stability criterion, and the results are shown in Table 4.11. The thermal stability of the films is consistent with that of the dyes evaluated from TGA, and ΔE_{ab} was lower than 1.21, which was superior to the industrial standard (< 3). The hybrid-type films showed higher thermal stability than the dye-type films, which resulted from thermally stable carbon black. ΔE_{ab} was found to decrease as the baking process was repeated. This tendency implies that the color change occurring during the baking process is within the predictable range and that the synthesized dyes are suitable for the black matrix.

Table 4.11. The ΔE_{ab} values of the fabricated black matrices.

	ΔE_{ab}		
	Pre-1st Post	1st Post-2nd Post	2nd Post-3rd Post
H_{ad}	0.63	0.69	0.24
H_{ae}	0.78	0.54	0.30
H_{bd}	0.85	0.60	0.11
H_{be}	1.04	0.62	0.25
H_{cd}	0.82	0.29	0.12
H_{ce}	1.21	0.40	0.25
D_{ad}	1.80	0.88	0.25
D_{ae}	2.28	1.70	0.83
D_{bd}	1.75	1.27	0.84
D_{be}	1.88	1.47	0.77
D_{cd}	1.25	0.54	0.75
D_{ce}	1.50	0.51	0.32

4.3.6 AFM images of the black matrices

The surface morphology of the fabricated films was investigated by non-contact mode AFM, and 3D images of the films are depicted in Fig. 4.9, and Fig. 4.10. The agglomerates were found in both the dye-type and hybrid-type films that did not exist in the surface of the carbon black-type film. These aggregates were considered to be formed by the dyes. The same weight of colorants was included in the dye-type and hybrid-type films, and thus, larger amounts of dyes were added to the dye-type film in place of carbon black. The higher dye concentration may increase the formation of aggregates, and this assumption was confirmed by a comparison between the 3D image of the hybrid-type and dye-type films.

The hybrid-type films had a smaller number of particles than dye-type films, while the surface was more rugged caused by the difference in miscibility between the solvated dyes and the dispersed carbon black. The Rq values listed in Table 4.12 indicate the flatness of the film and the Rq of the hybrid-type films had a maximum value of 1.48, which is lower than the criterion of the color filter production (< 4). The Rq of the dye-type film (0.36–0.76, Table 4.13) deviated from the influence of the carbon black and was lower than that of the hybrid-type film.

The 3D images of the H_{cd} and D_{ce} containing 5c showed a larger distribution of particles, clearly suggesting that the solubility of the dye strongly affects the formation of aggregates on the surface of the films. However, the height of the particles was less than 12 nm, and Rq of the films was not significantly affected by

the low-height particles.

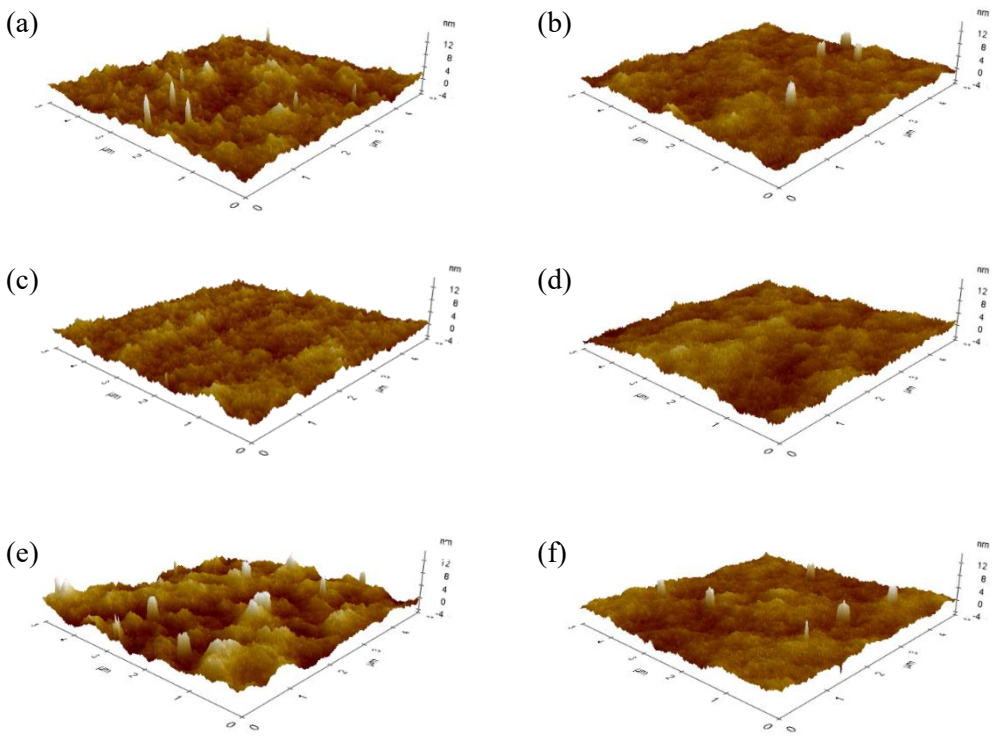

Figure 4.9. AFM images of the hybrid-type black matrices: (a) H_{ad}; (b) H_{ae}; (c) H_{bd}; (d) H_{be}; (e) H_{cd}; (f) H_{ce}.

Table 4.12. Surface roughness (Rq) of the hybrid-type black matrices after postbaking.

	H_{ad}	H_{ae}	H_{bd}	H_{be}	H_{cd}	H_{ce}
Rq	0.96	0.89	0.86	0.96	1.48	0.76

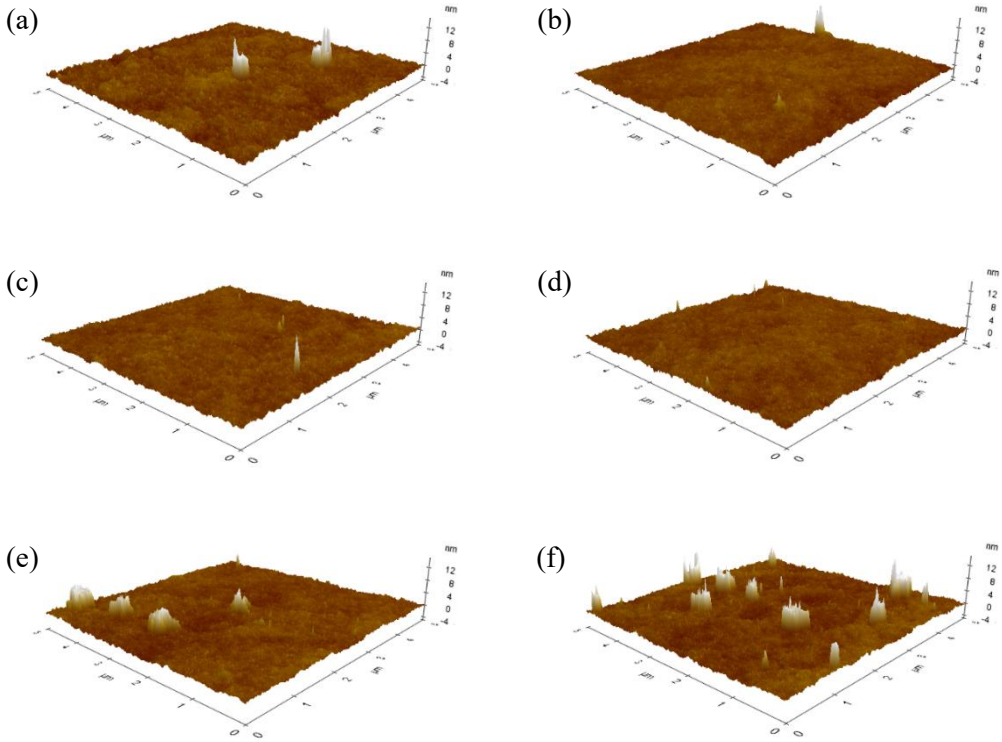

Figure 4.10. AFM images of the dye-type black matrices: (a) D_{ad}; (b) D_{ae}; (c) D_{bd}; (d) D_{be}; (e) D_{cd}; (f) D_{ce}.

Table 4.13. Surface roughness (Rq) of the dye-type black matrices after postbaking.

	D_{ad}	D_{ae}	D_{bd}	D_{be}	D_{cd}	D_{ce}
Rq	0.66	0.41	0.36	0.39	0.67	0.91

4.3.7 Dielectric constant of the black matrices

A low dielectric constant is required in the black matrix because of the adjacent electrically sensitive TFT layer. In the display industry, the dielectric constant of the black matrix should be less than 7. The carbon black-type film cannot satisfy the industrial standard and hence, the development of a material that can lower the dielectric constant is required [36].

In this research, hybrid-type films were fabricated using highly soluble dimeric PDIs mixed with dispersed carbon black. The dielectric constants of the films are listed in Table 4.14. The addition of the dyes was effective in lowering the dielectric constant of the films. In particular, the dye-type films showed a significantly lower value (0.99–7.58, Table 4.15) than the carbon black-type film (> 17). The hybrid-type films had a higher dielectric constant than dye-type films due to the effect of highly conductive carbon black, but the value was measured to be as low as applicable to the black matrix. The dielectric constant of the films gradually decreased as the frequency increased from 0.1 to 1,000 kHz. This was attributed to the lack of dipole reorientation of the dyes in high frequency [37].

Table 4.14. Dielectric constants of hybrid-type black matrices at various frequency.

Frequency (kHz)	Dielectric constant (ε_r)					
	H_{ad}	H_{ae}	H_{bd}	H_{be}	H_{cd}	H_{ce}
0.1	10.56	10.53	8.97	9.15	7.45	9.07
1	7.93	10.11	7.74	7.91	6.15	7.97
10	7.49	8.99	6.09	6.20	6.08	7.91
100	7.19	8.23	5.65	5.94	5.82	7.45
200	5.47	6.62	5.16	5.54	5.10	6.92
400	4.80	5.61	4.68	5.07	4.12	4.92
600	4.87	4.04	4.68	5.04	4.35	4.63
800	4.30	3.71	4.21	4.83	3.96	4.50
1,000	4.12	2.90	4.06	4.70	3.51	3.69

Table 4.15. Dielectric constants of dye-type black matrices at various frequency.

Frequency (kHz)	Dielectric constant (ε_r)					
	D_{ad}	D_{ae}	D_{bd}	D_{be}	D_{cd}	D_{ce}
0.1	7.01	7.58	6.42	6.82	6.65	6.83
1	6.80	6.15	5.06	5.94	5.84	5.05
10	6.16	6.13	4.41	4.95	4.49	3.03
100	5.27	5.90	3.89	4.12	4.06	2.88
200	4.03	3.89	3.23	3.63	2.34	2.07
400	3.02	2.70	2.17	3.26	1.62	1.35
600	3.04	2.92	2.28	3.33	1.71	1.40
800	2.63	2.52	1.85	3.01	1.31	1.21
1,000	2.38	2.37	1.41	2.59	1.04	0.99

4.4 Conclusions

Dimeric PDIs were synthesized linked with diphenyl compound, and their optical and thermal properties were measured and compared with those of monomeric PDIs. The dimers showed a broader absorption range and higher absorbance than monomers in a solution state. Additionally, the ICT character generated by the donating group at the bay position of the dye and fluorescence QY of the dyes was lower than that of unsubstituted PDI. In film state, additional fluorescence quenching occurred, and the fluorescence band was shifted to the infrared region so that transmittance of the film was kept low in the visible region. By the presence of carbon black, the hybrid-type film had better optical and physical properties than dye-type films while surface roughness and dielectric constant increased slightly.

Dimerization of PDI is a molecular design strategy for improving spectral properties of dyes and increasing the solubility of dyes in PGMEA. The DFT calculation of the synthesized dimers resulted in a twisting angle of 66.99° between the PDI planes, and the solubility of the dimers increased up to 2.45 times that of monomers. The bulky substituents introduced at the bay and imide positions of the PDI core also contributed to the solubility enhancement by inducing the core distortion of the PDI and interrupting intermolecular π–π stacking. In previous studies, the dye content of the films was limited due to the low solubility of the dyes. However, in this study, hybrid-type black matrices with improved absorptivity were prepared using highly soluble dimers. In particular, the OD values of H_{ad} and H_{ae} were found sufficient for industrial application. Therefore, dimeric PDIs with

enhanced solubility in PGMEA can be an effective approach for enhancing the optical properties of the black matrix.

4.5 References

[1] Horn D, Rieger J. Organic Nanoparticles in the Aqueous Phase—Theory, Experiment, and Use. Angewandte Chemie International Edition. 2001;40(23):4330-61.

[2] Kurokawa N, Yoshikawa H, Hirota N, Hyodo K, Masuhara H. Size-dependent spectroscopic properties and thermochromic behavior in poly(substituted thiophene) nanoparticles. Chemphyschem. 2004;5(10):1609-15.

[3] Norris DJ, Sacra A, Murray CB, Bawendi MG. Measurement of the size dependent hole spectrum in CdSe quantum dots. Phys Rev Lett. 1994;72(16):2612-5.

[4] Yagita Y, Matsui K. Size-dependent optical properties of 9,10-bis(phenylethynyl)anthracene crystals. Journal of Luminescence. 2015;161:437-41.

[5] Asahi T, Sugiyama T, Masuhara H. Laser fabrication and spectroscopy of organic nanoparticles. Accounts of Chemical Research. 2008;41(12):1790-8.

[6] Oikawa H, Mitsui T, Onodera T, Kasai H, Nakanishi H, Sekiguchi T. Crystal Size Dependence of Fluorescence Spectra from Perylene Nanocrystals Evaluated by

Scanning Near-Field Optical Microspectroscopy. Japanese Journal of Applied Physics. 2003;42(Part 2, No. 2A):L111-L3.

[7] Kasai H, Kamatani H, Okada S, Oikawa H, Matsuda H, Nakanishi H. Size-Dependent Colors and Luminescences of Organic Microcrystals. Japanese Journal of Applied Physics. 1996;35(Part 2, No. 2B):L221-L3.

[8] Tsuda K. Colour filters for LCDs. Displays. 1993;14(2):115-24.

[9] Choi J, Lee W, Namgoong JW, Kim T-M, Kim JP. Synthesis and characterization of novel triazatetrabenzcorrole dyes for LCD color filter and black matrix. Dyes and Pigments. 2013;99(2):357-65.

[10] Choi J, Sakong C, Choi J-H, Yoon C, Kim JP. Synthesis and characterization of some perylene dyes for dye-based LCD color filters. Dyes and Pigments. 2011;90(1):82-8.

[11] Sakong C, Kim YD, Choi J-H, Yoon C, Kim JP. The synthesis of thermally-stable red dyes for LCD color filters and analysis of their aggregation and spectral properties. Dyes and Pigments. 2011;88(2):166-73.

[12] Namgoong JW, Chung S-W, Jang H, Kim YH, Kwak MS, Kim JP. Improving nanoparticle dispersions of pigment and its application to a color filter: New phthalocyanine derivatives as synergist. Journal of Industrial and Engineering Chemistry. 2018;58:266-77.

[13] Lee W, Choi J, Kim SH, Park J, Kim JP. Analysis and Characterization of Dye-Based Black Matrix Film of Low Dielectric Constant Containing Phthalocyanine and

Perylene Dyes. Journal of Nanoscience and Nanotechnology. 2015;15(1):295-302.

[14] Lee W, Yuk SB, Choi J, Jung DH, Choi S-H, Park J, et al. Synthesis and characterization of solubility enhanced metal-free phthalocyanines for liquid crystal display black matrix of low dielectric constant. Dyes and Pigments. 2012;92(3):942-8.

[15] Koo H-S, Chen M, Pan P-C. LCD-based color filter films fabricated by a pigment-based colorant photo resist inks and printing technology. Thin Solid Films. 2006;515(3):896-901.

[16] Sabnis RW. Color filter technology for liquid crystal displays. Displays. 1999;20(3):119-29.

[17] Yuk SB, Lee W, Kim SH, Namgoong JW, Lee JM, Kim JP. Application of perylene dyes for low dielectric hybrid-type black matrices. Journal of Industrial and Engineering Chemistry. 2018;64:237-44.

[18] Yuk SB, Lee W, Namgoong JW, Choi J, Chang JB, Kim SH, et al. Synthesis and characterization of bay-substituted perylene dyes for LCD black matrix of low dielectric constant. Journal of Inclusion Phenomena and Macrocyclic Chemistry. 2015;82(1):187-94.

[19] Huang C, Barlow S, Marder SR. Perylene-3,4,9,10-tetracarboxylic acid diimides: synthesis, physical properties, and use in organic electronics. J Org Chem. 2011;76(8):2386-407.

[20] Kozma E, Catellani M. Perylene diimides based materials for organic solar cells.

Dyes and Pigments. 2013;98(1):160-79.

[21] Chao CC, Leung MK, Su YO, Chiu KY, Lin TH, Shieh SJ, et al. Photophysical and electrochemical properties of 1,7-diaryl-substituted perylene diimides. J Org Chem. 2005;70(11):4323-31.

[22] Auweter H, Haberkorn H, Heckmann W, Horn D, Lüddecke E, Rieger J, et al. Supramolecular Structure of Precipitated Nanosize β-Carotene Particles. Angewandte Chemie International Edition. 1999;38(15):2188-91.

[23] Jia W-b, Wang H-w, Yang L-m, Lu H-b, Kong L, Tian Y-p, et al. Synthesis of two novel indolo[3,2-b]carbazole derivatives with aggregation-enhanced emission property. Journal of Materials Chemistry C. 2013;1(42):7092-101.

[24] Daub J, Engl R, Kurzawa J, Miller SE, Schneider S, Stockmann A, et al. Competition between Conformational Relaxation and Intramolecular Electron Transfer within Phenothiazine−Pyrene Dyads. The Journal of Physical Chemistry A. 2001;105(23):5655-65.

[25] Sumalekshmy S, Gopidas KR. Photoinduced Intramolecular Charge Transfer in Donor−Acceptor Substituted Tetrahydropyrenes. The Journal of Physical Chemistry B. 2004;108(12):3705-12.

[26] Inan D, Dubey RK, Westerveld N, Bleeker J, Jager WF, Grozema FC. Substitution Effects on the Photoinduced Charge-Transfer Properties of Novel Perylene-3,4,9,10-tetracarboxylic Acid Derivatives. J Phys Chem A. 2017;121(24):4633-44.

[27] Bryantsev VS, Firman TK, Hay BP. Conformational Analysis and Rotational Barriers of Alkyl- and Phenyl-Substituted Urea Derivatives. The Journal of Physical Chemistry A. 2005;109(5):832-42.

[28] Bradley JS. Homogeneous carbon monoxide hydrogenation to methanol catalyzed by soluble ruthenium complexes. Journal of the American Chemical Society. 1979;101(24):7419-21.

[29] Li H, Guo Y, Li G, Xiao H, Lei Y, Huang X, et al. Aggregation-Induced Fluorescence Emission Properties of Dicyanomethylene-1,4-dihydropyridine Derivatives. The Journal of Physical Chemistry C. 2015;119(12):6737-48.

[30] Wurthner F. Perylene bisimide dyes as versatile building blocks for functional supramolecular architectures. Chem Commun (Camb). 2004(14):1564-79.

[31] Bodapati JB, Icil H. Highly soluble perylene diimide and oligomeric diimide dyes combining perylene and hexa(ethylene glycol) units: Synthesis, characterization, optical and electrochemical properties. Dyes and Pigments. 2008;79(3):224-35.

[32] Farooqi MJ, Penick MA, Burch J, Negrete GR, Brancaleon L. Characterization of novel perylene diimides containing aromatic amino acid side chains. Spectrochimica Acta Part A: Molecular and Biomolecular Spectroscopy. 2016;153:124-31.

[33] Li M, Xu J-R, Zeng Y, Ben H-J, Yao F-L, Yang S, et al. Ionic self-assembled derivatives of perylene diimide: Synthesis, aggregated structure and molecular packing behavior. Dyes and Pigments. 2017;139:79-86.

[34] Agnihotri S, Mukherji S, Mukherji S. Size-controlled silver nanoparticles synthesized over the range 5–100 nm using the same protocol and their antibacterial efficacy. RSC Advances. 2014;4(8):3974-83.

[35] Hou J, Chen TL, Zhang S, Huo L, Sista S, Yang Y. An Easy and Effective Method To Modulate Molecular Energy Level of Poly(3-alkylthiophene) for High-Voc Polymer Solar Cells. Macromolecules. 2009;42(23):9217-9.

[36] Zhao H, Zhang Y-y, Xu H, He Z-m, Zhang Z-L, Zhang H-q. Synthesis and properties of perylene diimide dyes bearing unsymmetrical and symmetrical phenoxy substituents at bay positions. Tetrahedron. 2015;71(40):7752-7.

[37] Tantra R, Jing S, Pichaimuthu SK, Walker N, Noble J, Hackley VA. Dispersion stability of nanoparticles in ecotoxicological investigations: the need for adequate measurement tools. Journal of Nanoparticle Research. 2011;13(9):3765-80.

[38] Yin X-z, Tan Y-q, Song Y-h, Zheng Q. Dispersion stability and rheological behavior of suspensions of polystyrene coated fumed silica particles in polystyrene solutions. Chinese Journal of Polymer Science. 2011;30(1):26-35.

[39] Nolte H, Schilde C, Kwade A. Determination of particle size distributions and the degree of dispersion in nanocomposites. Composites Science and Technology. 2012;72(9):948-58.

[40] Ciardelli F, Ruggeri G, Pucci A. Dye-containing polymers: methods for preparation of mechanochromic materials. Chemical Society Reviews. 2013;42(3):857-70.

[41] Olhero SM, Ferreira JMF. Influence of particle size distribution on rheology and particle packing of silica-based suspensions. Powder Technology. 2004;139(1):69-75.

[42] Lee PTC, Chiu C-W, Chang L-Y, Chou P-Y, Lee T-M, Chang T-Y, et al. Tailoring Pigment Dispersants with Polyisobutylene Twin-Tail Structures for Electrowetting Display Application. ACS Applied Materials & Interfaces. 2014;6(16):14345-52.

Chapter 5

Characterization of the optical properties of the donor-acceptor structure of perylene dyes in liquid state and analysis of film characteristics

5.1 Introduction

Organic compounds have different chemical and physical properties as the particle size varies from isolated molecules to bulk crystals [1-4], and their dependence on the size of the organic compounds has been observed for particles of larger than several tens of nanometers [5]. Even in the case of perylene, the excimer fluorescence is gradually blue-shifted without changing the monomer fluorescence peak as the perylene particles of several hundreds of nanometers decrease in size [6, 7]. To realize the desired optical properties of an organic compound, it is, therefore, necessary to precisely control the aggregation behavior of the molecules.

A color filter, which is one of the major components in organic light-emitting diodes (OLEDs) and liquid crystal displays (LCDs), plays an important role in converting the unrefined light into red, green, and blue colors [8]. An unintended color change of a film may occur owing to an aggregation of the colorant molecules during the color filter manufacturing process, particularly the heat treatment [9-11], and thus the control of the molecular aggregation is required during this process.

Two different methods applied during the wet process for this purpose have been studied, namely, a dispersion method for pulverizing an insoluble pigment through physical treatment, and a dissolution method for a soluble dye through dissolving in organic solvents [12-14].

Pigments are the most commonly used materials in a display [15, 16]. In general, the solubility of the pigments in an industrial solvent (PGMEA) is exceedingly low due to its strong aggregation arising from an intermolecular interaction. For this reason, pigments have been applied to color filters through the dispersion method [11]. The pigment grinding process and the development of a suitable dispersion agent for each pigment are essential for a highly dispersed system [12]. In addition, newly added materials for the dispersion method should be compatible with the other elements of the photoresist, such as a photoinitiator or a binder polymer. Additional studies are needed for the stabilization of a dispersed solution according to the respective pigment structure.

By contrast, a dissolution method using a soluble dye has certain advantages in that the film manufacturing process is simpler than the dispersion method because no additional materials are required. However, the solubility of the dyes is a critical parameter for the dissolution method and the black matrices fabricate with the dyes of low solubility cannot satisfy the optical density (OD) above 2.5 as required in the industry [9-11]. In the previous study, the hybrid-type film using highly soluble dyes (11.45 and 12.81 wt%) exhibited the OD of 2.64 while OD of 0.49 was measured from the film using the dyes with low solubility (3.20 and 4.60 wt%) [17]. The introduction of substitutions to reduce intermolecular packing or to increase the

miscibility of the dyes from the medium is a typical strategy for the solubility enhancement of the dyes.

Therefore, in this study, dyes with low solubility were applied to film processing in the dispersion method. The dyes with high optical properties and low solubility in PGMEA were selected for this purpose. The optical properties and dispersibility were evaluated in a liquid state, and the optical and surface morphology were investigated in film state. In addition, a comparison analysis was conducted with the films fabricated by the dissolution method using highly soluble dyes developed in the previous chapter. This research into the fabrication of films using colorants of a similar structure allows a more accurate analysis of the film characteristics according to the manufacturing method applied.

5.2 Experimental section

5.2.1 Materials and instrumentation

Perylene-3,4,9,10-tetracarboxylic dianhydride, 2,6-diisopropylaniline, m-cresol, iodine, sulfuric acid, bromine, acetic acid, propionic acid, and potassium carbonate anhydrous purchased from Sigma-Aldrich, 3,4,5-trimethoxybenzyl alcohol, 3-isopropoxypropylamine and 3,4,5-trimethoxybenzyl amine purchased from TCI were used as received. All the other reagents and solvents were reagent-grade and obtained from commercial suppliers. Transparent glass substrates were provided by

Paul Marienfeld GmbH & Co. KG, and acrylic binder, dispersed millbase and black matrix resist were supplied by ChemE Inc.

^{1}H and ^{13}C NMR spectra were recorded on a Bruker Avance 500 spectrometer (National Center for Inter-university Research Facilities at Seoul National University) at 500 MHz using chloroform-d and TMS, as the solvents and internal standard, respectively. Matrix Assisted Laser Desorption/Ionization Time of Flight (MALDI-TOF) mass spectra were collected on a Voyager-DE STR Biospectrometry Workstation (National Center for Inter-university Research Facilities at Seoul National University) with α-cyano-4-hydroxycinnamic acid (CHCA) as the matrix. Absorption and transmittance spectra were measured using a Perkin-Elmer Lambda 25 spectrophotometer and fluorescence spectra were measured using a Perkin-Elmer LS 55. Thermogravimetric analysis (TGA) was conducted in a nitrogen atmosphere at a heating rate of 10 °C min^{-1} using a TA instruments Thermogravimetric Analyzer 2050. Chromatic characteristics of the black matrices were analyzed on a Scinco color spectrometer. The particle size of dyes in dispersion and solution state were evaluated using a dynamic light scattering (DLS) method using a Litesizer 500 Particle Analyzer. The viscosity of the dispersed and dissolved dyes and carbon black were measured using an Advanced Rheometric Expansion System. Dielectric constants of the black matrices were measured using an Edward E306 thermal evaporator and an HP 4294A precision impedance analyzer. The thickness of the black matrices was measured using a KLA-TENCOR Nanospec AFT/200 alpha step. The OD value of the black matrices was measured using X-rite 301 densitometer. The roughness of the black matrices was measured using NX-10 and typical surface morphology of the black matrices were imaged with merlin-compact FE-SEM and

JSM-7800F prime, using accelerating voltage of 2.0 kV at a working distance of 4.9-8.9 mm. In addition, to reduce charging of non-conductive sample surface on SEM analysis, Pt was coated by sputtering (JEOL MSC-101) onto the samples for 40 secs at a current strength of 40 mA.

5.2.2 Synthesis

The dyes **2**, **3, 4a-d and dimer 4a-b** are already known structures and were synthesized according to the previously reported procedures.

5.2.2.1 N,N'-Bis(2,6-diisopropylphenyl)-1-bromo-7-(3,4,5-trimethoxybenzyloxy)-perylene-3,4,9,10-tetracarboxylicdiimide (4a)

3 (1.00 g, 1.15 mmol), 3,4,5-trimethoxybenzyl alcohol (1.14 g, 5.76 mmol) and potassium carbonate (0.80 g, 5.76 mmol) in DMF (60 ml) was stirred under nitrogen atmosphere for 3h at 80 ℃. The reaction mixture was cooled to room temperature and poured into 0.5 M HCl (300 ml). The precipitate was filtered repeatedly washed with water, and dried in vacuum at 80 ℃. The crude product was purified by silica gel column chromatography with CH_2Cl_2 as eluent to obtain unreacted **3** (0.33 g, 33% yield) and desired **4a** as red solid compound (0.60 g, 53% yield). ^{1}H NMR ($CDCl_3$, 500 MHz): δ 9.67 (d, 1H, *J* = 13.6 Hz), 9.57 (d, 1H, *J* = 4.8 Hz), 9.03 (s, 1H), 8.72

(s, 1H), 8.72 (d, 1H, *J* = 2.4 Hz), 8.71 (d, 1H, *J* = 2.4 Hz), 7.54-7.50 (m, 2H), 7.38-7.35 (m, 4H), 6.80 (s,2H), 5.57 (s, 2H), 3.87 (s, 3H), 3.85 (s, 6H), 2.79-2.70 (septet, 4H), 1.20-1.18 (m, 24H); ^{13}C NMR (125 MHz, $CDCl_3$): δ 163.53, 162.89, 157.14, 153.91, 145.83, 145.78, 138.36, 137.05, 134.67, 134.02, 133.50, 131.76, 130.56, 130.51, 130.08, 130.02, 129.91, 129.20, 128.93, 128.80, 128.25, 124.51, 124.37, 124.33, 123.33, 122.62, 121.81, 121.40, 120.20, 119.34, 105.47, 77.48, 77.22, 76.97, 72.93, 61.13, 56.44, 29.46, 24.20; MALDI-TOF (m/z): calcd for $[M+3H]^{3+}$: 987.30. Found: 987.34; Elemental analysis: Calcd for $C_{58}H_{53}N_2O_8$: C 70.65; H 5.42; N 2.84; O 12.98. Found: C 70.62; H 5.49; N 2.75; O 12.73.

5.2.2.2 N,N'-Bis(2,6-diisopropylphenyl)-1-bromo-7-(3-isopropoxypropyl (anmino))-perylene-3,4,9,10-tetracarboxylicdiimide (4b)

4b was synthesized following the same procedure for **4a** using **3** (1.00 g, 1.15 mmol) and 3-isopropoxypropylamine (0.60 g, 5.76 mmol) in DMF (60 ml). The crude product was purified by silica gel column chromatography with CH_2Cl_2 as eluent to obtain **4b** as green solid compound (0.67 g, 64% yield). ^{1}H NMR ($CDCl_3$, 500 MHz): δ 9.49 (d, 1H, *J* = 13.6 Hz), 9.07 (d, 1H, *J* = 12.8 Hz), 8.98 (s, 1H), 8.71 (d, 1H, *J* = 12.8 Hz), 8.52 (d, 1H, *J* = 12.8 Hz), 8.31 (s, 1H), 7.52-7.48 (m, 2H), 7.36 (d, 4H, *J* = 12.8 Hz), 3.66-3.62 (m, 4H), 3.47-3.43 (m, 1H), 2.79-2.71 (septet, 4H), 2.15-2.12 (m, 2H), 1.20-1.66 (m, 24H), 0.86 (d, 6H, *J* = 9.6 Hz); ^{13}C NMR (125 MHz, $CDCl_3$): δ 163.88, 163.34, 163.01, 148.02, 145.87, 145.84, 145.81, 145.74, 138.71, 135.96, 135.31, 134.22, 132.32, 132.23, 131.85, 130.81, 130.74, 130.68,

129.87, 129.85, 129.14, 128.78, 126.06, 124.80, 124.32, 124.27, 123.46, 122.62, 121.96, 121.61, 119.58, 119.47, 119.34, 118.58, 114.72, 77.48, 77.22, 76.97, 72.46, 68.56, 45.31, 29.90, 29.44, 29.41, 29.05, 24.21, 24.18, 21.95, 21.89; MALDI-TOF (m/z): calcd for $[M+3H]^{3+}$: 906.31. Found: 906.29; Elemental analysis: Calcd for $C_{54}H_{54}N_3O_5$: C 71.67; H 6.01; N 4.64; O 8.84. Found: C 71.72; H 6.06; N 4.67; O 8.85.

5.2.2.3 N,N'-Bis(2,6-diisopropylphenyl)-1-bromo-7-(3-methoxybutoxy)-perylene-3,4,9,10-tetracarboxylicdiimide (4c)

4c was synthesized following the same procedure for **4a** using **3** (1.00 g, 1.15 mmol), 3-methoxy-1-butanol (0.60 g, 5.76 mmol) and potassium carbonate (0.80 g, 5.76 mmol) in *N,N*-dimethylmethanamide (DMF) (60 ml). The crude product was purified by silica gel column chromatography with CH_2Cl_2 as eluent to obtain unreacted **3** (0.65 g, 65% yield) and desired **4c** as red solid compound (0.19 g, 19% yield). ^{1}H NMR ($CDCl_3$, 500 MHz): δ 9.66 (d, 1H, *J* = 12.8 Hz), 9.55 (d, 1H, *J* = 13.6 Hz), 9.03 (s, 1H), 8.78 (d, 1H, *J* = 13.6 Hz), 8,71 (d, 1H, *J* = 12.8 Hz), 8.62 (s, 1H), 7.53-7.50 (m, 2H), 7.38-7.36 (m, 4H), 4.70-4.64 (m, 2H), 3.72 (sextet, 1H), 3.39 (s, 3H), 2.80 (septet, 4H), 2.25-2.73 (m, 2H), 1.32 (d, 4H, *J* = 10.4 Hz), 1.20-1.89 (m, 24H); ^{13}C NMR (125 MHz, $CDCl_3$): δ 163.61, 163.59, 163.56, 162.97, 157.83, 145.86, 145.82, 138.56, 134.77, 134.22, 133.42, 131.87, 130.62, 130.58, 130.09, 129.96, 129.83, 129.15, 128.67, 128.54, 128.30, 124.37, 124.34, 123.33, 122.53, 121.65, 120.75, 119.98, 118.85, 77.48, 77.22, 76.97, 73.83, 67.96, 56.46,

36.75, 29.45, 24.23, 19.46; MALDI-TOF (m/z): calcd for $[M+3H]^{3+}$: 893.20. Found: 893.42; Elemental analysis: calcd for $C_{53}H_{51}N_2O_6$: C, 71.37; H, 5.76; N, 3.14; O, 10.76. Found: C, 71.35; H, 5.90; N, 3.00; O, 10.84.

5.2.2.4 N,N'-Bis(2,6-diisopropylphenyl)-1-bromo-7-(1-butoxy-2-propanyloxy)-perylene-3,4,9,10-tetracarboxylicdiimide (4d)

4d was synthesized following the same procedure for **4a** using **3** (1.00 g, 1.15 mmol), 1-butoxy-2-propanol (0.76 g, 5.76 mmol) and potassium carbonate (0.80 g, 5.76 mmol) in DMF (60 ml). The crude product was purified by silica gel column chromatography with CH_2Cl_2 as eluent to obtain unreacted **3** (0.61 g, 61% yield) and desired **4d** as red solid compound (0.17 g, 0.16% yield). ^{1}H NMR ($CDCl_3$, 500 MHz): δ 9.64 (d, 1H, J = 12.8 Hz), 9.62 (d, 1H, J = 10.4 Hz), 9.02 (s, 1H), 8.76 (d, 1H, J = 12.8 Hz), 8.69 (d, 1H, J = 12.8 Hz), 8.63 (s, 1H), 7.53-7.50 (m, 2H), 7.37-7.36 (m, 4H), 5.22-5.20 (m, 1H), 3.84-3.76 (m, 2H), 3.56-3.51 (m, 2H), 2.79-2.72 (septet, 4H), 1.57-1.56 (m, 2H), 1.55 (s, 1H), 1.20-1.19 (m, 24H), 0.85 (t, 3H, J = 12.0 Hz); ^{13}C NMR (125 MHz, $CDCl_3$): δ 163.66, 163.60, 163.56, 163.50, 163.01, 157.69, 157.42, 157.16, 145.82, 138.45, 134.77, 133.40, 131.89, 130.65, 130.61, 130.10, 130.00, 129.96, 129.93, 129.86, 129.08, 129.05, 128.49, 128.21, 123.28, 122.51, 121.69, 121.55, 120.49, 119.89, 118.85, 74.16, 71.76, 69.31, 31.92, 29.44, 24.23, 19.44, 17.39, 14.04; MALDI-TOF (m/z): calcd for $[M+3H]^{3+}$: 921.32. Found: 921.49; Elemental analysis: Calcd for $C_{55}H_{55}N_2O_6$: C 71.81; H 6.03; N 3.05; O 10.43. Found: C 71.85; H 6.17; N 3.17; O 10.18.

5.2.2.5 N,N'-Bis(2,6-diisopropylphenyl)-1-bromo-7-(3,4,5-trimethoxybenzyl (amino))-perylene-3,4,9,10-tetracarboxylicdiimide (4e)

4e was synthesized following the same procedure for **4a** using **3** (1.00 g, 1.15 mmol) and 3,4,5-trimethoxybenzyl amine (2.27 g, 11.51 mmol) in *N,N*-dimethylmethanamide (DMF) (60 ml) was stirred under nitrogen atmosphere for 2.5 h at 80 ℃. The reaction mixture was cooled to room temperature and poured into 0.5 M HCl (300 ml). The precipitate was filtered, repeatedly washed with water, and dried in vacuum at 80 ℃. The crude product was purified by silica gel column chromatography with CH_2Cl_2 as eluent to obtain **4e** as green solid compound (0.51 g, 45% yield). ^{1}H NMR ($CDCl_3$, 500 MHz): δ 9.52 (d, 1H), 9.00 (d, 1H), 8.99 (s, 1H), 8.68 (d, 1H), 8.56 (d, 1H), 8.45 (s, 1H), 7.52 (m, 2H), 7.37 (m, 4H), 6.67 (s,2H), 6.31 (t, 1H), 4.64 (d, 2H), 3.86 (s, 6H), 3.85 (s, 3H), 2.77 (septet, 4H), 1.57 (m, 24H); ^{13}C NMR (125 MHz, $CDCl_3$): δ 163.73, 163.35, 162.94, 162.89, 154.06, 147.29, 147.02, 145.83, 145.76, 138.87, 138.21, 135.72, 135.19, 134.81, 132.57, 132.47, 131.87, 131.74, 130.72, 130.68, 130.62, 130.03, 129.97, 129.93, 129.86, 129.24, 128.91, 127.24, 126.69, 124.45, 124.36, 124.32, 123.52, 123.03, 121.80, 121.45, 120.25, 120.25, 119.80, 119.03, 115.49, 105.36, 77.48, 77.22, 76.97, 61.10, 56.50, 49.69, 29.91, 29.43, 24.20; MALDI-TOF (m/z): calcd for $[M+3H]^{3+}$: 983.31. Found: 986.30; Elemental analysis: Calcd for $C_{58}H_{53}N_2O_8$: C 70.73; H 5.53; N 4.27; O 11.37. Found: C 70.33; H 5.73; N 4.28; O 11.00.

5.2.2.6 4,4'-(Biphenyl)bis(N,N'-bis(2,6-diisopropylphenyl)-1-bromo-7-(3,4,5-trimethoxybenzyloxy)-perylene-3,4,9,10-tetracarboxylicdiimide) (dimer 4a)

4a (0.60 g, 0.61 mmol), biphenyl-4,4'-diboronic acid bis(pinacol) ester (0.12 g, 0.31 mmol) and $Pd(PPh_3)_4$ (0.4 g, 0.03 mmol) were added in degassed aqueous 2M potassium carbonate (24 ml) and tetrahydrofuran (THF, 48 ml). The reaction mixture was heated at reflux under nitrogen atmosphere for 18 h. After cooled to room temperature, the mixture was diluted with ethyl acetate and the aqueous layer was removed. Upon drying over anhydrous $MgSO_4$, the organic layer was condensed in vacuum. The crude products were purified by silica gel column chromatography with CH_2Cl_2 as eluent to obtain **dimer 4a** as red solid compound (0.29 g, 49% yield). ^{1}H NMR ($CDCl_3$, 500 MHz): δ 9.65 (d, 2H, *J* = 16.0 Hz), 8.78 (s, 2H), 8.74 (s, 2H), 8.72 (d, 2H, *J* = 4.8 Hz), 8.23-8.19 (m, 4H), 7.87 (d, 4H, *J* = 13.6 Hz), 7.72 (d, 4H, *J* = 5.6 Hz), 7.52-7.48 (m, 4H), 7.37-7.32 (m, 8H), 6.84 (s, 4H), 5.60 (s, 4H), 3.85 (s, 6H), 3.88 (s, 6H), 3.87 (s, 12H), 2.81-2.70 (m, 8H), 1.20-1.14 (m, 48H); ^{13}C NMR (125 MHz, $CDCl_3$): δ 163.85, 163.82, 163.57, 163.54, 157.43, 157.06, 153.90, 145.79, 142.41, 142.32, 142.05, 140.51, 140.45, 140.37, 138.56, 136.07, 135.19, 135.00, 134.62, 133.50, 132.83, 131.69, 131.22, 130.79, 130.71, 130.62, 130.29, 129.99, 129.92, 129.88, 129.80, 129.60, 129.34, 129.19, 128.80, 128.75, 128.63, 124.86, 124.31, 124.17, 122.27, 122.23, 122.16, 121.98, 119.56; MALDI-TOF (m/z): calcd for $[M+H]^+$: 1964.83. Found: 1965.00; Elemental analysis: Calcd for $C_{128}H_{114}N_4O_{16}$: C 78.27; H 5.85; N 2.85; O 13.03. Found: C 78.28; H 5.97; N 2.76; O 12.39.

5.2.2.7 4,4'-(Biphenyl)bis(N,N'-bis(2,6-diisopropylphenyl)-1-bromo-7-(3-isopropoxypropyl(amino))-perylene-3,4,9,10-tetracarboxylicdiimide) (dimer 4b)

Dimer 4b was synthesized following the same procedure for **dimer 4a** using **4b** (0.60 g, 0.66 mmol), biphenyl-4,4'-diboronic acid bis(pinacol) ester (0.13 g, 0.33 mmol) and $Pd(PPh_3)_4$ (0.4 g, 0.03 mmol) in degassed aqueous 2 M potassium carbonate (24 ml) and THF (48 ml). The crude products were purified by silica gel column chromatography with CH_2Cl_2 as eluent to obtain **dimer 4b** as green solid compound (0.48 g, 81% yield). ^{1}H NMR ($CDCl_3$, 500 MHz): δ 9.10 (d, 2H, *J* = 12.8 Hz), 8.74 (s, 2H), 8.72 (d, 2H, *J* = 12.8 Hz), 8.31 (s, 2H), 8.06-8.01 (m, 4H), 7.84 (d, 4H, *J* = 11.2 Hz), 7.72 (d, 4H, *J* = 12.8 Hz), 7.51-7.45 (m, 4H), 7.36-7.31 (m, 8H), 3.69-3.68 (m, 4H), 3.67-3.63 (m, 4H), 3.53-3.48 (m, 2H), 2.81-2.72 (septet, 8H), 2.16-2.14 (m, 4H), 1.21-1.16 (m, 48H), 0.95 (d, 12H, *J* = 9.6 Hz); ^{13}C NMR (125 MHz, $CDCl_3$): δ 163.95, 163.74, 147.83, 145.84, 142.24, 140.27, 139.06, 136.84, 136.20, 134.22, 132.98, 132.19, 131.11, 130.88, 130.32, 130.16, 129.87, 129.76, 129.33, 128.98, 126.19, 124.52, 124.29, 124.23, 122.90, 122.26, 121.81, 121.31, 119.89, 119.58, 119.66, 77.48, 77.22, 76.97, 72.51, 68.35, 45.21, 29.91, 29.43, 29.33, 29.26, 24.27, 24.20, 22.07, 21.93; MALDI-TOF (m/z): calcd for $[M+H]^+$: 1802.88. Found: 1802.97; Elemental analysis: Calcd for $C_{120}H_{116}N_6O_{10}$: C 79.97; H 6.49; N 4.66; O 8.88. Found: C 79.81; H 6.46; N 4.42; O 8.36.

5.2.3 Preparation of dispersed of dyes

4a and 4b were mixed a dispersant polymer in PGMEA, respectively. Zr beads were then introduced into the mixture. After mixing, a pre-milling (60 min) was performed using a paint shaker, followed by main-milling (120 min) with 550 times/min. The pigment dispersion was isolated by vacuum filtering.

5.2.4 Preparation of black matrices

Two kinds of black matrices (M_{ab}, $M_{ab}C$) using dispersed dyes (4a and 4b) and two kinds of black matrices (D_{ab}, $D_{ab}C$) using dissolved dyes (dimer 4a and dimer 4b) were fabricated. The solutions for M_{ab} was composed of the dispersed solution of the dyes (0.10 g), PGMEA (3.34 g), acrylic binder (0.16 g). The solutions for $M_{ab}C$ was composed of the dispersed solution of the dyes (0.10 g), PGMEA (2.13 g), acrylic binder (0.97 g), and carbon black resist (0.02 g). The solutions D_{ab} was composed of the dyes (0.08 g), PGMEA (4.27 g) and acrylic binder (0.13 g). The solutions for $M_{ab}C$ was composed of the dispersed solution of the dyes (0.08 g), PGMEA (3.14 g), acrylic binder (0.97 g), and carbon black resist (0.03 g). The prepared solutions were coated on a transparent glass substrate using a MIDAS System SPIN-1200D spin coater. The coating speed was initially 250 rpm for 20 sec, which was then increased to 400 rpm and kept constant for 10 sec. The wet coated black matrices were then dried at 40 °C for 20 min, prebaked 100 °C for 100 sec, and

post baked at 230 ℃ for three times every 30 min. After each step, the coordinate values of the black matrices were measured.

5.2.5 Geometry optimization of the synthesized dyes

The geometry and electric structure of the studied dyes are optimized by the density functional theory (DFT) method at the B3LYP/6-31G (d, p) performed on Gaussian 09 program.

5.3 Results and Discussion

5.3.1 Synthesis

The PDI dyes were chosen for their high stability and light absorbing ability [19, 20]. In addition, substituents capable of inducing fluorescence quenching were introduced at the bay position of the dyes to prevent an unwanted light generation. The synthesis procedure and the structure of the dyes are depicted in scheme 5.1. 4a, 4b, dimer 4a, and dimer 4b were chosen for a comparative study of the dissolved and dispersed states, respectively, due to their low-fluorescence quantum yield. 4a, 4b,

dimer 4a, dimer 4b, E1, and E2 were synthesized in the previous chapter, and A1 was newly synthesized to evaluate the effects of the aryl compound on the fluorescence of the dye as compared to alkyl-group substituted dyes (4b, E1, and E2). Perylene-3,4,9,10-tetracarboxylic dianhydride was refluxed in H_2SO_4 with bromine to obtain 1,7-dibromo PDI. A highly soluble dibromo PDI was obtained through the imidization of 2,6-diisopropyl aniline on the periphery position of the dyes. The imidized aniline ring is twisted at a large angle to the perylene core, which contributes to the prevention of the intermolecular stacking and the enhancement of solubility of the dye. Electron donating groups, such as ether and amino groups, were introduced at the PDI bay position to develop the dyes in various light-absorbing regions. The monomeric PDIs were synthesized to dimeric PDIs (dimer 4a and 4b) containing diphenyl group as a linker through the Suzuki–Miyaura coupling reaction. The structures of the intermediates and dyes were confirmed by ^{1}H NMR, ^{13}C NMR, and MALDI-TOF spectroscopy and elemental analyses.

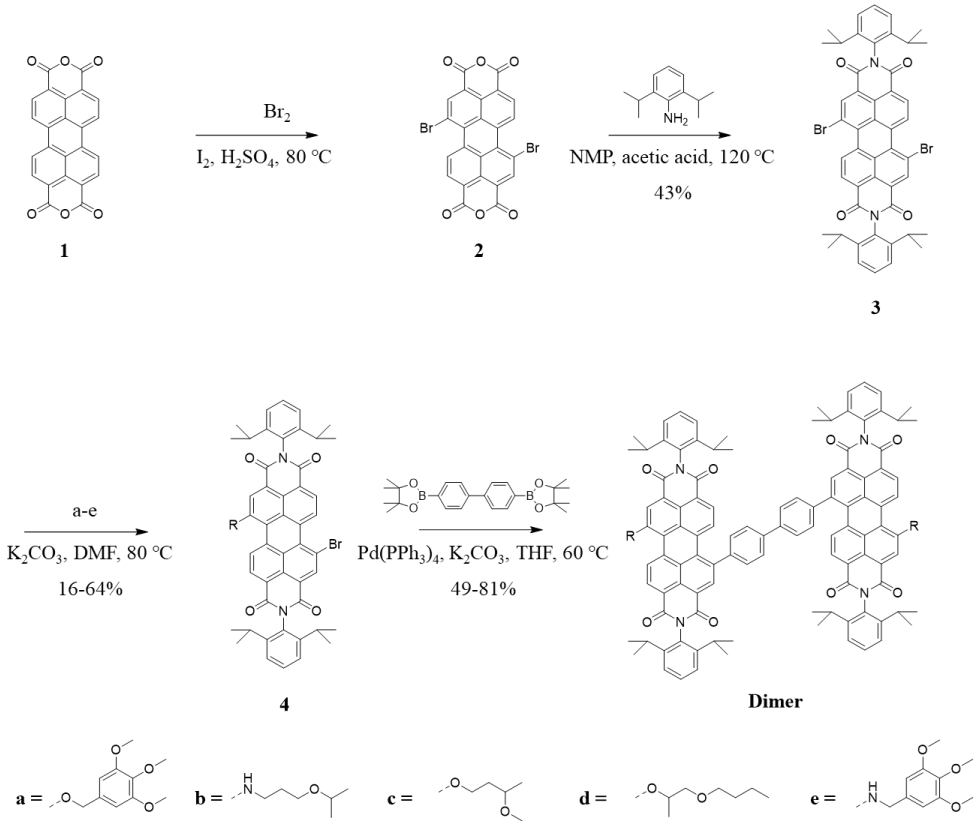

Scheme 5.1. Synthesis of PDI dyes.

5.3.2 Spectral properties of the dyes in a liquid state

Since the dispersion solution (5 wt%, 0.051 and 0.055 M for 4a and 4b, respectively) showed a high absorbance above the measurement limit of the instrument, the spectroscopic properties of the dyes in liquid state were measured as a diluted solution at a concentration of 10^{-5} M and presented in Fig. 5.1 and Table 5.1.

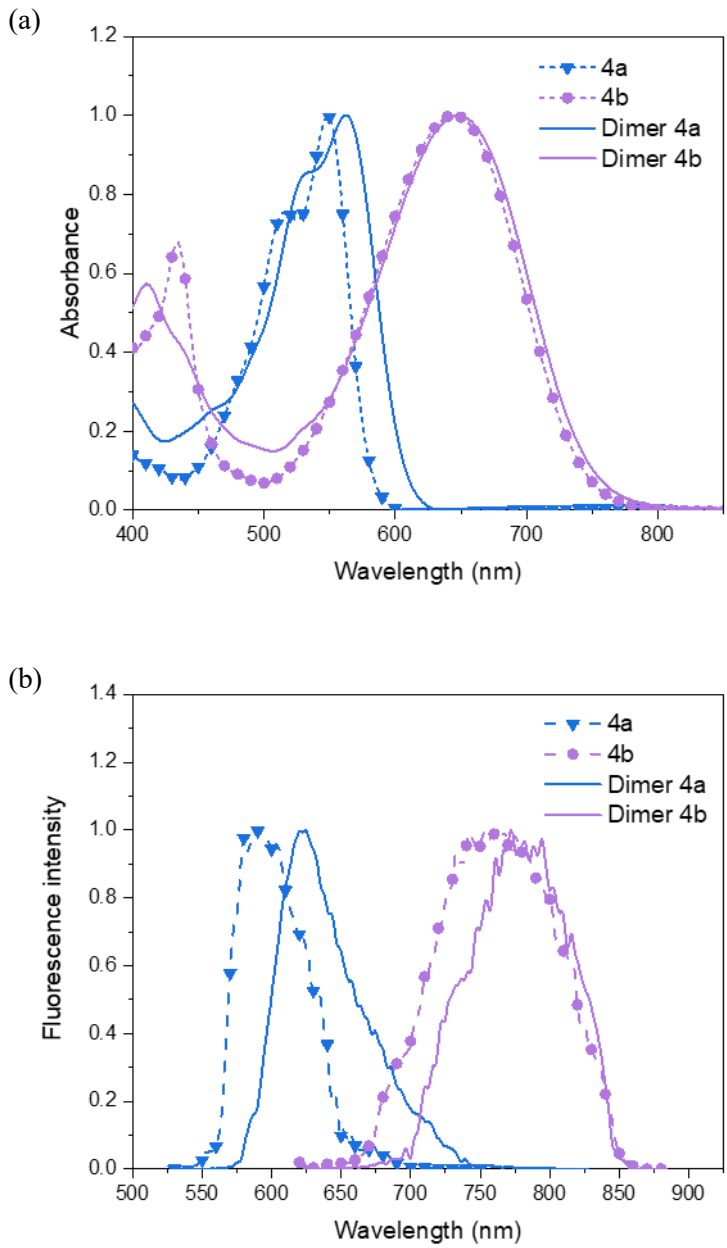

Figure 5.1. Normalized absorption (a) and normalized emission (b), of the dyes in PGMEA.

Table 5.1. Spectroscopic data of the dyes in PGMEA.

Dye	λ_{abs} (nm)	λ_{em} (nm)	ε (10^4 M^{-1} cm^{-1})
4a	549	598	4.92
4b	648	597	4.11
Dimer 4a	562	624	6.05
Dimer 4b	647	782	5.44

4a and 4b showed significantly different band shapes and this spectral characteristic, as investigated in a previous chapter, is due to the difference in the core distortion angle of the dyes [21]. The core distortion angle of 4b (21.17°) is larger than that of 4a (14.71°), which is caused by a steric hindrance occurring between the H atom of the substituted amino group and the H atom of the adjacent bay position of the PDI. As a result, the vibronic coupling is weakened and a broad absorption spectrum is obtained in 4b. By contrast, in the case of 4a, the 0-0 and 0-1 transitions were clearly shown in the absorption spectrum due to the stronger vibronic coupling than in 4b.

The fluorescence of the synthetic dyes showed low intensity, and the fluorescence quantum yields were lower than 0.04, whereas a near unity fluorescence quantum yield was measured for an unsubstituted PDI (0.92). This fluorescence quenching can occur through an intramolecular charge transfer (ICT), which is generated from a covalently bonded donor (amine and ether group)-acceptor (perylene) molecular structure [24, 25]. As the excited dipole moment induced from ICT increases, the

energy level of the excited molecule is decreased through non-radiative decay, such as intersystem crossing and solvent relaxation [26]. The ICT determined by Lippert–Mataga plot, which shows the Stokes shift of the dye ($\Delta\nu$) according to the polarizability of the solvent (Δf), and the plots for 4a and 4b are shown in Fig. 5.2 and Table 5.2. Both 4a and 4b demonstrated a positive slope in the Lippert–Mataga plots, confirming that ICT clearly occurred.

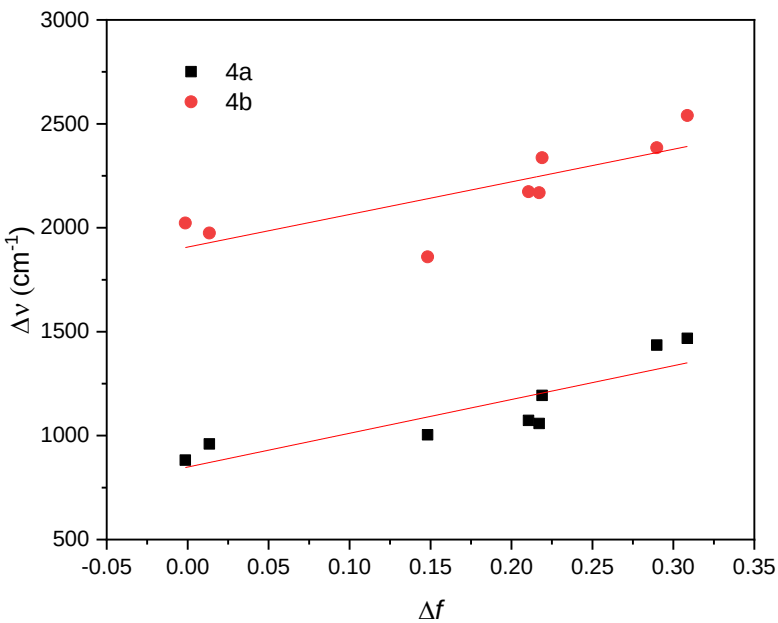

Figure 5.2. Lippert-Mataga plot for the dyes in various solvents.

Table 5.2. Summary of spectroscopic data of the dissolved dyes in various solvents. Solvents are listed in their order of the orientation polarizability.

		Hexane	Toluene	CF	THF	MC	EtOH	MeOH
	Δf	0	0.014	0.148	0.210	0.217	0.289	0.309
4a	λ_{abs} (nm)	540	553	553	550	554	552	551
	λ_{em} (nm)	567	584	586	584	588	600	600
	ε (10^4 M^{-1} cm^{-1})	4.48	4.02	4.25	4.07	4.27	4.18	4.04
	Φ_F	0.13	0.26	0.10	0.05	0.03	0.02	0.02
4b	λ_{abs} (nm)	617	643	647	646	651	658	659
	λ_{em} (nm)	705	737	736	751	758	780	791
	ε (10^4 M^{-1} cm^{-1})	3.47	3.49	3.89	3.54	4.11	3.53	3.62
	Φ_F	0.03	0.02	0.02	0.01	0.01	0.01	0.00

The chemical shift of the H atoms indicated in Fig. 5.3 changed according to the electron donating power of the substituents. An amino group moved the chemical shift of the H atoms toward the upper-field compared to the H atoms of the ether group. This change in chemical shift demonstrates that the electron donating power of the amino group is stronger than that of the ether group. The high electron donating ability of 4b enhances the charge transfer between the donor and acceptor in an excited state, and the fluorescent quantum yield of 4b showed a lower value than that of 4a due to a non-radiative decay occurring during this process [26].

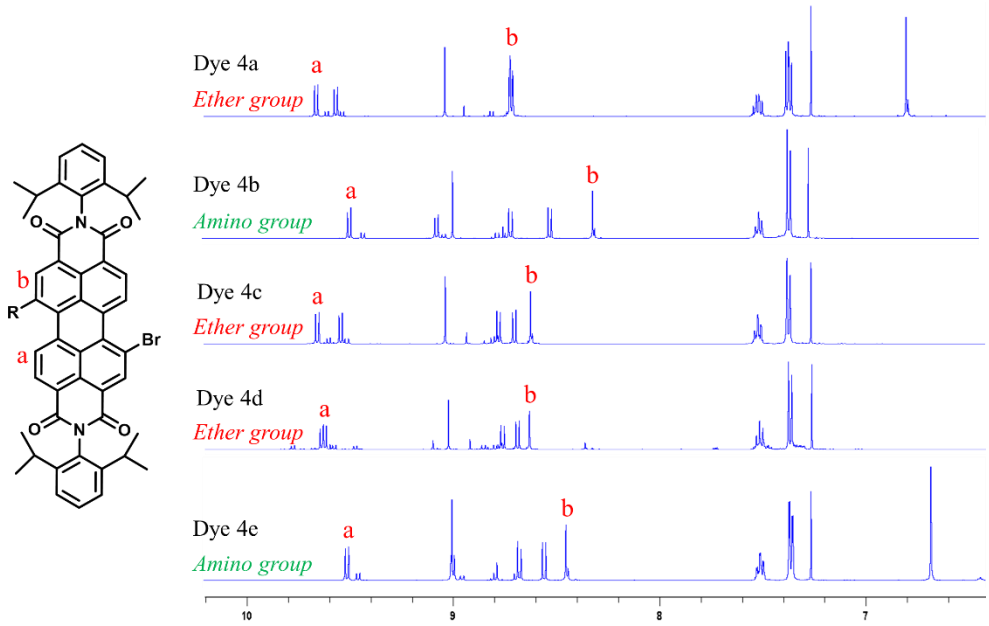

Figure 5.3. ^{1}H NMR (500 MHz) spectra of the aromatic region of the dyes containing ether group (4a, 4c and 4d) and amino group (4b and 4e). The labeled peaks correspond to the protons of PDI core adjacent to the O or N atoms of the dyes.

Because the chemical shifts of the H atoms in the aromatic region of the ether group with a substituted 4a, 4c, and 4d have similar values, it is considered that 4a does not show a significant difference in the electron donating power of the substituents as compared with 4c and 4d. However, the fluorescence quantum yield of the dyes is significantly different, as listed in Table 5.3. This suggests that the fluorescence of the PDI is influenced not only by the electron donating ability attached to the bay position.

Table 5.3. Fluorescence quantum yield of the dyes in PGMEA.

	4a	4b	4c	4d	4e	Unsubstituted PDI
Fluorescence QY	0.04	0.0	0.81	0.75	0.02	0.92

The major structural difference between 4a and dye 4c and 4d is the presence of an aromatic ring. According to the computational calculations [21, 22], the aromatic ring has a larger rotational energy barrier than the alkyl group bonded to the same resonance structure [27, 28]. Because a rotational motion in the molecules is one of the typical reasons for the dissipation of the molecular excitation energy through a non-radiative pathway [29, 30], the fluorescence properties of the dyes were measured by varying the rotational motion. The viscosity of the solvent was controlled by varying the amount of glycerol mixed in ethanol, thereby influencing the intramolecular rotation, and the changes in the fluorescence and absorption by viscosity are plotted in Figs. 5.4 and 5.5.

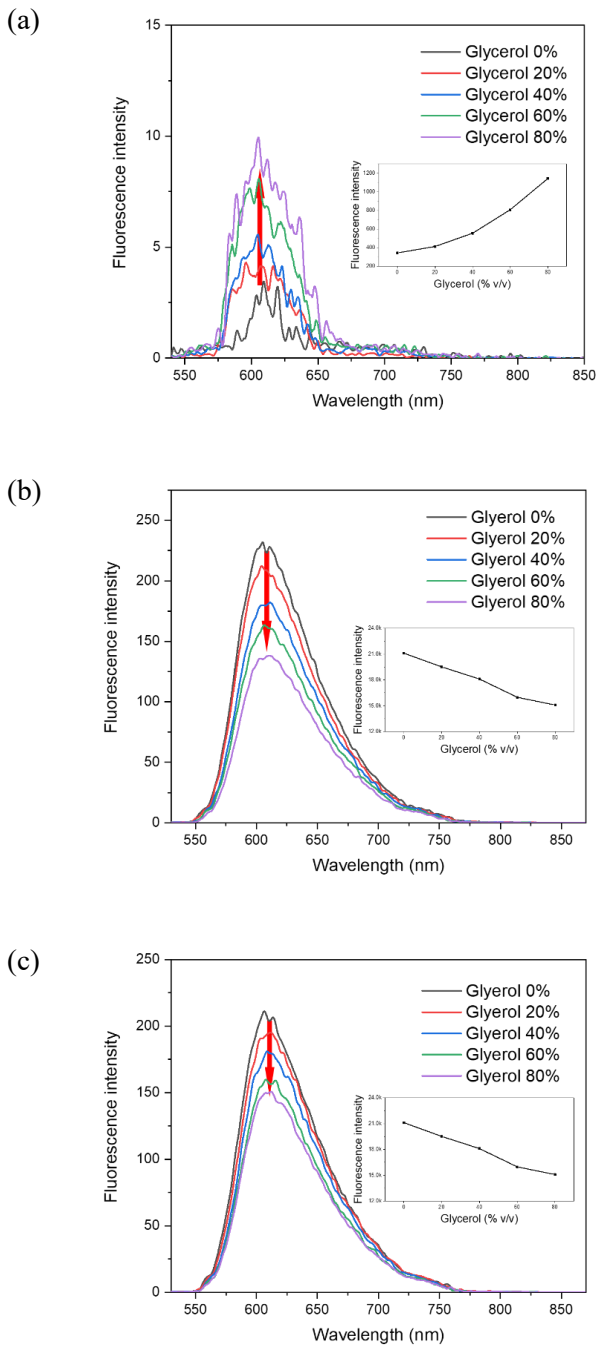

Figure 5.4. Emission spectra of the dyes with ether group in various viscosity: (a) 4a; (b) 4c; (c) 4d. The fluorescence of 4a, 4c, and 4d was measured using a filter reducing the intensity to 1% due to instrumental limitations.

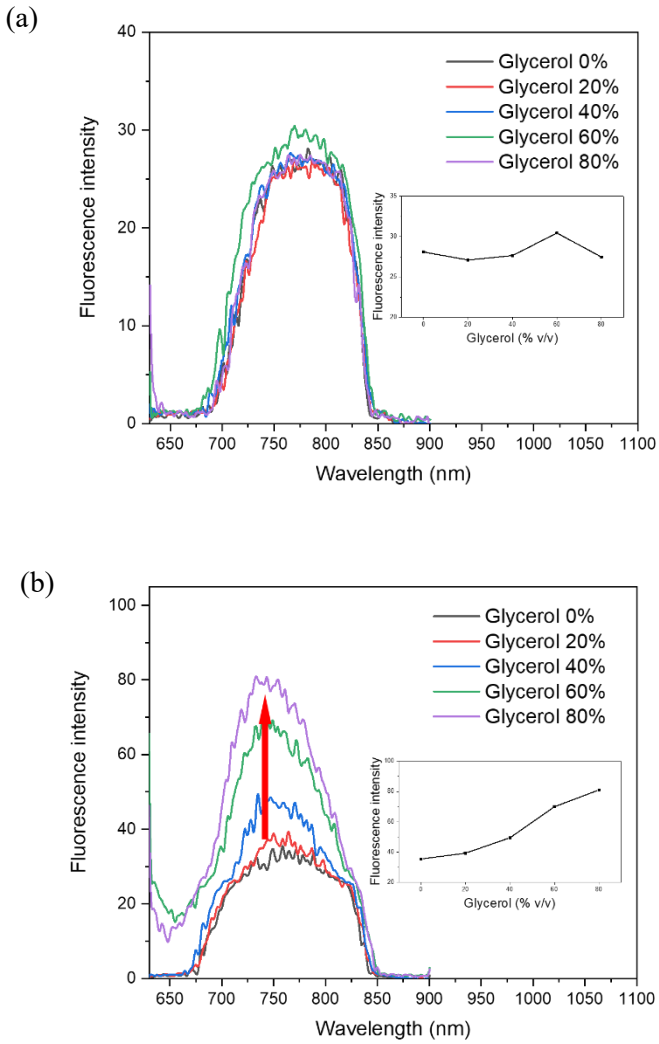

Figure 5.5. Emission spectra of the dyes with amino group in various viscosity: (a) 4b; (b) 4e.

According to the fluorescence spectra shown in Fig. 5.4, the fluorescence intensity of 4c and 4d, which were substituted with an alkoxy group, tends to decrease with an increase in the solvent viscosity. This reduction in the fluorescence is considered to be aggregation-caused quenching under a high glycerol concentration. On the other hand, an aromatic ring attached 4a showed an increasing fluorescence intensity as the viscosity is increased. This change in fluorescence intensity of 4a is due to the restricted intramolecular rotation (RIR) of the aromatic ring in the solutions of high viscosity, which converts the non-radiative decay into radiative decay. The same fluorescence tendency of the aryl and alkyl groups was also observed in the alkyl-amino substituted 4b and aryl-amino substituted 4e (Fig. 5.5).

As shown in Figs. 5.6 and 5.7, the absorption intensities of the dyes were almost equivalent regardless of the glycerol concentration, unlike the fluorescence intensities of the dyes. However, the aggregation phenomena of dyes with an increasing glycerol volume ratio were also observed through the band shape of the absorption spectra. The most typical spectral change in the absorption induced from the aggregation of PDI is presented in the absorption peak intensity ratio (I_{0-0}/I_{0-1}), which tends to be reduced by the aggregation [31-33]. As listed in Table 5.4, the peak intensity ratio of 4a and 4c showed a smaller value at a concentration with 80% glycerol than that under the other concentrations. These results indicate that 4a and 4c, which have low solubility in glycerol, aggregated as the volume ratio of glycerol was increased. The 0-0 and 0-1 vibrational transitions of 4b, 4d and 4e in absorption spectra are difficult to separate. However, as shown in Table 5.5, the increase in full width at half maximum (FWHM) with an increasing glycerol content was observed in 4b and 4e, indicating that aggregation had occurred [34].

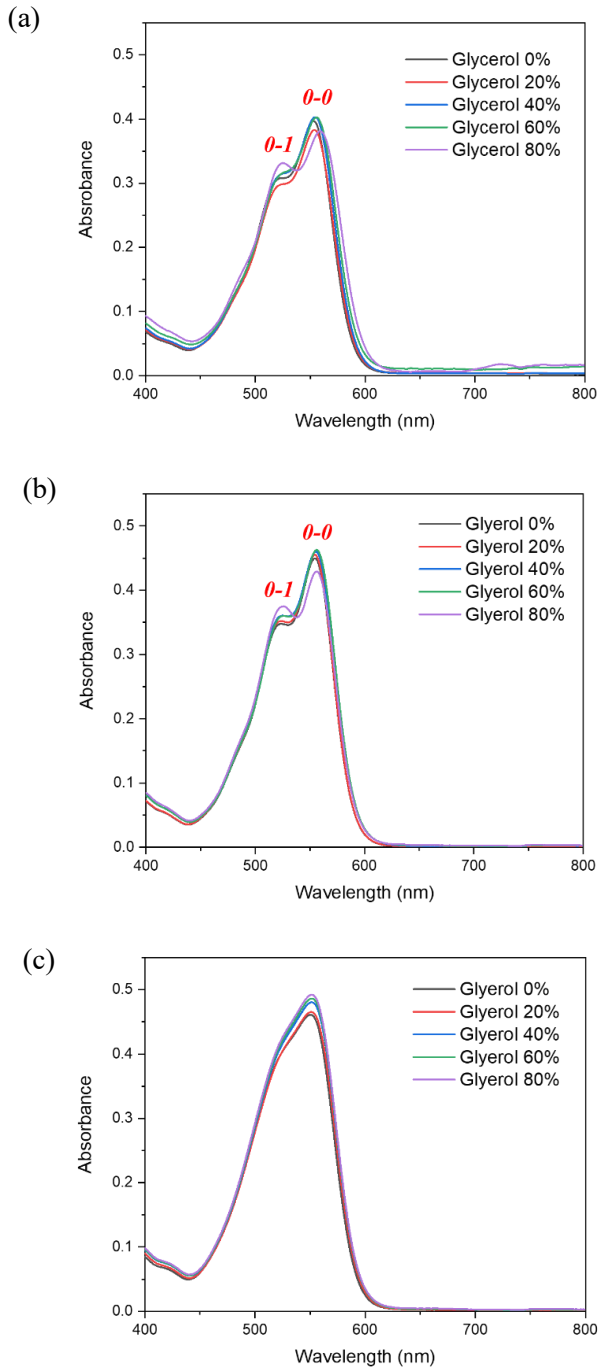

Figure 5.6. Absorption spectra of the dyes with ether group in various viscosity: (a) 4a; (b) 4c; (c) 4d.

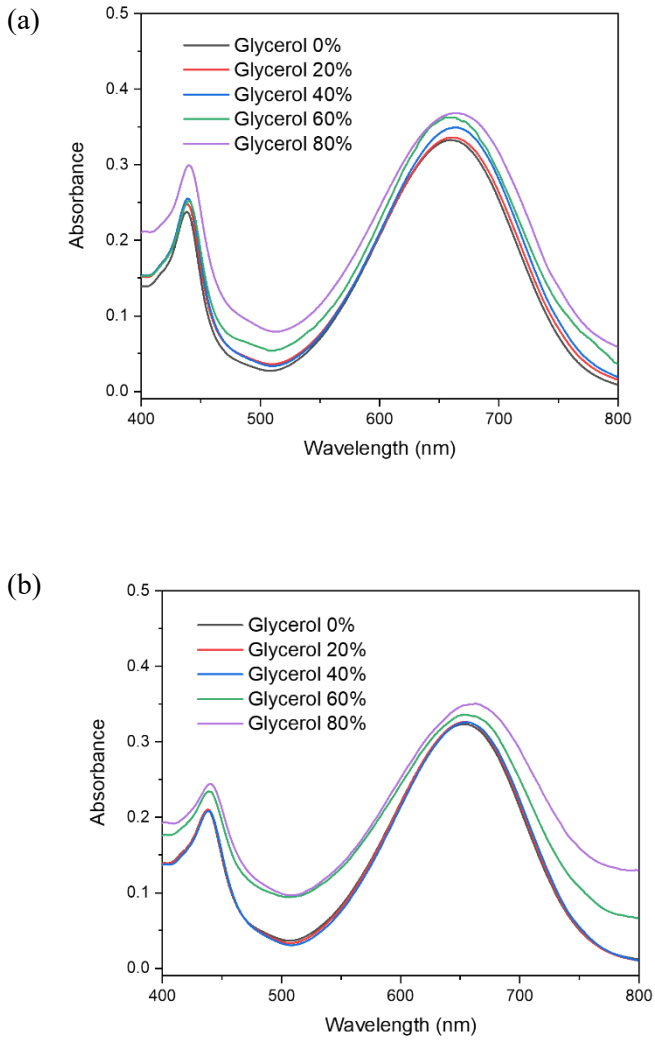

Figure 5.7. Absorption spectra of the dyes with amino group in various viscosity: (a) 4b; (b) 4e.

Table 5.4. Peak intensity ratio (I_{0-0}/I_{0-1}) of 4a and 4b.

	Glycerol 0%	Glycerol 20%	Glycerol 40%	Glycerol 60%	Glycerol 80%
4a	1.30	1.29	1.29	1.30	1.15
E1	1.29	1.29	1.28	1.29	1.15

Table 5.5. FWHM[a] of 4b and 4e.

	Glycerol 0%	Glycerol 20%	Glycerol 40%	Glycerol 60%	Glycerol 80%
4b	126	130	125	145	143
A1	117	118	117	140	157

[a] The FWHM value was estimated by doubling the right half-width of the absorption band

5.3.3 Computational studies of the dyes

The electron densities of the dyes were predicted by DFT calculations and the frontier molecular orbitals, and the energy levels in the highest occupied molecular orbital (HOMO) and lowest unoccupied molecular orbital (LUMO) resulting from the calculations are shown in Fig. 5.8. The energy gap between the HOMO and LUMO tends to decrease through an increase in the HOMO level by the substitution of the donating group at the bay position of the PDI without changes in the LUMO level [35]. The calculated HOMO and LUMO levels showed that decreasing the energy gap by increasing the electron donating ability of the bay substituent occurs

in the order of 4b > 4a > unsubstituted PDI. These results correlate with increasing maximum absorption wavelengths of the dyes (522 nm for unsubstituted PDI, 549 nm for 4a, and 648 nm for 4b).

The planarity of the PDI core is influenced by the bay position substituent and is reflected in the vibronic structure of the absorption spectrum. The dihedral angles of the dyes between two naphthalene units attached at central benzene ring were calculated by DFT to confirm the relationship of the core planarity and the absorption band shape. The distortion angle of the bromine-substituted bay position was calculated to be similar for 4a and 4b at 21.63° and 21.97°, respectively. However, the distortion angles of the donating group-substituted bay position were calculated to different angles (14.71° for 4a and 21.73° for 4b). The O atom of the ether group and the H atom of the adjacent bay position are at a distance of 2.06 Å, and weak hydrogen bonding is possible at this distance [36], whereas the amine group was sterically hindered owing to the H atom of the amine group. The core distortion angle of 4b is larger than that of 4a because of these structural features. The low planarity of 4b interferes with the vibronic coupling of the molecule, and as shown in Fig. 5.1. (a), the absorption spectrum of 4b indicates a broad-band shape with no visible vibrational peaks. By contrast, the planar 4a, as compared to 4b, exhibited an absorption spectrum with evident 0-0 and 0-1 electronic-vibrational transitions.

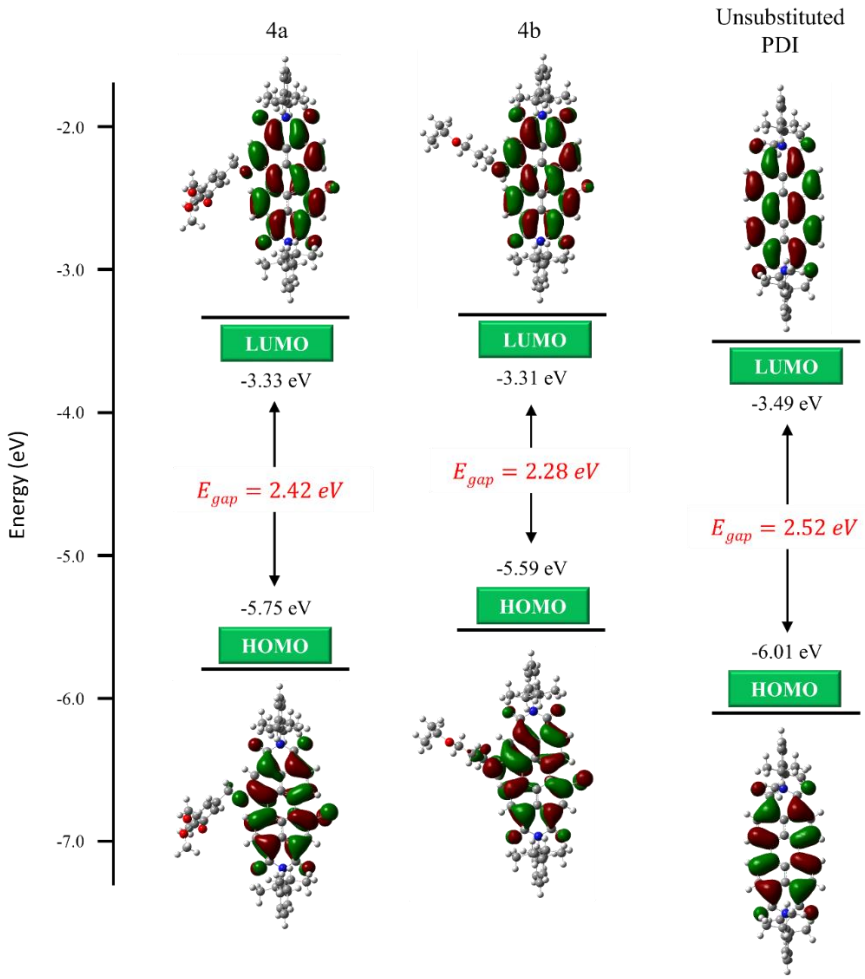

Figure 5.8. The frontier molecular orbitals of the LUMO and HOMO of 4a and 4b calculated by DFT at B3LYP/6-31G level.

5.3.4 Evaluation of dispersion properties

The particle sizes of the dispersed dyes and carbon black were measured through dynamic light scattering (DLS). The results of the DLS are shown in Fig. 5.9 and Table 5.6. The average particle sizes of the dispersed dyes and carbon black showed similar values of approximately 122.12–129.96 nm and the polydispersity index was increased in the order of carbon black, 4b, and 4a. The polydispersity index is a dimensionless measure of the broadness of the size distribution, and the high polydispersity index of 4a indicates that more agglomerates were formed at 4a than at 4b and carbon black [37].

The dispersibility of the dyes was also observed through the steady-state rheology behavior. The viscosity of the dye solutions mixed with a binder polymer was measured according to the shear rate at the same temperature (23 ℃) for this purpose [38, 39]. The same linear cardo binder was added under the same concentration in all solutions to minimize the effect of the binder polymer. In a solution with high dispersibility, a sufficient distance between the particles is maintained by the dispersion agent, and the short-range van der Waals attraction force is reduced. The internal resistance does not change with respect to the change in shear stress in this highly dispersed solution, and thus, the viscosity remains constant [40]. In this respect, the dispersed dyes and carbon black can be considered to maintain a well-dispersed state at a shear rate of between 10 and 1,000, as observed in Fig. 5.10. However, increased viscosities were observed at a shear rate of below 10 for the dyes. This increase in viscosity is due to the rearrangement of the structure, which occurs

at a low shear rate in a dispersion where particles of different sizes are randomly located. The particles were arranged in an ordered structure as the shear rate increased by more than 10, and the viscosity of the dispersed dyes was then maintained at a constant level [41].

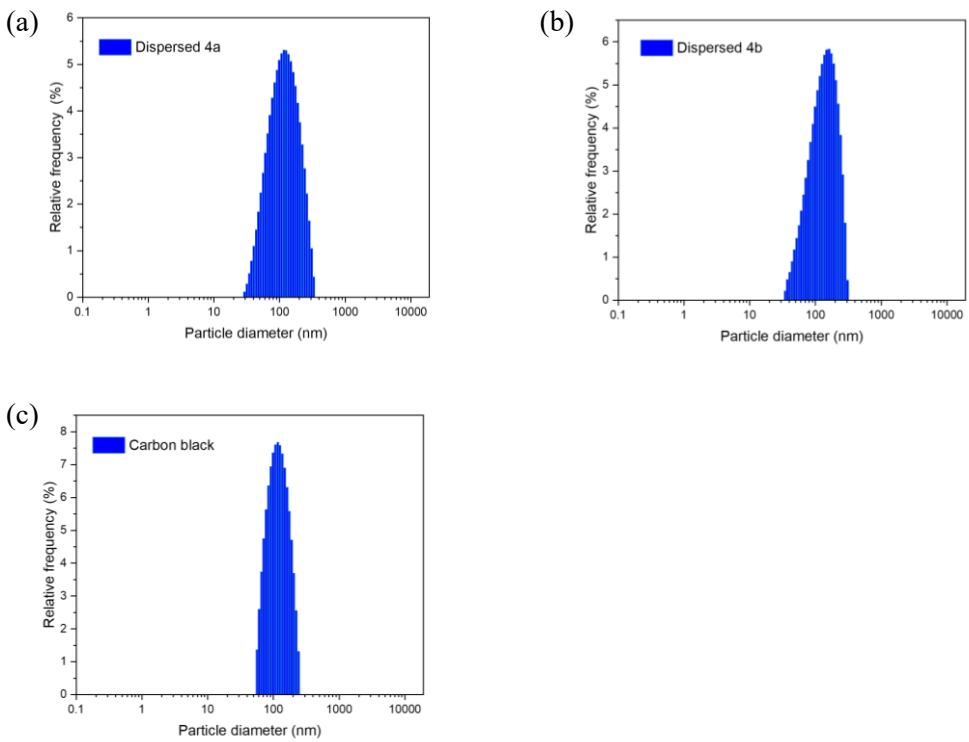

Figure 5.9. DLS results of the dyes and carbon black.

Table 5.6. Particle size and polydispersity index of the dyes and carbon black.

Dye / Pigment	4a	4b	Carbon black
Average particle size (nm)	122.12	129.96	123.44
Polydisperse index	1.32	1.29	1.13

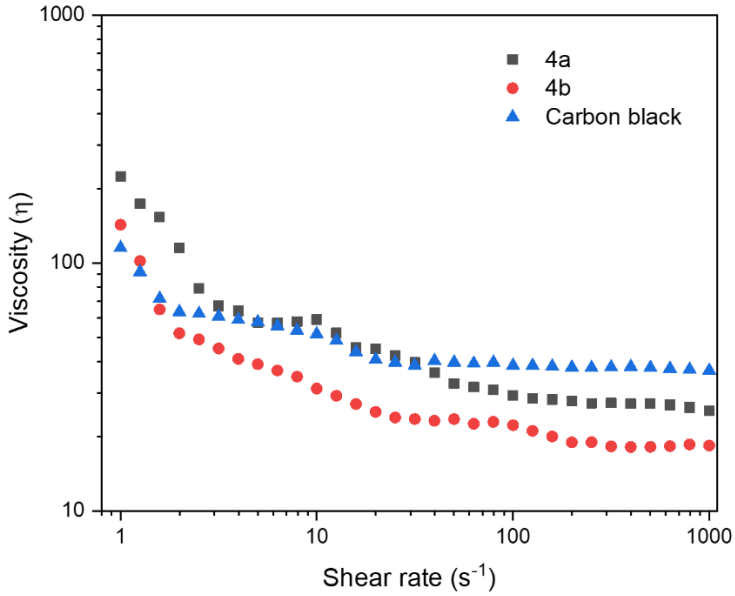

Figure 5.10. Steady-state viscosity as a function of shear rate for suspension of the dyes/carbon black with binder polymer from 1 to 10^3 s^{-1}.

5.3.5 Optical and thermal properties of black matrices

Black matrices were fabricated using the dispersed dye solutions, and the films were analyzed with a focus on the difference in their optical characteristics. Films using highly soluble dimeric PDIs were also fabricated with the dissolution method for comparison. In order to minimize the effect of structural difference on the film characteristics, dimeric PDIs with the same bay-substituents as 4a and 4b, respectively were chosen. The content of the dyes and carbon black in the fabricated dye-type and hybrid-type films were presented in Table 5.7.

Table 5.7. Blend ratio of fabricated black matrices.

Type		Film	Dye		Carbon black (wt%)
			4a (wt%)	4b (wt%)	
Dispersed solution	Hybrid-type	$M_{ab}C$	0.78	0.78	1.56
	Dye-type	M_{ab}	0.78	0.78	-
Dissolved solution	Hybrid-type	$D_{ab}C$	1.83	1.83	3.66
	Dye-type	D_{ab}	1.83	1.83	-

One prebaking and three postbaking stages were applied for the film fabrication; the color differences (ΔE_{ab}) of the films between each baking step are listed in Table 5.8 and Fig. 5.11, and the transmittance spectra of the films are shown in Fig. 5.12. The ΔE_{ab} and transmittance spectra during the baking process are the criteria for evaluating the thermal stability of the film. The black matrices fabricated with dissolution method exhibited better optical and thermal properties than black matrices fabricated with dispersion method.

Table 5.8. The ΔE_{ab} values of the fabricated black matrices.

	ΔE_{ab}		
	Pre-1st Post	1st Post-2nd Post	2nd Post-3rd Post
$M_{ab}C$	4.37	1.14	0.23
M_{ab}	7.75	5.42	2.57
$D_{ab}C$	1.21	0.40	0.25
D_{ab}	1.50	0.51	0.32

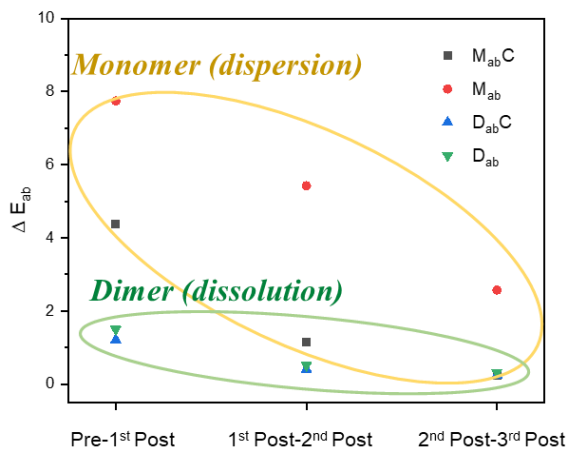

Figure 5.11. The ΔE_{ab} values of the fabricated black matrices.

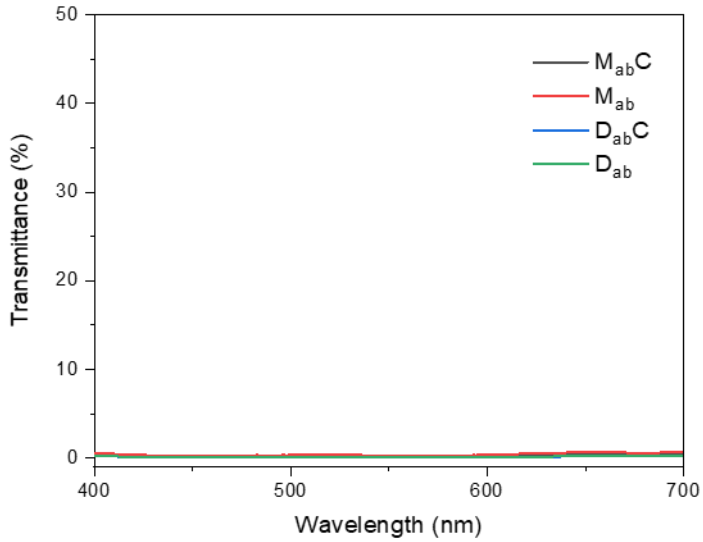

Figure 5.12. Transmittance spectra of the fabricated black matrices after 3rd postbake.

Table 5.9. Transmittance of the fabricated black matrices at specific wavelength after 3rd postbake.

	Dispersion method		Dissolution method	
	$M_{ab}C$	M_{ab}	$D_{ab}C$	D_{ab}
550 nm	0.23	0.30	0.11	0.12
700 nm	0.44	0.75	0.23	0.25

The thermal stability of dimers and monomers in the solid state was analyzed by TGA in the previous chapter and the results are shown in Table 5.10. The dimers have a smaller weight loss at 30 min of the isothermal region at 230 ℃ than the monomers. This difference in thermal stability of the dyes was reflected in that of the films. ΔE_{ab} of the dye-type film with the dissolved dimers (D_{ab}, 0.31–1.50) showed a lower value than the dye-type film with a dispersed solution (M_{ab}, 2.57–7.75). The same tendency in the color difference was also exhibited between the hybrid-type films, $D_{ab}C$ (0.25–1.21) and $M_{ab}C$ (0.23–4.37).

Table 5.10. Weight loss (%) of the dyes during 30 min of isothermal region at 230 ℃ examined by TGA.

4a	4b	Dimer 4a	Dimer 4b
0.77	6.24	0.19	0.63

The thermal stability of the film is also related to the presence of the carbon black. The hybrid-type films containing thermally stable carbon black exhibited a higher heat resistance than the dye-type films, and the thermal stability of the hybrid-type films revealed a low ΔE_{ab} with a small difference in the transmittance during the baking process.

The fluorescence of the fabricated films is shown in Fig. 5.13, and the fluorescence of the film 4a was detected in the visible region. This optical property is consistent with the liquid state fluorescence property of 4a, in which the

fluorescence intensity increases in a high viscosity medium. The intramolecular rotation of the substituent was limited in the film state as well, and an aggregation-induced emission occurred. However, as can be seen in the low fluorescence intensity of the other films, the fluorescence generated from 4a in the film state was reabsorbed by 4b or carbon black and did not affect the optical properties of the black matrices.

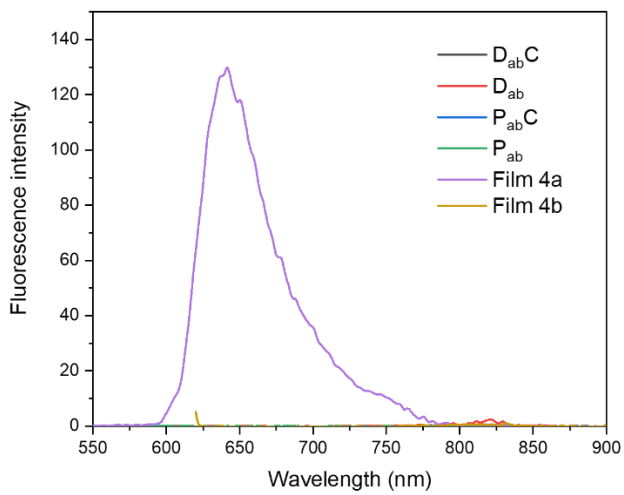

Figure 5.13. Emission spectra of the fabricated films after 3rd postbake.

5.3.6 Surface investigation of the fabricated film using AFM and FE-SEM

The roughness of the films (Rq) was investigated by scanning their surface using a non-contact mode AFM, and the results are shown in Fig. 5.14. The films fabricated with dispersed dyes or carbon black showed rough surface compare to D_{ab}. The highest Rq value among the fabricated films, namely, 2.47, was found at the $M_{ab}C$,

which was fabricated with the solution containing both dispersed dyes and carbon black.

The aggregated particles were found on the surface of M_{ab} in a 3D image, which is consistent with the DLS results of a dispersed solution measured in a liquid state. The surface of the D_{ab} exhibited more uniform surface than that of M_{ab}. However, Rq value of D_{ab} was increased due to large particles. It is considered that the coagulation process occurred in the baking process from dimer 4a, which have lower solubility than dimer 4b.

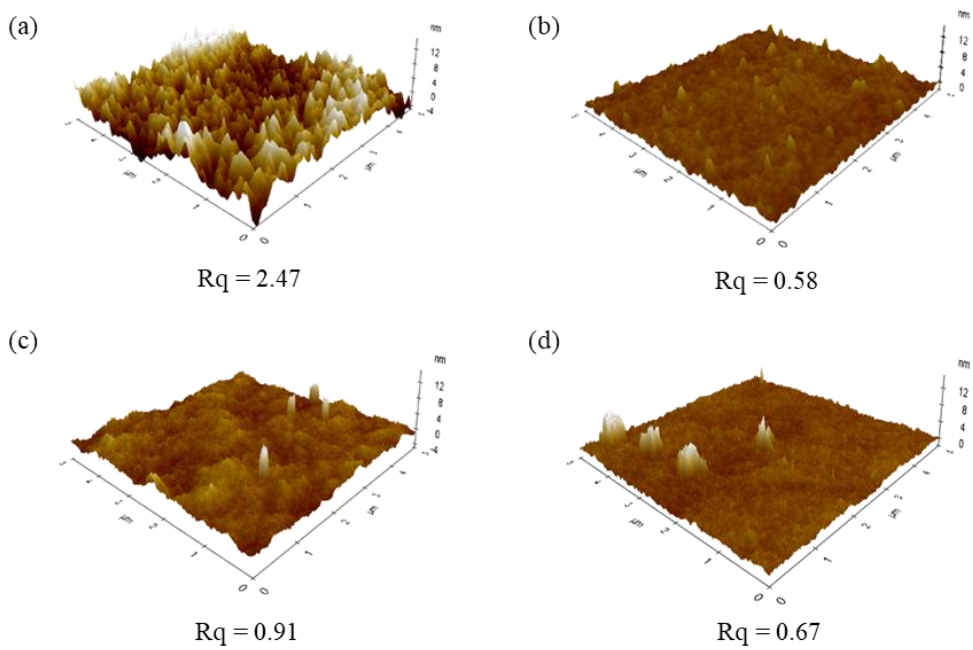

Figure 5.14. AFM images and surface roughness (Rq) of the fabricated black matrices: (a) $M_{ab}C$; (b) M_{ab}; (c) $D_{ab}C$; (d) D_{ab}.

FE-SEM measurement was also conducted to analyze the surface properties of the black matrices. According to the SEM images shown in Fig. 5.15, particles on the surface of M_{ab} were observed at an uneven size. In particular, particles of about 200 nm were formed in the surface of $M_{ab}C$ due to the effect of carbon black. On the other hand, the surface of D_{ab} displayed evenly dispersed particles of approximately 100 nm in size. $D_{ab}C$ particles were more heterogeneous than D_{ab}. However, $D_{ab}C$ exhibited high light absorbing ability than D_{ab} by the carbon black. Therefore, $D_{ab}C$ is considered to be more suitable for the black matrix.

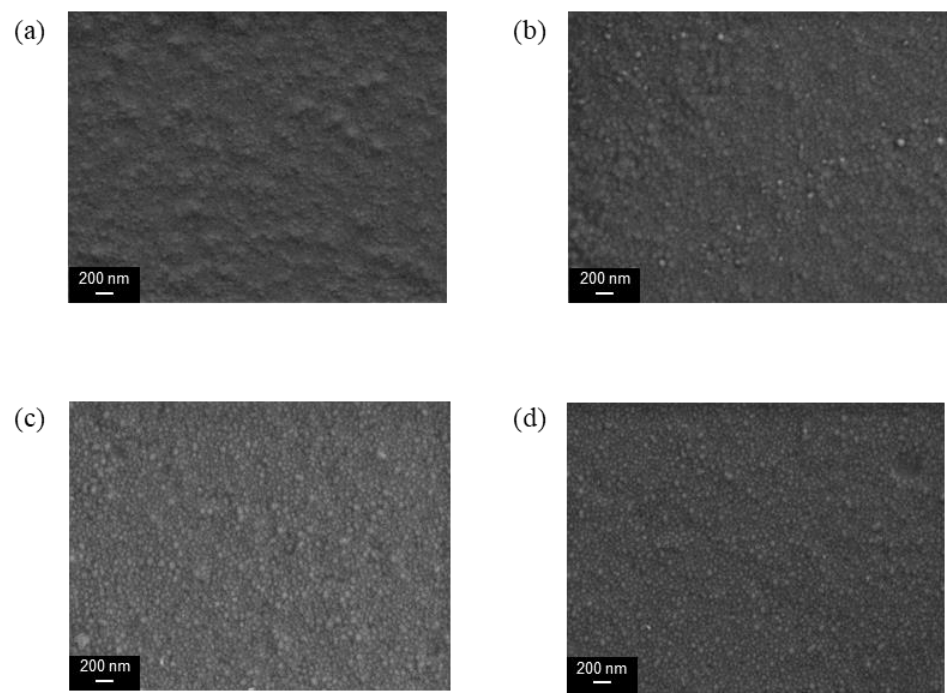

Figure 5.15. SEM images of the fabricated black matrices: (a) $M_{ab}C$; (b) M_{ab}; (c) $D_{ab}C$; (d) D_{ab}.

5.4 Conclusions

In this study, dispersed solutions were formulated for the dyes of low solubility, and the optical and physical properties of the dyes in both the liquid and film states were analyzed. The dyes were designed based on a PDI structure, which exhibits a high absorption ability and low fluorescence intensity suitable for a black matrix.

The fluorescence intensity of 4b was dramatically decreased compared to unsubstituted PDI due to ICT induced from the amino substituent of a high electron donating ability. The fluorescence quenching also occurred in 4a through ICT; however, an aggregation-induced emission appeared through the RIR of the benzyl substituent. The dispersibility of each dispersed dye was evaluated based on viscosity measurements of the steady-state rheology and a stable dispersibility of both dyes was confirmed according to the measured viscosity data.

The black matrices were fabricated by dispersion and dissolution method using monomers and dimers, respectively. Films $D_{ab}C$ and D_{ab} showed stronger light shielding ability and high thermal stability than films $M_{ab}C$ and M_{ab}. These results showed that the dissolution method is a better option for a black matrix with high optical and physical properties.

The microscopic structure of the films was examined using AFM and FE-SEM. The dispersion properties in a liquid state were similarly observed on the surface of the films. The Rq value of the films was less than 2.47, which is applicable to a black matrix. From the SEM images, even particle sizes and smooth surfaces were

observed at D_{ab} and $D_{ab}C$ compared to the films using the dispersed method.

The dyes applied to the hybrid-type black matrix through the dispersion method exhibited sufficient thermal stability and light-absorption ability. However, the film surface was less suitable for the black matrix compared with the films using the dissolution method. Therefore, this study suggests that the black matrices using highly soluble dimers by the dissolution method showed better optical and physical properties than black matrices using monomers of low solubility by the dispersion method.

5.5 References

[1] Horn D, Rieger J. Organic Nanoparticles in the Aqueous Phase—Theory, Experiment, and Use. Angewandte Chemie International Edition. 2001;40(23):4330-61.

[2] Kurokawa N, Yoshikawa H, Hirota N, Hyodo K, Masuhara H. Size-dependent spectroscopic properties and thermochromic behavior in poly(substituted thiophene) nanoparticles. Chemphyschem. 2004;5(10):1609-15.

[3] Norris DJ, Sacra A, Murray CB, Bawendi MG. Measurement of the size dependent hole spectrum in CdSe quantum dots. Phys Rev Lett. 1994;72(16):2612-5.

[4] Yagita Y, Matsui K. Size-dependent optical properties of 9,10-

bis(phenylethynyl)anthracene crystals. Journal of Luminescence. 2015;161:437-41.

[5] Asahi T, Sugiyama T, Masuhara H. Laser fabrication and spectroscopy of organic nanoparticles. Accounts of Chemical Research. 2008;41(12):1790-8.

[6] Oikawa H, Mitsui T, Onodera T, Kasai H, Nakanishi H, Sekiguchi T. Crystal Size Dependence of Fluorescence Spectra from Perylene Nanocrystals Evaluated by Scanning Near-Field Optical Microspectroscopy. Japanese Journal of Applied Physics. 2003;42(Part 2, No. 2A):L111-L3.

[7] Kasai H, Kamatani H, Okada S, Oikawa H, Matsuda H, Nakanishi H. Size-Dependent Colors and Luminescences of Organic Microcrystals. Japanese Journal of Applied Physics. 1996;35(Part 2, No. 2B):L221-L3.

[8] Tsuda K. Colour filters for LCDs. Displays. 1993;14(2):115-24.

[9] Choi J, Lee W, Namgoong JW, Kim T-M, Kim JP. Synthesis and characterization of novel triazatetrabenzcorrole dyes for LCD color filter and black matrix. Dyes and Pigments. 2013;99(2):357-65.

[10] Choi J, Sakong C, Choi J-H, Yoon C, Kim JP. Synthesis and characterization of some perylene dyes for dye-based LCD color filters. Dyes and Pigments. 2011;90(1):82-8.

[11] Sakong C, Kim YD, Choi J-H, Yoon C, Kim JP. The synthesis of thermally-stable red dyes for LCD color filters and analysis of their aggregation and spectral properties. Dyes and Pigments. 2011;88(2):166-73.

[12] Namgoong JW, Chung S-W, Jang H, Kim YH, Kwak MS, Kim JP. Improving

nanoparticle dispersions of pigment and its application to a color filter: New phthalocyanine derivatives as synergist. Journal of Industrial and Engineering Chemistry. 2018;58:266-77.

[13] Lee W, Choi J, Kim SH, Park J, Kim JP. Analysis and Characterization of Dye-Based Black Matrix Film of Low Dielectric Constant Containing Phthalocyanine and Perylene Dyes. Journal of Nanoscience and Nanotechnology. 2015;15(1):295-302.

[14] Lee W, Yuk SB, Choi J, Jung DH, Choi S-H, Park J, et al. Synthesis and characterization of solubility enhanced metal-free phthalocyanines for liquid crystal display black matrix of low dielectric constant. Dyes and Pigments. 2012;92(3):942-8.

[15] Koo H-S, Chen M, Pan P-C. LCD-based color filter films fabricated by a pigment-based colorant photo resist inks and printing technology. Thin Solid Films. 2006;515(3):896-901.

[16] Sabnis RW. Color filter technology for liquid crystal displays. Displays. 1999;20(3):119-29.

[17] Yuk SB, Lee W, Kim SH, Namgoong JW, Lee JM, Kim JP. Application of perylene dyes for low dielectric hybrid-type black matrices. Journal of Industrial and Engineering Chemistry. 2018;64:237-44.

[18] Yuk SB, Lee W, Namgoong JW, Choi J, Chang JB, Kim SH, et al. Synthesis and characterization of bay-substituted perylene dyes for LCD black matrix of low dielectric constant. Journal of Inclusion Phenomena and Macrocyclic Chemistry. 2015;82(1):187-94.

[19] Huang C, Barlow S, Marder SR. Perylene-3,4,9,10-tetracarboxylic acid diimides: synthesis, physical properties, and use in organic electronics. J Org Chem. 2011;76(8):2386-407.

[20] Kozma E, Catellani M. Perylene diimides based materials for organic solar cells. Dyes and Pigments. 2013;98(1):160-79.

[21] Chao CC, Leung MK, Su YO, Chiu KY, Lin TH, Shieh SJ, et al. Photophysical and electrochemical properties of 1,7-diaryl-substituted perylene diimides. J Org Chem. 2005;70(11):4323-31.

[22] Auweter H, Haberkorn H, Heckmann W, Horn D, Lüddecke E, Rieger J, et al. Supramolecular Structure of Precipitated Nanosize β-Carotene Particles. Angewandte Chemie International Edition. 1999;38(15):2188-91.

[23] Jia W-b, Wang H-w, Yang L-m, Lu H-b, Kong L, Tian Y-p, et al. Synthesis of two novel indolo[3,2-b]carbazole derivatives with aggregation-enhanced emission property. Journal of Materials Chemistry C. 2013;1(42):7092-101.

[24] Daub J, Engl R, Kurzawa J, Miller SE, Schneider S, Stockmann A, et al. Competition between Conformational Relaxation and Intramolecular Electron Transfer within Phenothiazine−Pyrene Dyads. The Journal of Physical Chemistry A. 2001;105(23):5655-65.

[25] Sumalekshmy S, Gopidas KR. Photoinduced Intramolecular Charge Transfer in Donor−Acceptor Substituted Tetrahydropyrenes. The Journal of Physical Chemistry B. 2004;108(12):3705-12.

[26] Inan D, Dubey RK, Westerveld N, Bleeker J, Jager WF, Grozema FC. Substitution Effects on the Photoinduced Charge-Transfer Properties of Novel Perylene-3,4,9,10-tetracarboxylic Acid Derivatives. J Phys Chem A. 2017;121(24):4633-44.

[27] Bryantsev VS, Firman TK, Hay BP. Conformational Analysis and Rotational Barriers of Alkyl- and Phenyl-Substituted Urea Derivatives. The Journal of Physical Chemistry A. 2005;109(5):832-42.

[28] Bradley JS. Homogeneous carbon monoxide hydrogenation to methanol catalyzed by soluble ruthenium complexes. Journal of the American Chemical Society. 1979;101(24):7419-21.

[29] Li H, Guo Y, Li G, Xiao H, Lei Y, Huang X, et al. Aggregation-Induced Fluorescence Emission Properties of Dicyanomethylene-1,4-dihydropyridine Derivatives. The Journal of Physical Chemistry C. 2015;119(12):6737-48.

[30] Wurthner F. Perylene bisimide dyes as versatile building blocks for functional supramolecular architectures. Chem Commun (Camb). 2004(14):1564-79.

[31] Bodapati JB, Icil H. Highly soluble perylene diimide and oligomeric diimide dyes combining perylene and hexa(ethylene glycol) units: Synthesis, characterization, optical and electrochemical properties. Dyes and Pigments. 2008;79(3):224-35.

[32] Farooqi MJ, Penick MA, Burch J, Negrete GR, Brancaleon L. Characterization of novel perylene diimides containing aromatic amino acid side chains. Spectrochimica Acta Part A: Molecular and Biomolecular Spectroscopy.

2016;153:124-31.

[33] Li M, Xu J-R, Zeng Y, Ben H-J, Yao F-L, Yang S, et al. Ionic self-assembled derivatives of perylene diimide: Synthesis, aggregated structure and molecular packing behavior. Dyes and Pigments. 2017;139:79-86.

[34] Agnihotri S, Mukherji S, Mukherji S. Size-controlled silver nanoparticles synthesized over the range 5–100 nm using the same protocol and their antibacterial efficacy. RSC Advances. 2014;4(8):3974-83.

[35] Hou J, Chen TL, Zhang S, Huo L, Sista S, Yang Y. An Easy and Effective Method To Modulate Molecular Energy Level of Poly(3-alkylthiophene) for High-Voc Polymer Solar Cells. Macromolecules. 2009;42(23):9217-9.

[36] Zhao H, Zhang Y-y, Xu H, He Z-m, Zhang Z-L, Zhang H-q. Synthesis and properties of perylene diimide dyes bearing unsymmetrical and symmetrical phenoxy substituents at bay positions. Tetrahedron. 2015;71(40):7752-7.

[37] Tantra R, Jing S, Pichaimuthu SK, Walker N, Noble J, Hackley VA. Dispersion stability of nanoparticles in ecotoxicological investigations: the need for adequate measurement tools. Journal of Nanoparticle Research. 2011;13(9):3765-80.

[38] Yin X-z, Tan Y-q, Song Y-h, Zheng Q. Dispersion stability and rheological behavior of suspensions of polystyrene coated fumed silica particles in polystyrene solutions. Chinese Journal of Polymer Science. 2011;30(1):26-35.

[39] Nolte H, Schilde C, Kwade A. Determination of particle size distributions and the degree of dispersion in nanocomposites. Composites Science and Technology.

2012;72(9):948-58.

[40] Ciardelli F, Ruggeri G, Pucci A. Dye-containing polymers: methods for preparation of mechanochromic materials. Chemical Society Reviews. 2013;42(3):857-70.

[41] Olhero SM, Ferreira JMF. Influence of particle size distribution on rheology and particle packing of silica-based suspensions. Powder Technology. 2004;139(1):69-75.

[42] Lee PTC, Chiu C-W, Chang L-Y, Chou P-Y, Lee T-M, Chang T-Y, et al. Tailoring Pigment Dispersants with Polyisobutylene Twin-Tail Structures for Electrowetting Display Application. ACS Applied Materials & Interfaces. 2014;6(16):14345-52.

Summary

Perylene dyes were synthesized using perylene-3,4,9,10-tetracarboxylic dianhydride (PTCDA) for application on the black matrix. Bulky substituents were introduced at the periphery and the bay position of PTCDA to enhance the solubility of the dyes in PGMEA. The introduced substituents also affected the absorption range and the band shape of the dyes.

Aniline derivative-substituted PDIs were synthesized, and a broad absorption range of the dyes was exhibited by the carbazole group attached at the bay position. The synthetic dyes exhibited a high thermal stability in the solid state, and this stability characteristic was reflected in the films fabricated with these dyes. And dye-type and hybrid-type films showed a lower dielectric constant compared with that of the carbon black-type film.

The conjugation-extended perylenetetracarboxylic bisbenzimidazole (PTCBI) was also synthesized for visible light absorption around 600–700 nm, the wavelength region of weakly absorbed by the carbazole-containing PDI dye. The black matrices that were fabricated with a mixture of PDI and PTCBI dyes showed a high thermal stability and a low dielectric constant. In addition, self-aggregation that occurred from dyes of different moieties was prevented by applying dyes based on the same perylene structure on the films.

The black matrix using the dissolved dyes can achieve OD values of industrial standards with a sufficient dye content. Therefore, high solubility of the dyes in

PGMEA is essential. Films with PDI monomers having insufficient solubility did not satisfy this industrially desired optical property. Dimerization of the PDIs was conducted to prevent intermolecular interaction between the monomeric PDIs, and therefore the solubility of the dimers was significantly improved. The optical properties and thermal stability were also enhanced by the dimerization of the dyes. Films fabricated with increased dye contents exhibited a high OD value of 2.76. Therefore, dyes with enhanced solubility can be an effective approach for enhancing the optical properties of the black matrix.

Dye-type black matrices have the lowest dielectric constant among the types of the film; however, the light in the visible region was not sufficiently absorbed. The hybrid-type black matrix was able to meet the commercial standards of optical characteristics while lowering the dielectric constant as compared with the carbon black-type black matrix. The films prepared using the dissolution method showed smoother surface properties with a lower Rq value than the films prepared using the dispersion method. Therefore, it is concluded that the hybrid-type black matrix prepared using highly soluble dyes via the dissolution method can replace the carbon black-type black matrix.

초 록

컬러 필터는 디스플레이 모듈의 주요한 요소 중 하나로, 정제되지 않은 빛을 적, 녹, 청 3 색의 빛으로 변환해 준다. 블랙 매트릭스는 이 RBG 픽셀 사이에 위치하여 원치 않는 색의 혼합을 방지해 준다. 또한 외부에서 모듈 내부로 들어오는 빛을 차단함으로써 외부 빛에 의한 TFT의 오작동을 방지할 수 있다. 이러한 역할을 수행하기 위해 블랙 매트릭스 재료는 가시광 영역에서의 강한 흡광 능력과 내구성이 요구된다.

현재 가장 많이 사용되고 있는 블랙 매트릭스 용 재료는 카본 블랙이다. 카본 블랙은 빛과 열에 대한 안정성이 높으며 가시광 전 영역에서 우수한 흡광 특성을 보인다. 하지만 전도도가 높은 카본 블랙의 특성으로 인해 카본 블랙 타입 블랙 매트릭스가 TFT 층에 인접할 경우 TFT에 잘못된 전기적 신호가 전달될 수 있다. 디스플레이 패널이 점점 박막화되면서 TFT 층과 컬러 필터 층의 간격이 줄어들고 있기 때문에 카본 블랙을 다른 물질로 대체하기 위한 연구가 지속적으로 요구되고 있다. 현재 필름의 유전율을 낮추기 위해 유기 안료를 카본 블랙과 혼합하여 사용하고 있지만 안료의 낮은 몰 흡광도 때문에 블랙 매트릭스의 광학 특성 달성에 어려움이 있다.

카본 블랙과 안료는 분자간 강한 인력으로 인해 공정 용매인 PGMEA에 대한 용해도가 낮다. 따라서 카본 블랙과 안료는 물리적, 화학적 처리

를 통해 작은 입자 크기를 유지시켜주는 분산법을 이용하여 블랙 매트릭스에 적용되고 있다. 분산된 재료는 입자 크기가 수백 나노미터 이하로 일정하게 제어되면서 단순 분산 형태가 유지되어야 하며 분산법을 통해 블랙 매트릭스를 제조하기 위해서는 추가 적인 분산 공정과 분산제와 같은 새로운 물질의 개발이 요구된다.

반면 유기 염료는 높은 몰 흡광도와 낮은 유전율 특성을 보이기 때문에 카본 블랙이나 유기 안료를 대체할 수 있다. 또한 PGMEA에 대한 충분한 용해도 특성을 보이는 염료는 용해법으로 블랙 매트릭스 제조에 적용이 가능하여 이를 통해 공정의 단순화가 가능하다. 하지만 유기 염료는 유기 안료나 블랙 매트릭스 비해 내구성이 낮은 특성이 있기 때문에 이를 보완하기 위한 염료 구조의 설계가 요구된다.

따라서 본 학위 논문에서는 PGMEA에 용해성을 보이는 유기 염료를 개발하고 이를 염료 형 및 염료와 카본 블랙을 혼합하여 사용하는 하이브리드 형 블랙 매트릭스에 적용하고자 했다. 안료를 이용한 필름과 마찬가지로 염료를 이용한 필름은 낮은 유전율 특성을 보이기 때문에 색 특성과 내구성을 만족할 경우 염료는 블랙 매트릭스에 더 적합한 재료로 평가할 수 있다.

염료의 기본 구조로 내구성이 뛰어난 perylene perylene-3,4,9,10-tetracarboxylic dianhydride (PTCDA)를 선정함으로써 일반적인 염료의 단점인 낮은 내구성을 보완하고자 했다. PTCDA는 높은 열안정성 뿐 아니라

우수한 열적, 화학적, 광화학적, 전기적 특성을 보이기 때문에 생화학적 응용, 유기 광전지, 발광 다이오드 및 박막 트랜지스터와 같은 다양한 산업분야에서 활용되어 왔다. 또한 periphery와 bay 위치의 치환기에 따라 쉽게 오비탈 에너지 레벨의 조정이 가능하므로 가시광 전 영역 흡수를 목적으로 하는 블랙 매트릭스 재료로 적합하다.

PTCDA를 블랙 매트릭스 재료로 개발하기 위해 먼저 PTCDA의 periphery 위치에 aniline 유도체가 도입된 perylene diimide (PDI)를 합성하고 PDI의 bay 위치에 전자 공여 치환기를 도입하여 흡광 영역을 조절하였다. 합성된 염료의 광학적, 열적 특성을 조사하고, 염료 형 및 하이브리드 형 의 광학, 열적 및 전기적 특성을 조사하였다. 두 종류의 필름 중, 하이브리드 형 블랙 매트릭스가 낮은 유전율, 낮은 투과율 및 높은 열안정성을 보였다.

추가적으로 염료의 분광 특성을 보완하기 위해 PTCDA의 장 축 방향으로 conjugation을 확장한 PTCDI를 합성하고 PDI 염료와 혼합하여 블랙 매트릭스 필름을 제조하였다. 제조된 필름의 광학적, 열적, 전기적 특성을 조사하였으며 추가적으로 원자 빔 현미경을 통해 필름의 표면을 관찰했다.

개발된 블랙 매트릭스 재료로 필름의 전기적 특성과 표면의 편평도를 산업적 수준 이상으로 달성할 수 있었지만 블랙 매트릭스의 광 흡수 능력을 평가하는 가장 중요한 요소 중 하나인 광학 밀도 (optical density, OD)

수치가 산업적인 표준 (2.5)에는 도달하지 못하였다. 따라서 OD 값을 향상시키기 위한 전략으로 PDI 단량체를 이합체화 하였으며 이를 이용하여 필름을 제조했다. 이합체화된 두 PDI는 perylene 판이 서로 뒤틀린 상태로 존재하기 때문에 동일한 bay 위치 치환기가 도입된 단량체에 비해 용해도가 크게 상승했다. 염료의 향상된 용해도를 통해 필름 제조에 염료의 함량이 증가할 수 있었으며 필름의 광학 밀도가 최대 2.76까지 증가했다. 또한 이합체화된 염료를 이용한 하이브리드 형 블랙 매트릭스는 이전에 개발된 블랙 매트릭스에 비해 높은 열적 안정성, 편평한 표면 상태 및 낮은 유전율을 나타냈다.

최종적으로 용해법을 이용한 블랙 매트릭스를 분산법을 이용한 블랙 매트릭스와 비교하여 실제 블랙 매트릭스에 염료의 적용 가능성을 평가해 보았다. 구조가 유사하면서 용해도에 차이를 보이는 perylene 염료를 이용하여 두 방법으로 제조된 블랙 매트릭스의 특성을 비교해 본 결과, 열적으로 안정적이면서 우수한 광학 및 표면 특성의 블랙 매트릭스 개발을 위해서는 perylene 염료의 용해도를 향상시킨 후 용해법으로 블랙 매트릭스에 적용하는 방법이 분산법을 이용하는 방법보다 더 유리함을 확인할 수 있었다.

결론적으로 카본 블랙과 유기 안료를 유기 염료로 대체함으로써 저유전율 블랙 매트릭스를 제조했다. 필름의 광, 열안정성 특성을 향상시키기 위해 염료는 빛 흡광 능력과 열 안정성이 뛰어난 perylene 구조를 기본으로 하여 합성하였다. 제조된 필름은 열처리 과정에서도 색변화가 크게

변하지 않아 열안정성이 높은 것으로 측정되었으며 표면 상태도 균일한 수준을 유지하여 블랙 매트릭스 개발의 요구 특성을 만족하였다. 또한 고용해성 PDI 이량체를 통해 OD의 산업적인 기준을 만족하였으며 실제 산업에 적용 가능한 수준의 하이브리드 형 블랙 매트릭스를 개발할 수 있었다.

List of Publications

Original Papers

1. **Yuk SB**, Lee W, Namgoong JW, Choi J, Chang JB, Kim SH, et al. Synthesis and characterization of bay-substituted perylene dyes for LCD black matrix of low dielectric constant. Journal of Inclusion Phenomena and Macrocyclic Chemistry. 2015;82(1):187-94.
2. **Yuk SB**, Lee W, Kim SH, Namgoong JW, Lee JM, Kim JP. Application of perylene dyes for low dielectric hybrid-type black matrices. Journal of Industrial and Engineering Chemistry. 2018;64:237-44.
3. **Yuk SB,** Lee JM, Namgoong JW, Sakong C, Kim SH, Hwang TG, Lee W, Kim JP. Synthesis of bay-linked perylene dimers with enhance solubility for high optical density black matrix material. Dyes and Pigments. 2019;171:107695.
4. Choi J, Lee W, Sakong C, **Yuk SB**, Park JS, Kim JP. Facile synthesis and characterization of novel coronene chromophores and their application to LCD color filters. Dyes and Pigments. 2012;94(1):34-9.
5. Lee W, **Yuk SB**, Choi J, Jung DH, Choi S-H, Park J, et al. Synthesis and characterization of solubility enhanced metal-free phthalocyanines for liquid crystal display black matrix of low dielectric constant. Dyes and Pigments. 2012;92(3):942-8.
6. Chang JB, **Yuk SB**, Park JS, Kim JP. Dichroic and spectral properties of anthraquinone-based azo dyes for PVA polarizing film. Dyes and Pigments. 2012;92(1):737-44.

7. Sakong C, Kim SH, **Yuk SB**, Namgoong JW, Park SW, Ko MJ, et al. Influence of Solvent and Bridge Structure in Alkylthio-Substituted Triphenylamine Dyes on the Photovoltaic Properties of Dye-Sensitized Solar Cells. Chemistry – An Asian Journal. 2012;7(8):1817-26.
8. Lee W, **Yuk SB**, Choi J, Kim HJ, Kim HW, Kim SH, et al. The effects of the number of anchoring groups and N-substitution on the performance of phenoxazine dyes in dye-sensitized solar cells. Dyes and Pigments. 2014;102:13-21.
9. Kim SH, Namgoong JW, **Yuk SB**, Kim JY, Lee W, Yoon C, et al. Synthesis and characteristics of metal-phthalocyanines tetra-substituted at non-peripheral (α) or peripheral (β) positions, and their applications in LCD color filters. Journal of Inclusion Phenomena and Macrocyclic Chemistry. 2015;82(1-2):195-202.
10. Kim JY, Choi J, Namgoong JW, Kim SH, Sakong C, **Yuk SB**, et al. Synthesis and characterization of novel perylene dyes with new substituents at terminal-position as colorants for LCD color filter. Journal of Inclusion Phenomena and Macrocyclic Chemistry. 2015;82(1):203-12.
11. Kim JY, Hwang TG, Woo SW, Lee JM, Namgoong JW, **Yuk SB**, et al. Simple modification of basic dyes with bulky &symmetric WCAs for improving their solubilities in organic solvents without color change. Sci Rep. 2017;7:46178.
12. Woo SW, Kim JY, Hwang TG, Lee JM, Kim HM, Namgoong J, **Yuk SB**. Effect of weakly coordinating anions on photo-stability enhancement of basic dyes in organic solvents. Dyes and Pigments. 2019;160:765-71.
13. Bae JH, Lim SJ, Choi J, **Yuk SB**, Namgoong JW, Ko JH, et al. Effects of introducing functional groups on the performance of phenoxazine-based dye-

sensitized solar cells. Dyes and Pigments. 2019;162:905-15.

14. Hwang TG, Kim JY, Namgoong JW, Lee JM, **Yuk SB**, Kim SH, et al. Aggregation induced emission of diketopyrrolopyrrole (DPP) derivatives for highly fluorescent red films. Photochem Photobiol Sci. 2019;18(5):1064-74.1.

List of Presentations

International

1. Lee W, **Yuk SB**, Choi JH, Kim JP, “Synthesis and characterization of highly soluble metal-free phthalocyanines for LCD black matrix”, International Conference on Porphyrins and Phthalocyanines, New Mexico, United states, 2010 - Poster
2. **Yuk SB**, Lee W, Sakong C, Namgoong JW, Kim JP, “The effect of additional electron donating group and conjugated linker on the efficiency of DSSCs based on phenoxazine dyes”, International Conference on Photochemistry, Los Angeles, United States, 2012 - Poster
3. **Yuk SB**, Lee W, Kim JP, “Synthesis and characterization of bay-substituted perylene diimide dyes for LCD black matrix of low dielectric constant”, International Symposium on Nano and Supramolecular Chemistry, 2014 - Oral
4. **Yuk SB**, Lee JM, Kim JP, “Synthesis and Spectral Studies of Perylene Diimide Dyes for LCD Color Filter Black Matrix”, International Conference on Photochemistry, Jeju, Korea, 2015 - Poster
5. Lee JM, **Yuk SB**, Choi S, Kim JP, “A study on improving thermal stability and dispersibility of LCD color filter by introducing ionic interaction between heat resistant cationic phthalocyanine dyes and an anionic binder”, International Conference on Porphyrins and Phthalocyanines, Nanjing, China, 2016 - Poster

Domestic

1. Lee W, **Yuk SB**, Kim JP, “Synthesis and properties of novel metal-free phthalocyanines derived from sterically hindered phenols”, Korean Chemical Society, 2009 - Poster

2. **Yuk SB**, Lee W, Kim JP, “Synthesis of bay-substituted perylene diimide dyes with low permittivity for black matrix”, Korean Chemical Society, 2010 - Poster

3. **Yuk SB**, Lee W, Kim JP, “Synthesis and characterization of highly soluble bay-substituted perylene diimide dyes for black matrix of liquid crystal display”, Korean Chemical Society, 2011 - Poster

4. **Yuk SB**, Kim SH, Kim, JP, “Synthesis and characterization of perylene based dyes for LCD color filter”, The Korean Society of Industrial and Engineering Chemistry, 2013 - Poster

5. **Yuk SB**, Lee JM, Lee W, Kim JP, “Analysis and characterization of dye-type and hybrid-type black matrices of low dielectric constant containing perylene dyes”, The Korean Society of Industrial and Engineering Chemistry, 2015 - Poster

6. **Yuk SB**, Lee JM, Lee W, Kim JP, “Application of perylene dyes for low dielectric hybrid-type black matrices”, Korean Chemical Society, 2017 - Poster